

Self-consistent mean-field models for nuclear structure

Michael Bender and Paul-Henri Heenen

*Service de Physique Nucléaire Théorique, Université Libre de Bruxelles,
B-1050 Bruxelles, Belgium*

Paul-Gerhard Reinhard

*Institut für Theoretische Physik II, Universität Erlangen-Nürnberg,
D-91058 Erlangen, Germany*

(Published 23 January 2003)

The authors review the present status of self-consistent mean-field (SCMF) models for describing nuclear structure and low-energy dynamics. These models are presented as effective energy-density functionals. The three most widely used variants of SCMF's based on a Skyrme energy functional, a Gogny force, and a relativistic mean-field Lagrangian are considered side by side. The crucial role of the treatment of pairing correlations is pointed out in each case. The authors discuss other related nuclear structure models and present several extensions beyond the mean-field model which are currently used. Phenomenological adjustment of the model parameters is discussed in detail. The performance quality of the SCMF model is demonstrated for a broad range of typical applications.

CONTENTS

I. Introduction	122	c. Gaussian overlap Hamiltonian kernel	140
A. The nuclear many-body problem	122	d. Collective Schrödinger equation	140
B. The Hartree-Fock-Bogoliubov method	123	e. Relationship between the collective Schrödinger equation and the Gaussian overlap approximation	141
1. Basics of a mean-field description	124	f. Extension of the generator coordinate method and the Gaussian overlap approximation	141
2. The Hartree-Fock-Bogoliubov equation	125	B. Symmetry restoration	141
3. Symmetries and constraints	126	1. Particle-number projection	141
4. The BCS approximation	126	a. General treatment	141
5. Local densities and currents, nonrelativistic	127	b. Variation before or after projection	141
6. Local densities and currents, relativistic	127	c. The Lipkin-Nogami prescription	142
C. Semiclassical approximations	128	2. Angular momentum projection	142
D. Motivation of a nuclear energy functional	128	a. Principle of the method	142
II. Choices for the Effective Interaction	129	b. Calculation of multipole moments and transition probabilities	143
A. Mean field	129	c. Density dependence of the effective interactions	143
1. The Gogny interaction	129	d. Rotational correction as approximate projection	143
2. Skyrme interactions	130	3. Center-of-mass projection	143
a. The Skyrme energy functional	130	C. Time-dependent mean-field approaches	144
b. Single-particle Hamiltonian	130	1. Time-dependent Hartree-Fock (Bogoliubov)	144
c. Time-odd fields	131	2. Quasiparticle random-phase approximation	145
d. Choices for the coupling constants	131	IV. Technicalities	146
e. Spin-orbit interaction	132	A. Representations	146
f. Tensor force	132	B. Algorithms	146
g. Density dependence	132	V. Parametrizations	147
h. Finite-range terms	133	A. Observables	147
i. The Fayans energy functional	133	1. Energies	147
3. Relativistic mean-field models	133	2. Charge form factor and radii	147
4. Links between relativistic mean-field and Skyrme Hartree-Fock models	135	3. Nuclear matter	148
5. The Coulomb interaction	136	a. Infinite nuclear matter	148
B. Pairing correlations	136	b. Semi-infinite nuclear matter	149
1. Pairing interactions	136	c. Relation to liquid-drop models	149
2. Pairing-active space	138	4. Stability	149
III. Beyond the Static Mean-Field Approach	138	5. Some words of caution	150
A. Configuration mixing	139	B. The pairing gap and odd-even staggering of masses	150
1. Generator coordinate method	139	C. Fit strategies	151
a. Review of the formalism	139	D. Global results	153
b. Conservation of the nucleon numbers	139		
c. Choice of the collective coordinate	140		
2. Gaussian overlap approximation	140		
a. Gaussian overlap kernel	140		
b. Canonical collective variable	140		

1. Nuclear matter properties	153
2. Average quality of bulk observables	154
VI. Applications	155
A. Binding energies	155
B. Shell structure	156
1. Single-particle energies	156
2. Signatures for shell closures	158
3. Shell quenching	158
4. Proton emitters	159
C. Observables of the density distribution	159
1. Systematics of charge radii	159
2. Neutron radii	160
D. Deformation	161
1. Medium-mass nuclei	161
2. Shell quenching in light nuclei	162
3. Fission barriers	163
4. Superdeformed states and fission isomers	164
5. Octupole deformation	164
E. Q_α values in superheavy elements	165
F. Excitations	166
1. Rotational bands	166
2. Low-energy spectra	167
a. Light nuclei	167
b. Deformation effects in medium-mass nuclei	168
c. Ground-state correlations and mass systematics	168
3. Giant resonances	169
4. Excitations of unnatural parity and β decay	170
VII. Conclusions and Outlook	171
Acknowledgments	172
Appendix A: Energy-Density Functional From The Two-Body Skyrme Force	172
Appendix B: The Nucleon Form Factor	172
References	173

I. INTRODUCTION

The remarkable experimental progress in producing and analyzing exotic nuclei has ushered in a renaissance of nuclear structure models. One very successful theoretical approach is with self-consistent mean-field models, perhaps the leading theory for describing and predicting properties of heavy nuclei.

Intense research in recent years has produced a large body of new material and insights. It is time to sort through and to review this work. This article tries to provide an up-to-date view of the self-consistent mean-field (SCMF) models for nuclear structure and excitations. In order to stay within the limits of a review article, we have reduced the material to the essentials and tried to provide extensive citations to sources where more details can be found. And yet we are sure that we are missing some references which might be equally useful. We apologize in advance and hope that this article will be, nonetheless, instructive for a broad readership.

A. The nuclear many-body problem

Models for nuclear structure have been developed since the early days of nuclear physics about 70 years ago. The production of more and more new isotopes has revived the interest in nuclear structure models in recent

years. The large variety of new modeling initiatives can be grouped into three different approaches: *ab initio* methods; self-consistent mean-field (SCMF) and shell-model theories; and macroscopic models with a touch of quantum shell structure. The present review concentrates on the various brands of SCMF theory. Nuclear SCMF models are in many respects analogs of density-functional theory (Hohenberg and Kohn, 1964; Kohn and Sham, 1965), which gives a very successful description of all kinds of many-electron systems (Jones and Gunnarsson, 1989; Parr and Yang, 1989; Dreizler and Gross, 1990; Nagy, 1998; Kohn, 1999; Singh and Deb, 1999; Calvayrac *et al.*, 2000; Onida *et al.*, 2002). In order to put this level of approximation into perspective, we briefly summarize here the status of the competing approaches, staying at a level of citations that is by no means comprehensive.

Traditional *ab initio* methods start from a given nucleon-nucleon potential, which is an effective interaction to describe nucleon-nucleon scattering data (Machleidt and Slaus, 2001). It has a large repulsive core, which means that nuclear matter is a strongly correlated quantum liquid. A description requires highly developed many-body theories like the relativistic Brueckner-Hartree-Fock (Serot and Walecka, 1986; Brockmann and Machleidt, 1990; Dickhoff and M uther, 1992) or correlated basis functions (Pandharipande *et al.*, 1997; Heiselberg and Pandharipande, 2000). All these treatments reproduce the basic features of nuclear saturation. At second glance, however, there is an interesting distinction: all approaches that employ strictly the given nucleon-nucleon potential fail to yield the saturation point of nuclear matter quantitatively, while those models that employ an additional (empirical) three-body force perform very well. The microscopic origin of this three-body force is still under discussion. Intrinsic nucleonic degrees of freedom may play a role, and very recently models have been proposed which try to draw lines directly from underlying QCD formulations to nuclear structure (Lutz *et al.*, 2000; Kaiser *et al.*, 2002). The methods are so involved that almost all of these investigations have been done in homogeneous nuclear (or neutron) matter. Very recent developments in computational techniques allow *ab initio* calculations of finite nuclei, currently reaching about as far as the carbon nuclei (Navratil *et al.*, 2000). The problem of a three-body force persists, of course, in these investigations as well.

The other extreme of nuclear models is the macroscopic nuclear liquid-drop model (Myers and Swiatecki, 1982), which parametrizes the energy in terms of global properties such as volume energy, asymmetry energy, surface energy, etc. The actual parameters are fitted phenomenologically. The liquid-drop model thus describes very well the average trends of nuclear binding energies. It is usually augmented by a shell-correction energy that approximates the quantal shell effects not taken into account in the liquid-drop model. This correction energy is calculated from the single-particle spectrum obtained using a phenomenologically adjusted single-particle po-

tential (Brack *et al.*, 1972). Both combined constitute the microscopic-macroscopic (mic-mac) method which has been tuned to very high descriptive power. The root-mean-square error on binding energies is nowadays below 0.7 MeV (Möller *et al.*, 1995). The mic-mac method, however, relies on a large amount of *ad hoc* modeling, particularly around the expected nuclear mean field. This leaves uncertainties when extrapolating the model into the unknown regime of exotic nuclei.

In between the two extremes of *ab initio* and liquid-drop models, there are two models that work at a microscopic level but employ effective interactions to allow a treatment in either restricted spaces or forms of many-body wave functions. The first of these are the shell-model approaches. In the shell model, one takes for the mean field a standard phenomenological single-particle model but then performs a configuration-mixing calculation involving all many-body states that can be constructed using a more or less broad band of single-nucleon states around the Fermi energy (Brown and Wildenthal, 1988). The residual interaction in the active space is usually fitted phenomenologically. Hjorth-Jensen *et al.* (1992) have recently come up with microscopic determinations using as effective interaction a G matrix from *ab initio* calculations. The problem of the proper saturation point which plagues *ab initio* models is circumvented by using a phenomenologically prescribed mean field. The dimensions of these shell-model calculations grow explosively with system size. Thus Monte Carlo techniques or specific diagonalization schemes have been developed to tackle heavier nuclei. A large body of surveys has been completed with these new methods (Koonin *et al.*, 1997a, 1997b; Caurier and Nowacki, 1999; Otsuka, 2001; Otsuka *et al.*, 2001).

The SCMF methods, to which the rest of this article will be devoted, also fall in between *ab initio* and mic-mac methods, but they take a different path than the shell model. They concentrate on an unprejudiced, self-consistent determination of the nuclear mean field. To this end, they employ effective interactions which are tuned to their primary use in mean-field calculations. The concept is closely related to energy-density-functional theory in electronic systems. Nuclear density functional theory is outlined by Petkov and Stoitsov (1991) and Fayans *et al.* (2000) for nonrelativistic models and by Speicher *et al.* (1991, 1993) and Schmid *et al.* (1995a) for relativistic ones.

However, electronic energy functionals of high accuracy may be derived *ab initio* from electron gas theory. In the nuclear problem, the corresponding approach has not yet been as successful. Attempts have been made to map nuclear matter theory onto mean-field models for finite nuclei using the local-density approximation (LDA; Müther *et al.*, 1990). These yield in a straightforward manner fair results for energies and radii, but for quantitative purposes, energy functionals with phenomenologically determined parameters are far more accurate. Thus one proceeds in a more phenomenological manner: the form of the effective energy functional is motivated from *ab initio* theory, but the actual param-

eters (around 10) are adjusted by extensive fits to nuclear structure data. This will be discussed in detail in the theoretical section of this review.

The nuclear SCMF models have been used extensively since the 1970s. Effective interactions were first derived at that time and applied to a large variety of problems. However, there were still several restrictions imposed on the models which limited the range of applications and left room for mic-mac models. The main restrictions were related to the symmetries of the wave functions, which limited application of the model to ground-state properties of even nuclei. The situation changed in the 1990s when nearly symmetry-unrestricted SCMF calculations became possible. Thanks to this development, studies of rotational bands in heavy nuclei could be systematically performed; in particular, the SCMF models encountered great success in studies of superdeformed rotational bands in isotopes around Dy and Hg. This result was not obvious, since the energy density functionals that were used were not at all adjusted to this kind of phenomenon. To give another example, systematic calculations of superheavy nuclei were also performed, throwing doubt on some of the conclusions drawn from macroscopic models. At the same time, intense experimental developments greatly increased our knowledge of nuclei far from stability. This in turn had an impact on effective interactions, which were improved in several ways over the last decade. The success of the SCMF method has now reached a point where one has to introduce correlations beyond the mean field to improve further on the quality of the description. Several developments along this line have been started in recent years and the first applications seem to be very promising.

We plan to review in this paper the present state of developments, considering the three most widely used variants of nuclear SCMF models. We try to give a comprehensive account of the underlying formal framework and to demonstrate model performance with a brief guided tour through a broad range of applications.

B. The Hartree-Fock-Bogoliubov method

This section is devoted to the general features of nuclear mean-field models. It starts with the basic building blocks and presents the formulation of the coupled mean-field equations at a level that is common to all mean-field models. The actual models are specified later in Sec. II by way of their effective energy functionals. For a more detailed introduction into the Hartree-Fock-Bogoliubov (HFB) method see Mang (1975), Goodman (1979), Ring and Schuck (1980), and Blaizot and Ripka (1985).

The notion of a “mean field” deserves further comment. We concentrate in this review on self-consistent models, where the potential well for nucleons is computed from the nucleonic wave functions. This produces a theory at the level of the Hartree-Fock approximation, which is inadequate for a description of nuclear properties that are strongly influenced by pairing correlations.

To take these correlations into account, one generalizes the mean-field concept to include a pairing field, calculated with the Hartree-Fock-Bogoliubov equations (known as the Bogoliubov–de Gennes equations in condensed-matter physics). Following common usage in the literature, we will use the expression “mean field” in a twofold manner. On the one hand, mean field will refer to methods and models that incorporate both the nucleon potential and the pairing field, but on the other hand we shall also use it to denote the particle-hole part (as contrasted to the particle-particle or pairing part) of the effective interaction or Hamiltonian in the HFB equation.

1. Basics of a mean-field description

The basic building block of any mean-field model is a set of single-nucleon wave functions,

$$\{\psi_i(\mathbf{x}), i=1, \dots, N_{\text{wf}}\}, \quad \mathbf{x}=(\mathbf{r}, \sigma, \tau), \quad (1)$$

where the number of single-particle wave functions N_{wf} is larger than the number of nucleons $A=Z+N$. \mathbf{r} stands for spatial coordinates, $\sigma=\pm 1$ for spin, and $\tau=\pm 1$ for isospin indices. Some authors use equivalently $\sigma, \tau=\pm 1/2$.

For formal purposes it is advantageous to introduce the creation operator \hat{a}_i^+ for a nucleon in the single-particle state $\psi_i(\mathbf{x})$. The coordinate-space representation employs creation operators \hat{a}_x^+ for eigenstates of position. The transformation to creation operators for states i reads

$$\hat{a}_i^+ = \int d^3r \sum_{\sigma\tau} \psi_i(\mathbf{x}) \hat{a}_x^+. \quad (2)$$

The simplest model based on these single-nucleon states is the independent-particle model in which the state of a nucleus, $|\Phi\rangle$, is described by a Slater determinant $|\Phi\rangle \equiv \det\{\psi_i(\mathbf{x}), i=1, \dots, A\}$. The independent-particle state can be characterized formally by $\hat{a}_i^+|\Phi\rangle=0$ for occupied states ($1 \leq i \leq A$) and $\hat{a}_i|\Phi\rangle=0$ for unoccupied states ($i > A$).

Pairing correlations are included by introducing the concept of independent quasiparticles defined by the Bogoliubov transformation (Ring and Schuck, 1980),

$$\hat{b}_n^+ = \sum_i (U_{in}\hat{a}_i^+ + V_{in}\hat{a}_i), \quad (3)$$

which connects single-particle states to quasiparticle states. In compact notation the transformation reads

$$\begin{pmatrix} \hat{b} \\ \hat{b}^+ \end{pmatrix} = \mathcal{W}^+ \begin{pmatrix} \hat{a} \\ \hat{a}^+ \end{pmatrix}, \quad \mathcal{W} = \begin{pmatrix} U & V^* \\ V & U^* \end{pmatrix}, \quad (4)$$

where the transformation matrix is unitary, i.e., $U^+U + V^+V=1$, $UU^+ + V^*V^T=1$, $U^TV + V^TU=0$, and $UV^+ + V^*U^T=0$. This transformation may be decomposed into the product of three simpler ones by virtue of the Bloch-Messiah theorem (Bloch and Messiah, 1962). The ground state of the system is given then by the quasiparticle vacuum condition,

$$\hat{b}_n|\Phi\rangle=0, \quad (5)$$

for all n . The quasiparticle states are defined here in terms of fermion operators. They can also be handled in terms of quasiparticle wave functions in coordinate space:

$$\phi_n = \begin{pmatrix} \phi_n^{(U)}(\mathbf{x}) \\ \phi_n^{(V)}(\mathbf{x}) \end{pmatrix} = \begin{pmatrix} \sum_i U_{in}\psi_i(\mathbf{x}) \\ \sum_i V_{in}\psi_i(\mathbf{x}) \end{pmatrix}. \quad (6)$$

These states are orthonormal due to the unitarity of the quasiparticle transformation, i.e.,

$$\int dx \phi_n^+(\mathbf{x}) \phi_m(\mathbf{x}) = \delta_{nm}, \quad \int dx = \int d^3r \sum_{\sigma\tau}. \quad (7)$$

A compact description for an independent-particle state is provided by the introduction of one-body density matrices. This is particularly useful for self-consistent mean-field models whose energy functionals are formulated in terms of these densities. For independent quasiparticles, one has to deal with two objects, a one-body density matrix ρ and a pair tensor κ , given as

$$\rho_{ij} = \langle \Phi | \hat{a}_j^+ \hat{a}_i | \Phi \rangle = (V^* V^T)_{ij} = \rho_{ji}^*, \quad (8a)$$

$$\kappa_{ij} = \langle \Phi | \hat{a}_j \hat{a}_i | \Phi \rangle = (V^* U^T)_{ij} = -\kappa_{ji}. \quad (8b)$$

These may be viewed as the components of a generalized quasiparticle density

$$\mathcal{R} = \begin{pmatrix} \rho & \kappa \\ -\kappa^* & 1 - \rho^* \end{pmatrix}. \quad (8c)$$

From the properties of ρ and κ , one can show that the eigenvalues of \mathcal{R} are equal to either 0 or 1.

The representation of the density matrices in configuration space is equivalent to a representation in coordinate space,

$$\rho(\mathbf{x}, \mathbf{x}') = \langle \Phi | \hat{a}_x^+ \hat{a}_{x'} | \Phi \rangle \equiv \sum_n \phi_n^{(V)}(\mathbf{x}) \phi_n^{(V)*}(\mathbf{x}'), \quad (9a)$$

$$\kappa(\mathbf{x}, \mathbf{x}') = \langle \Phi | \hat{a}_{x'} \hat{a}_x | \Phi \rangle \equiv \sum_n \phi_n^{(U)}(\mathbf{x}) \phi_n^{(V)*}(\mathbf{x}'). \quad (9b)$$

Instead of the antisymmetric pair tensor κ , the pair density matrix $\tilde{\rho}$, which is obtained by time inversion of one of the indices of κ , turns out to be more useful for the formulation of local energy-density functionals (Dobaczewski *et al.*, 1984):

$$\begin{aligned} \tilde{\rho}(\mathbf{x}, \mathbf{x}') &= -\sigma' \langle \Phi | \hat{a}_{r', -\sigma', \tau'} \hat{a}_x | \Phi \rangle \\ &= -\sigma' \kappa(\mathbf{x}, \mathbf{r}', -\sigma', \tau'). \end{aligned} \quad (10)$$

\mathcal{R} is then constructed by replacing κ with $\tilde{\rho}$. Each of the three forms, (\hat{b}^+, \hat{b}) , ϕ_n , and \mathcal{R} , represents an independent-quasiparticle state or Hartree-Fock-Bogoliubov state. Each representation has its advantages and disadvantages. Which form is to be preferred depends on the actual application.

2. The Hartree-Fock-Bogoliubov equation

The ground state $|\Phi\rangle$ of the HFB method is obtained by minimization of the total energy

$$E = \langle \Psi | \hat{H} | \Psi \rangle = E[\rho, \kappa, \kappa^*], \quad (11)$$

with constraints on proton and neutron numbers $\langle \Psi | \hat{N}_q | \Psi \rangle = N_q$. Any expectation value of an operator with an HFB state can be expressed in terms of the one-body densities only. In fact, we shall later use effective energy-density functionals in which only the energy functional $E[\rho, \kappa, \kappa^*]$ is given without explicit knowledge of an underlying Hamiltonian \hat{H} .

The minimization of the total Routhian $E^\lambda = E - \lambda_q \langle \Psi | \hat{N}_q | \Psi \rangle$ leads to the HFB equation, which can be expressed in terms of the U and V transformation matrices

$$\mathcal{H} \begin{pmatrix} U_n \\ V_n \end{pmatrix} = e_n \begin{pmatrix} U_n \\ V_n \end{pmatrix}, \quad (12a)$$

$$\mathcal{H} = \begin{pmatrix} h - \lambda & \Delta \\ -\Delta^* & -h^* + \lambda \end{pmatrix} \quad (12b)$$

with

$$h_{ij} = \frac{\delta E}{\delta \rho_{ji}} = h_{ji}^*, \quad \Delta_{ij} = \frac{\delta E}{\delta \kappa_{ij}^*} = -\Delta_{ji}, \quad (13)$$

where the quasiparticle energies e_n are the Lagrangian multipliers introduced to constrain the orthonormalization of the quasiparticle states. For a standard Hamiltonian $\hat{H} = \hat{T} + \hat{V}$ where \hat{V} is a two-body interaction, the matrix elements of the mean-field and gap Hamiltonians are given by

$$h_{ij} = T_{ij} + \sum_{kl} V_{ikjl} \rho_{lk}, \quad \Delta_{ij} = \frac{1}{2} \sum_{kl} V_{ijkl} \kappa_{kl}, \quad (14)$$

where V_{ikjl} is the antisymmetrized two-body matrix element. The HFB spectrum $\{e_n\}$ is unbound from above and below. The eigenvalues show up in pairs $\pm e_n$ where one state for each pair already carries the full information. One must keep only one of the two states in the Fermion algebra to maintain the proper fermionic anti-commutation relations. For that, one usually takes the branch that is bound from below. A very compact form of the static HFB equation is given in terms of the generalized density (8c) as $[\mathcal{H}, \mathcal{R}] = 0$.

The solution of the HFB equation can be expressed in terms of several complete sets of individual states. Each of them corresponds to the diagonalization of a different operator. The *quasiparticle basis* ϕ_n , Eq. (6), is defined by the diagonalization of the generalized one-body matrix \mathcal{R} which can be performed since this matrix commutes with \mathcal{H} . The *natural orbital* or *canonical basis* ψ_i is obtained by diagonalization of the density ρ . In this basis, the pair tensor κ is in its canonical form, the U_{ni} matrix is diagonal, and the V_{ni} matrix is decomposed into 2×2 antidiagonal matrices. This basis provides a very compact representation of the HFB state which has sometimes been exploited for numerical solutions of the

HFB equation (Mühlhans *et al.*, 1984; Reinhard *et al.*, 1997; Tajima, 2000). A third basis is the *Hartree-Fock basis*, in which the mean-field Hamiltonian \hat{h} is diagonal. This basis still requires the full HFB matrices U_{ni} and V_{ni} , but only on a smaller subset of pairing-active states. Many HFB calculations use this double step, first diagonalizing \hat{h} and then solving the HFB equations in this basis.

Equation (12) can be rewritten in coordinate space as (Dobaczewski *et al.*, 1984)

$$\int dx' \mathcal{H}(\mathbf{x}, \mathbf{x}') \phi_n(\mathbf{x}') = e_n \phi_n(\mathbf{x}). \quad (15)$$

Expressing \mathcal{R} and \mathcal{H} in terms of the pair density $\bar{\rho}$, this representation is the appropriate tool for discussing the asymptotic properties of the HFB spectrum (Bulgac, 1980; Dobaczewski *et al.*, 1984). The density matrix and the pair density matrix $\bar{\rho}$ are localized over the nucleus. The interaction terms $h(\mathbf{x}, \mathbf{x}')$ and $\tilde{h}(\mathbf{x}, \mathbf{x}') = \delta E / \delta \bar{\rho}(\mathbf{x}', \mathbf{x})$ tend to zero asymptotically, and the kinetic energy and λ term are the only ones remaining for $|\mathbf{r}| \rightarrow \infty$:

$$-\frac{\hbar^2}{2m} \Delta \phi_n^{(U)}(\mathbf{x}) = (\lambda + e_n) \phi_n^{(U)}(\mathbf{x}), \quad (16)$$

$$-\frac{\hbar^2}{2m} \Delta \phi_n^{(V)}(\mathbf{x}) = (\lambda - e_n) \phi_n^{(V)}(\mathbf{x}). \quad (17)$$

The asymptotic forms of $\phi^{(U)}$ and $\phi^{(V)}$ depend on the signs of $\lambda + e_n$, and $\lambda - e_n$, respectively: $\phi^{(U)}$ becomes a plane wave for $\lambda + e_n > 0$ and a decreasing exponential for $\lambda + e_n < 0$, while $\phi^{(V)}$ becomes a plane wave for $\lambda - e_n > 0$ and a decreasing exponential for $\lambda - e_n < 0$.

For $\lambda > 0$, the whole spectrum is continuous, while for $\lambda < 0$, it is either discrete ($|e_n| < -\lambda$) or continuous ($|e_n| > -\lambda$). As for $e_n > 0$ and $\lambda < 0$, the lower components of $\phi^{(V)}$ are localized functions. One can write the density matrices only in terms of bound wave functions:

$$\rho(\mathbf{x}, \mathbf{x}') = \sum_{\mathcal{J}} \phi_n^{(V)}(\mathbf{x}) \phi_n^{(V)*}(\mathbf{x}'), \quad (18a)$$

$$\bar{\rho}(\mathbf{x}, \mathbf{x}') = \sum_{\mathcal{J}} \phi_n^{(U)}(\mathbf{x}) \phi_n^{(U)*}(\mathbf{x}'), \quad (18b)$$

where

$$\sum_{\mathcal{J}} \dots = \sum_{0 < e_n < -\lambda} \dots + \int_{-\lambda}^{\infty} \dots$$

These wave functions are always localized. The HFB state is defined by the occupation of all the states with negative energy, the quasiparticle states with positive energy defining the excitations of the system.

The fact that the density matrix vanishes asymptotically has the important consequence that the natural orbitals must vanish for $|\mathbf{r}| \rightarrow \infty$. This property is crucial to describing pairing correlations in nuclei far from stability for which the Fermi level is close to zero. In the Hartree-Fock basis, pairing correlations couple bound

states to states in the continuum. However, the diagonalization of the full HFB matrix still allows the construction of localized densities.

3. Symmetries and constraints

The Bogoliubov transformation, Eq. (3), is very general and no symmetry is imposed *a priori* on the wave functions. Two kinds of symmetry can be introduced: (i) symmetry related to the shape of the nucleus and (ii) time-reversal symmetry; see also Dobaczewski *et al.* (2000a, 2000b) for a general discussion.

Space symmetries are usually imposed through the basis on which the wave functions are expanded or the mesh that is used to discretize the wave function. Very general shapes can be described at this point and several codes exist which allow us to study nuclear densities exhibiting triaxial quadrupole or octupole deformations. The energy landscape as a function of a spatial degree of freedom can be explored with the help of constraints. The equations of motion are obtained by minimization of a Routhian,

$$E = \langle \hat{H} \rangle - \sum_{q=p,n} \lambda_q \langle \hat{N}_q \rangle - \sum_{\alpha} \lambda_{\alpha} \langle \hat{Q}_{\alpha} \rangle, \quad (19)$$

subject to the constraint $\langle \hat{Q}_{\alpha} \rangle = Q_{\alpha}$, where λ_q and λ_{α} are Lagrange multipliers, and where $\langle \hat{Q}_{\alpha} \rangle$ denotes the expectation value $\langle \Psi | \hat{Q}_{\alpha} | \Psi \rangle$. The operators \hat{Q}_{α} correspond to the spatial degrees of freedom that one wants to explore. A quadratic constraint is frequently used in the form

$$E = \langle \hat{H} \rangle - \sum_{q=p,n} \lambda_q \langle \hat{N}_q \rangle + \frac{1}{2} \sum_{\alpha} C_{\alpha} (\langle \hat{Q}_{\alpha} \rangle - \mu_{\alpha})^2, \quad (20)$$

where C_{α} is a constant, and μ_{α} is the desired value of the operator expectation $\langle \hat{Q}_{\alpha} \rangle$. This form is better suited to explore energy curves with several extrema. It is equivalent to a linear constraint with λ_{α} varying over the iterations and equal to $C_{\alpha}(\mu_{\alpha} - \langle \hat{Q}_{\alpha} \rangle)$ (Ring and Schuck, 1980), see Sec. IV for more details.

Time-reversal symmetry limits the systems that can be studied to even-even nonrotating nuclei and to two-quasiparticle excited states of those even nuclei when the quasiparticles are a pair of time-reversed orbits. These orbitals are then Kramers degenerate and correspond to the two eigenvalues $\pm i$ of the signature operator

$$\hat{R}_x = e^{i\pi \hat{J}_x}, \quad (21)$$

where J_x is the x component of the angular momentum operator. For axially symmetric nuclei, the two degenerate states have opposite angular momentum projection on the symmetry axis. The creation of a quasiparticle (to study odd nuclei) or the rotation of a nucleus (driven by a constraint $\omega \hat{J}_x$) breaks time-reversal symmetry. The orbitals paired by pairing correlations are no longer connected by the signature symmetry and therefore are not known *a priori*. The BCS approximation (see Sec. I.B.4)

is then suspect. However, the single-particle wave functions may remain eigenstates of signature. In this case, the HFB matrices are divided into blocks and their dimensions can be reduced by a factor of 2.

According to a well-established procedure (Goodman, 1974), the matrices U and V can be written in a block form:

$$U = \begin{pmatrix} u & 0 \\ 0 & \tilde{u}^* \end{pmatrix}; \quad V = \begin{pmatrix} 0 & \tilde{v}^* \\ -v & 0 \end{pmatrix}, \quad (22)$$

where the u , v and \tilde{u} , \tilde{v} matrices refer to the signature blocks. This leads to simplifications for ρ and κ :

$$\rho = \begin{pmatrix} r & 0 \\ 0 & \tilde{r}^* \end{pmatrix}; \quad \kappa = \begin{pmatrix} 0 & k \\ -k^T & 0 \end{pmatrix}; \quad \begin{cases} r = \tilde{v} \tilde{v}^+ \\ \tilde{r} = v v^+ \\ k = \tilde{v} \tilde{u} \end{cases}, \quad (23)$$

and for h and Δ :

$$h = \begin{pmatrix} h & 0 \\ 0 & \tilde{h}^* \end{pmatrix}; \quad \Delta = \begin{pmatrix} 0 & d \\ -d^T & 0 \end{pmatrix}. \quad (24)$$

Then the HFB equations, (12a) and (12b), reduce to the following problem:

$$\begin{pmatrix} h & d \\ d^+ & -\tilde{h} \end{pmatrix} \begin{pmatrix} u & \tilde{v} \\ -v & \tilde{u} \end{pmatrix} = \begin{pmatrix} u & \tilde{v} \\ -v & \tilde{u} \end{pmatrix} \begin{pmatrix} E_i^{\omega} \delta_{ij} & 0 \\ 0 & -E_i^{\omega} \delta_{ij} \end{pmatrix}. \quad (25)$$

In a similar manner, to study one-quasiparticle or two-quasiparticle states, the U and V components of eigenvectors are exchanged and the sign of v is reversed.

4. The BCS approximation

The BCS approximation is a widely used simplification of the HFB method for time-reversal-invariant systems. It requires an *a priori* knowledge of pairing partner states and for this reason is well defined only in the case of time-reversal invariance. There is then a Kramers degeneracy of the single-particle states $\epsilon_n = \epsilon_{\bar{n}}$ which come in pairs of time-conjugate partners φ_n , $\varphi_{\bar{n}}$. We associate the elements of the pair by the shorthand notation n , \bar{n} .

The HFB approach is cumbersome because the number of coupled equations that must be solved is double that of the BCS approximation. This is a consequence of the noncommutative properties of the mean-field and pairing Hamiltonians. However, one can expect that their commutator is close to zero in well-bound nuclei where time-reversal invariance can be imposed. The BCS approximation consists in forcing the pairing potential \hat{d} to be diagonal in the basis of the eigenstates of the mean-field Hamiltonian \hat{h} , i.e.,

$$d_{n\bar{m}} = \delta_{nm} d_{n\bar{m}}, \quad \hat{h} \varphi_n = \epsilon_n \varphi_n. \quad (26)$$

The two-component wave functions become simply $\phi_n^{(U)} = u_n \varphi_n$ and $\phi_n^{(V)} = v_n \varphi_n$. The pairing problem reduces to determining the occupation amplitudes (u_n, v_n) by means of the gap equation

$$(\epsilon_n - \lambda)(u_n^2 - v_n^2) + 2d_{n\bar{n}} u_n v_n = 0. \quad (27)$$

The density matrices then become

$$\rho(\mathbf{x}, \mathbf{x}') = 2 \sum_{n>0} v_n^2 \varphi_n(\mathbf{x}) \varphi_n^*(\mathbf{x}'), \quad (28a)$$

$$\tilde{\rho}(\mathbf{x}, \mathbf{x}') = -2 \sum_{n>0} u_n v_n \varphi_n(\mathbf{x}) \varphi_n^*(\mathbf{x}'). \quad (28b)$$

This provides a much simpler scheme altogether. It is the reason the BCS approximation is introduced for most mean-field calculations dealing with nuclei that are well bound and for which time-reversal invariance can be imposed.

However, the asymptotic conditions of the HFB method are lost since the pairing potential Δ is not zero asymptotically. The pair densities calculated in the BCS approximation are not localized when the Fermi level tends to zero. It is thus compulsory to switch to full HFB when dealing with exotic nuclei near the drip lines or to determine fission barriers.

5. Local densities and currents, nonrelativistic

The full density matrix $\rho(\mathbf{x}, \mathbf{x}') = \rho(\mathbf{r}\sigma\tau, \mathbf{r}'\sigma'\tau')$, as computed, for example in BCS, Eq. (28a) and Eq. (28b), can be decomposed into four separate spin-isospin terms,

$$\begin{aligned} \rho(\mathbf{r}\sigma\tau, \mathbf{r}'\sigma'\tau') &= \frac{1}{4} \left\{ [\rho_{00}(\mathbf{r}, \mathbf{r}') \delta_{\sigma\sigma'} + \mathbf{s}_{00}(\mathbf{r}, \mathbf{r}') \cdot \boldsymbol{\sigma}_{\sigma'\sigma}] \delta_{\tau\tau'} \right. \\ &\quad \left. + \sum_{\alpha=-1}^{+1} [\rho_{1\alpha}(\mathbf{r}, \mathbf{r}') \delta_{\sigma\sigma'} + \mathbf{s}_{1\alpha}(\mathbf{r}, \mathbf{r}') \cdot \boldsymbol{\sigma}_{\sigma'\sigma}] (\tau_{\tau'\tau})_{\alpha} \right\}. \end{aligned} \quad (29)$$

The decomposition uses the fact that the three Pauli matrices together with the unit matrix form a complete basis in both spin and isospin spaces. The $\boldsymbol{\sigma}_{\sigma'\sigma}$ and $\boldsymbol{\tau}_{\tau'\tau}$ are matrix elements of the Pauli matrices in spin and isospin space,

$$\boldsymbol{\sigma}_{\sigma'\sigma} = (\sigma' | \hat{\boldsymbol{\sigma}} | \sigma), \quad \boldsymbol{\tau}_{\tau'\tau} = (\tau' | \hat{\boldsymbol{\tau}} | \tau). \quad (30)$$

In what follows we shall consider pure proton and neutron states. In this case, only the $\alpha=0$ components of the isovector densities contribute. This restriction suffices for almost all applications. A generalization to isospin nondiagonal contributions is straightforward when needed (for situations with $T=0$ pairing or to describe β decay in the quasiparticle random-phase approximation, for example). There are six local densities and currents that can be derived from the full density matrix. With $T=0$ or 1, and omitting the second index in the densities entering Eq. (29), we have

$$\rho_0(\mathbf{r}) = \rho_0(\mathbf{r}, \mathbf{r}) = \sum_{\sigma\tau} \rho(\mathbf{r}\sigma\tau; \mathbf{r}\sigma\tau),$$

$$\rho_1(\mathbf{r}) = \rho_1(\mathbf{r}, \mathbf{r}) = \sum_{\sigma\tau} \rho(\mathbf{r}\sigma\tau; \mathbf{r}\sigma\tau) \tau,$$

$$\begin{aligned} \mathbf{s}_0(\mathbf{r}) = \mathbf{s}_0(\mathbf{r}, \mathbf{r}) &= \sum_{\sigma\sigma'\tau} \rho(\mathbf{r}\sigma\tau; \mathbf{r}\sigma'\tau) \boldsymbol{\sigma}_{\sigma'\sigma}, \\ \mathbf{s}_1(\mathbf{r}) = \mathbf{s}_1(\mathbf{r}, \mathbf{r}) &= \sum_{\sigma\sigma'\tau} \rho(\mathbf{r}\sigma\tau; \mathbf{r}\sigma'\tau) \boldsymbol{\sigma}_{\sigma'\sigma} \tau, \end{aligned} \quad (31)$$

$$\mathbf{j}_T(\mathbf{r}) = \frac{i}{2} (\nabla' - \nabla) \rho_T(\mathbf{r}, \mathbf{r}') |_{\mathbf{r}=\mathbf{r}'},$$

$$\mathbf{J}_T(\mathbf{r}) = \frac{i}{2} (\nabla' - \nabla) \otimes \mathbf{s}_T(\mathbf{r}, \mathbf{r}') |_{\mathbf{r}=\mathbf{r}'},$$

$$\boldsymbol{\tau}_T(\mathbf{r}) = \nabla \cdot \nabla' \rho_T(\mathbf{r}, \mathbf{r}') |_{\mathbf{r}=\mathbf{r}'},$$

$$\mathbf{T}_T(\mathbf{r}) = \nabla \cdot \nabla' \mathbf{s}_T(\mathbf{r}, \mathbf{r}') |_{\mathbf{r}=\mathbf{r}'}. \quad (32)$$

These are the density, spin density, current, spin-current tensor, kinetic density, and kinetic spin density, respectively. See Dobaczewski and Dudek (1996) for a detailed discussion of their properties. Isoscalar ($T=0$) densities are total densities (e.g., $\rho_0 = \rho_n + \rho_p$), while isovector ($T=1$) densities account for proton-neutron differences (e.g., $\rho_1 = \rho_n - \rho_p$). The spin-current tensor is usually approximated by the spin-orbit current

$$\mathbf{J} = \sum_{ijk} \epsilon_{ijk} \mathbf{J}_{jk} \mathbf{e}_i, \quad (32)$$

where ϵ_{ijk} is the Levi-Civita symbol. A similar decomposition exists for the pair density matrix $\tilde{\rho}(\mathbf{x}, \mathbf{x}')$, Eq. (10). In most applications, only the local pair density is needed

$$\tilde{\rho}_0(\mathbf{r}) = \sum_{\sigma\tau} \tilde{\rho}(\mathbf{r}\sigma\tau; \mathbf{r}\sigma\tau),$$

$$\tilde{\rho}_1(\mathbf{r}) = \sum_{\sigma\tau} \tilde{\rho}(\mathbf{r}\sigma\tau; \mathbf{r}\sigma\tau) \tau. \quad (33)$$

While the local density $\rho_0(\mathbf{r})$ describes the probability of finding a nucleon at \mathbf{r} , the local pair density $\tilde{\rho}_0(\mathbf{r})$ is related to the enhancement of the probability of finding a pair of nucleons with opposite spin due to correlations; see Dobaczewski, Nazarewicz, Werner, *et al.* (1996).

6. Local densities and currents, relativistic

A very similar line of development can be followed for relativistic models. The generalization consists of letting the Pauli spinor wave functions $\phi_n^{(U)}$, $\phi_n^{(V)}$, or φ_n in the nonrelativistic HFB method, grow to four-component Dirac spinor wave functions. There are 16 independent bilinear covariants $\bar{\psi}(\mathbf{r}) \Gamma \psi(\mathbf{r})$ that can be constructed using the relativistic 4×4 Dirac matrices. Choosing $\Gamma^S = 1$, $\Gamma_\mu^V = \gamma_\mu$, $\Gamma_{\mu\nu}^T = (i/2)(\gamma_\mu \gamma_\nu - \gamma_\nu \gamma_\mu)$, $\Gamma^P = \gamma_5$, and $\Gamma_\mu^A = \gamma_\mu \gamma_5$ gives the local scalar, vector, tensor, pseudoscalar, and pseudovector (axial) densities, which can be constructed as isoscalar or isovector densities. A simplification arises in that only three of these are required in standard relativistic mean-field theories, namely, the isoscalar and isovector (four-)vector densities and the isoscalar scalar density,

$$\rho_{\mu 0}(\mathbf{r}) = \sum_{\sigma\sigma'\tau} \rho(\mathbf{r}\sigma\tau; \mathbf{r}\sigma'\tau) (\gamma_{\mu})_{\sigma'\sigma}, \quad (34a)$$

$$\rho_{\mu 1}(\mathbf{r}) = \sum_{\sigma\sigma'\tau} \rho(\mathbf{r}\sigma\tau; \mathbf{r}\sigma'\tau) (\gamma_{\mu})_{\sigma'\sigma} \tau, \quad (34b)$$

$$\rho_{s0}(\mathbf{r}) = \sum_{\sigma\sigma'\tau} \rho(\mathbf{r}\sigma\tau; \mathbf{r}\sigma'\tau), \quad (34c)$$

where σ, σ' now run over four spinor components. The summation in the densities is usually restricted to positive energy states only; states from the Dirac sea are omitted. The related vacuum polarization effects are supposed to be effectively contained in the parameters of the model.

C. Semiclassical approximations

There is a straightforward link from the SCMF approach to the mic-mac methods. The basic idea of the mic-mac approach is a separation of the total energy into two parts (Strutinsky, 1967),

$$E = \bar{E} + \delta E, \quad (35)$$

$$\delta E = \sum_{\alpha} \varepsilon_{\alpha} - \int_{-\infty}^{\bar{\varepsilon}_F} d\varepsilon \sum_{\alpha} g(\varepsilon - \varepsilon_{\alpha}), \quad (36)$$

where $g(\varepsilon)$ is a Gaussian smoothing function whose width is of the order of the shell spacing. The shell-correction energy δE is an oscillating function of particle number and deformation. It is calculated from the single-particle energies ε_{α} which are obtained either from parametrized single-particle models like the modified harmonic oscillator, Woods-Saxon, or folded Yukawa potentials, or from fully self-consistent mean-field calculations. In the latter case, δE provides a useful tool for analyzing trends in SCMF models and their parametrizations; see, for example, Kleban *et al.* (2002) and Kruppa *et al.* (2000). The remaining component \bar{E} represents a smooth background energy. The idea behind the mic-mac models is to parametrize \bar{E} with high accuracy. For details of the method and typical results see Brack *et al.* (1972); Pauli (1973); Myers and Swiatecki (1974, 1982); Myers (1977); Ragnarsson *et al.* (1987); Brack (1992); Nilsson and Ragnarsson (1995); Möller *et al.* (1997), and references therein.

A direct path from the SCMF energy to the smooth energy \bar{E} is obtained by means of semiclassical approximations. The simplest one is the Thomas-Fermi approximation. The next step is the extended Thomas-Fermi method in which gradient corrections to the kinetic-energy functional are taken into account. It has been shown that the extended Thomas-Fermi energy gives a good approximation to the smooth background \bar{E} (Brack and Quentin, 1975). At the same time, the extended Thomas-Fermi method is also able to describe many local features of SCMF models (Bartel and Bencheikh, 2002). It has been exploited to approximate SCMF calculations with Skyrme interactions by adding

shell corrections (Aboussir *et al.*, 1992). This approach has allowed for the first time systematic large-scale calculations using Skyrme interactions over the whole chart of nuclei, irrespective of their deformation (Aboussir *et al.*, 1995).

There is also a large body of work concerning relativistic Thomas-Fermi and extended Thomas-Fermi methods; see, for example, Centelles *et al.* (1998), and references therein.

D. Motivation of a nuclear energy functional

As argued in Sec. I.A, a full-fledged *ab initio* treatment of finite nuclei is still beyond present-day capabilities. One employs effective interactions which are tuned for use in connection with self-consistent mean-field models. The short range of the nuclear interaction and the long wavelength of the single-nucleon states suggest an expansion in terms of zero-range interactions. This is called the density-matrix expansion and serves as a formal derivation of the ansatz for the Skyrme energy functional (Negele and Vautherin, 1972, 1975; Campi and Bouyssy, 1978). We sketch it here for the simple example of a local two-body interaction $v(\mathbf{r}-\mathbf{r}')$ using a compact notation in terms of the one-body density matrix ρ as introduced in Sec. I.B.1. We concentrate here on the spatial part and skip the spin and isospin indices, thus dealing with $\rho(\mathbf{r}_1, \mathbf{r}_2)$ to simplify the notation. Including spin and isospin is straightforward. The interaction energy contains a direct term and an exchange term,

$$E_{\text{dir}} = \frac{1}{2} \int \int d^3r d^3r' \rho(\mathbf{r}, \mathbf{r}) v(\mathbf{r}-\mathbf{r}') \rho(\mathbf{r}', \mathbf{r}'), \quad (37)$$

$$E_{\text{ex}} = \frac{1}{2} \int \int d^3r d^3r' \rho(\mathbf{r}, \mathbf{r}') v(\mathbf{r}-\mathbf{r}') \rho(\mathbf{r}', \mathbf{r}). \quad (38)$$

Handling the full one-body density matrix in the exchange term is numerically expensive. It is also to some extent unnecessary because $\rho(\mathbf{r}, \mathbf{r}')$ falls off quickly with increasing $\mathbf{r}-\mathbf{r}'$. This suggests an expansion of order $(\mathbf{r}-\mathbf{r}')^n$ of the density matrix around $\bar{\mathbf{r}} = (\mathbf{r} + \mathbf{r}')/2$,

$$\begin{aligned} \rho(\mathbf{r}, \mathbf{r}') &\approx \rho(\bar{\mathbf{r}}) i(\mathbf{r}-\mathbf{r}') \cdot \mathbf{j}(\bar{\mathbf{r}}) \\ &+ \frac{1}{2} (\mathbf{r}-\mathbf{r}')^2 \left[\tau(\bar{\mathbf{r}}) - \frac{1}{4} \Delta_{\bar{\mathbf{r}}} \rho(\bar{\mathbf{r}}) \right] \end{aligned} \quad (39)$$

with local density ρ , current \mathbf{j} , and kinetic density τ as defined in Sec. II.A.2. This yields for the square of the one-body density matrix

$$\begin{aligned} |\rho(\mathbf{r}, \mathbf{r}')|^2 &\approx \rho^2(\bar{\mathbf{r}}) - (\mathbf{r}-\mathbf{r}')^2 \left[\rho(\bar{\mathbf{r}}) \tau(\bar{\mathbf{r}}) \right. \\ &\quad \left. - \mathbf{j}^2(\bar{\mathbf{r}}) - \frac{1}{4} \rho(\bar{\mathbf{r}}) \Delta_{\bar{\mathbf{r}}} \rho(\bar{\mathbf{r}}) \right], \end{aligned} \quad (40)$$

which gives a local exchange energy-density functional

$$E_{\text{ex}} = \frac{1}{2} \int d^3r \left[V_0 \rho^2 + V_2 \left(\rho \tau - \mathbf{j}^2 - \frac{1}{4} \rho \Delta \rho \right) \right], \quad (41)$$

$$V_n = \int d^3(r-r') v(\mathbf{r}-\mathbf{r}') (\mathbf{r}-\mathbf{r}')^n. \quad (42)$$

These are precisely the terms we shall recognize later on in the Skyrme energy functional (see Sec. II.A.2). The direct term, Eq. (37), is already formulated in terms of the local density. It can be easily handled and there are models with finite-range direct terms. See, for example, the Bonche-Koonin-Negele force (Bonche *et al.*, 1976) and the relativistic mean-field models in Sec. II.A.3. Nonetheless it is consistent with the spirit of a zero-range force to expand this term as well. Using

$$\rho(\mathbf{r}) \approx \rho(\bar{\mathbf{r}}) + \frac{1}{2}(\mathbf{r}-\mathbf{r}') \cdot \nabla_{\bar{\mathbf{r}}} \rho(\bar{\mathbf{r}}) + \frac{1}{8}(\mathbf{r}-\mathbf{r}')^2 \Delta_{\bar{\mathbf{r}}} \rho(\bar{\mathbf{r}})$$

yields after a partial integration

$$E_{\text{dir}} = \frac{1}{2} \int d^3r \left(V_0 \rho^2 + \frac{1}{2} V_2 \rho \Delta \rho \right). \quad (43)$$

The term $\propto \rho \Delta \rho$ has already appeared in the exchange energy. Since it shows up here without the $\rho \tau$ term it may be parametrized independently. However, the combination $(\rho \tau - \mathbf{j}^2)$ in Eq. (41) has to be kept together. This guarantees Galilean invariance of the energy-density functional.

Altogether, this simple model shows the basic steps of a density-matrix expansion. The actual effective two-body interaction is the \mathcal{T} matrix in the nuclear medium. It can be obtained from the microscopic nucleon-nucleon force by many-body calculations like these, for example, of Brueckner-Hartree-Fock. The matrix is a density-dependent and nonlocal operator yielding the potential energy

$$E_{\text{pot}} = \frac{1}{2} \int \int \int \int dx dx' dy dy' \rho(\mathbf{x}, \mathbf{x}') \times \mathcal{T}(\mathbf{x}, \mathbf{x}'; \mathbf{y}, \mathbf{y}') \rho(\mathbf{y}, \mathbf{y}'). \quad (44)$$

An expansion similar to that above then yields all the terms as they are used in the Skyrme energy-density functional (Negele and Vautherin, 1972, 1975; Campi and Bouyssy, 1978).

The basic energy functional of the relativistic mean-field model can be motivated by a similar expansion while adjusting the concepts to a covariant formulation which is appropriate in the relativistic domain. The notion of a two-body force does not fit so well here and needs to be replaced by (effective) meson fields as mediators of the effective interaction. For a more detailed discussion see Reinhard and Maruhn (1999).

Thus far the density-matrix expansion looks straightforward. It is to be noted, however, that its quantitative success is very limited. A derivation of the parameters of the expansion from given Brueckner-Hartree-Fock calculations has provided only a fair reproduction of nuclear properties in subsequent mean-field calculations (Marcos *et al.*, 1989; Elsenhans *et al.*, 1990; Brockmann and Toki, 1992), but fails at a quantitative level. It is not yet clear to what extent this is a problem of the local-density approximation or of the Brueckner-Hartree-Fock calculations, which do not yet reproduce the

nuclear binding properties precisely enough. It is thus standard procedure to take the above density-matrix expansion as a motivation for the form of the mean-field energy functional, whose actual parameters are then adjusted phenomenologically (see Sec. V.C).

II. CHOICES FOR THE EFFECTIVE INTERACTION

Self-consistent Hartree-Fock calculations for closed-shell nuclei were first performed in the mid 1960s (Muthukrishnan and Baranger, 1965; Davies *et al.*, 1966; Kerman *et al.*, 1966; Bassichis *et al.*, 1967; Saunier and Pearson, 1967). The idea of a local-density approximation for such calculations was first explored by Negele (1970). In all these studies attempts were made to derive finite-range momentum-dependent or separable effective interactions directly from the bare nucleon-nucleon interaction. The calculations reproduced qualitatively the basic features of the nuclei, but failed on a more quantitative level. The breakthrough came when the connection to the bare nucleon-nucleon force was abandoned and effective interactions tailored for use in mean-field calculations were directly adjusted to observables of finite nuclei. The rediscovery of Skyrme's interaction by Vautherin and Vénéroni (1969) and Vautherin and Brink (1972), the introduction of the Gogny force (Gogny, 1973), and finally the formulation of the relativistic mean-field model (Walecka, 1974; Boguta and Bodmer, 1977) led to three "standard models" for the nuclear mean field which are widely used today and able to compete with the mic-mac method on a quantitative level.

A. Mean field

1. The Gogny interaction

Finite-range interactions have been introduced by Brink and Boeker (1967) in the form of the sum of two Gaussians with space-, spin-, and isospin-exchange mixtures. However such a form does not permit one to reproduce correctly the binding energies at the Hartree-Fock level of approximation. Gogny (1973, 1975) suggested adding a density dependence in the interaction and also a spin-orbit term. Dechargé and Gogny (1980) subsequently proposed a parametrization for an interaction which is now called the Gogny force:

$$\begin{aligned} \hat{v}_{\text{Gogny}}(\mathbf{r}_{12}) = & \sum_{j=1}^2 e^{-(r_{12}/\mu_j)^2} (W_j + B_j \hat{P}_\sigma - H_j \hat{P}_\tau \\ & - M_j \hat{P}_\sigma \hat{P}_\tau) + t_3 (1 + x_0 \hat{P}_\sigma) \delta(\mathbf{r}_{12}) \\ & \times \rho^\alpha \left(\frac{\mathbf{r}_1 + \mathbf{r}_2}{2} \right) + i W_{ls} (\hat{\boldsymbol{\sigma}}_1 + \hat{\boldsymbol{\sigma}}_2) \cdot \hat{\mathbf{k}}^\dagger \times \delta(\mathbf{r}_{12}) \hat{\mathbf{k}}, \end{aligned} \quad (45)$$

where $\hat{P}_\sigma = \frac{1}{2}(1 + \hat{\boldsymbol{\sigma}}_1 \cdot \hat{\boldsymbol{\sigma}}_2)$ is the spin-exchange operator, $\hat{P}_\tau = \frac{1}{2}(1 + \hat{\tau}_1 \cdot \hat{\tau}_2)$ the isospin-exchange operator, $\mathbf{r}_{12} = \mathbf{r}_1 - \mathbf{r}_2$, and $\hat{\mathbf{k}} = -(i/2)(\nabla_1 - \nabla_2)$. The quantities B_j , H_j , M_j , W_j , μ_j , t_3 , x_0 , α , and W_{ls} are parameters of the

interaction. The density-dependent zero-range force has been chosen with a spin-exchange mixture $x_0=1$ such that it does not contribute to the $T=1$ pairing channel. In this way, the usual problem of divergence of a zero-range interaction in the pairing channel is avoided, which enables one to use the Gogny interaction simultaneously in both mean-field and pairing channels. For the spin-orbit interaction the zero-range force introduced by Bell and Skyrme (1956; Skyrme, 1959b) is used.

The interaction has been adjusted with the direct Coulomb and Coulomb exchange terms calculated exactly. The energy of the spurious center-of-mass motion (see Sec. III.B.3) is subtracted from the total energy and is taken into account variationally. It has an anti-spin-orbit effect and if ignored requires a decrease in the strength of the spin-orbit interaction.

All terms are taken into account in the pairing channel, including the Coulomb contributions. The information going into the adjustment of the Gogny forces is summarized later on in Table I. Since the fit was done assuming spherical symmetry, the one-quasiparticle excitations describing odd nuclei were obtained by averaging all degenerate orbitals of a subshell. Moreover, odd nuclei are not described with the same level of accuracy as even ones are described by the HFB method. For this reason, an underestimate of 300 keV of the ground-state energy has been taken into account for odd- A nuclei. The original parametrization D1 has been readjusted by Berger *et al.* (1984, 1991) to correct for a too-large surface coefficient leading to an overestimate of the fission barrier of ^{240}Pu . Most calculations use this interaction, labeled D1S.

2. Skyrme interactions

In the Skyrme Hartree-Fock approach, the total binding energy is given by the sum of the kinetic energy, the Skyrme energy functional that models the effective interaction between nucleons, the Coulomb energy, the pair energy, and corrections for spurious motion:

$$E = E_{\text{kin}} + \int d^3r \mathcal{E}_{\text{Sk}} + E_{\text{Coul}} + E_{\text{pair}} - E_{\text{corr}}. \quad (46)$$

As the Skyrme energy functional is local, it has several technical advantages over the Gogny force. All exchange terms have the same structure as the direct terms, which greatly reduces the number of integrations when solving the Skyrme Hartree-Fock equations.

a. The Skyrme energy functional

It is useful to separate out the Skyrme energy functional as

$$\mathcal{E}_{\text{Sk}} = \sum_{T=0,1} (\mathcal{E}_T^{\text{even}} + \mathcal{E}_T^{\text{odd}}). \quad (47)$$

The time-odd part \mathcal{E}^{odd} contains all dependences on time-odd currents. They need to appear in bilinear form to render the functional time-reversal invariant. The term $\mathcal{E}^{\text{even}}$ contains only time-even densities. It is the only part which contributes in stationary calculations of

even-even nuclei. The sum runs over the isospin T . The time-even energy density is given by

$$\begin{aligned} \mathcal{E}_T^{\text{even}} = & C_T^\rho \rho_T^2 + C_T^{\Delta\rho} \rho_T \Delta\rho_T + C_T^\tau \rho_T \tau_T + C_T^J \mathbf{j}_T^2 \\ & + C_T^{\nabla J} \rho_T \nabla \cdot \mathbf{J}_T, \end{aligned} \quad (48)$$

while the time-odd part reads

$$\begin{aligned} \mathcal{E}_T^{\text{odd}} = & C_T^s \mathbf{s}_T^2 + C_T^{\Delta s} \mathbf{s}_T \cdot \Delta \mathbf{s}_T + C_T^{sT} \mathbf{s}_T \cdot \mathbf{T}_T + C_T^{\nabla s} (\nabla \cdot \mathbf{s}_T)^2 \\ & + C_T^j \mathbf{j}_T^2 + C_T^{\nabla j} \mathbf{s}_T \cdot \nabla \times \mathbf{j}_T. \end{aligned} \quad (49)$$

“Time-odd” refers to the densities $\mathcal{E}_T^{\text{odd}}$ is constructed from, not a property of $\mathcal{E}_T^{\text{odd}}$ itself, which is of course time even. In most applications, the coefficients C are taken to be constants except for C_T^ρ and C_T^s which depend on density according to the parametrization

$$C_T[\rho_0] = C_T[0] + (C_T[\rho_{0,\text{eq}}] - C_T[0]) \left(\frac{\rho_0}{\rho_{0,\text{eq}}} \right)^\alpha, \quad (50)$$

where $\rho_{0,\text{eq}}$ is the saturation density in infinite nuclear matter. For other choices see Sec. II.A.2.g below. Invariance under local gauge transformations links three pairs of time-even and time-odd terms in the energy functional

$$C_T^j = -C_T^\tau, \quad C_T^J = -C_T^{sT}, \quad C_T^{\nabla j} = +C_T^{\nabla J} \quad (51)$$

(see Dobaczewski and Dudek, 1995). This is a generalization of the Galilean invariance of the Skyrme interaction discussed by Engel *et al.* (1975).

b. Single-particle Hamiltonian

The single-particle Hamiltonian \hat{h}_q is obtained from the energy functional by using the variational principle. In what follows we now assume as is done in most applications, that protons and neutrons do not mix. For discussion of the single-particle Hamiltonian, it is simpler to recouple the isoscalar and isovector densities to proton and neutron densities. The contribution from the Skyrme interaction to the single-particle Hamiltonian for the nucleon species $q=p,n$ is then given by

$$\begin{aligned} \hat{h}_q = & U_q - \nabla \cdot B_q \nabla - \frac{i}{2} \{ \mathbb{W}_q, \nabla \sigma \} \\ & + \mathbf{S}_q \cdot \hat{\sigma} - \nabla \cdot (\hat{\sigma} \cdot \mathbf{C}_q) \nabla - \frac{i}{2} \{ \mathbf{A}_q, \nabla \}, \end{aligned} \quad (52)$$

where $\{ \mathbb{W}_q, \nabla \sigma \} = \sum_{ij} \{ W_{ij}, \nabla_i \hat{\sigma}_j \}$. The various local potentials are calculated as

$$\text{time-even: } U_q = \frac{\delta E}{\delta \rho_q}, \quad B_q = \frac{\delta E}{\delta \tau_q}, \quad \mathbb{W}_q = \frac{\delta E}{\delta \mathbb{J}_q}, \quad (53)$$

$$\text{time-odd: } \mathbf{A}_q = \frac{\delta E}{\delta \mathbf{j}_q}, \quad \mathbf{S}_q = \frac{\delta E}{\delta \mathbf{s}_q}, \quad \mathbf{C}_q = \frac{\delta E}{\delta \mathbf{T}_q}. \quad (54)$$

Here $B_q = \hbar^2/2m_q^*$ is proportional to the inverse effective mass, which in general depends on \mathbf{r} . Ground-state properties of even-even nuclei (which cover most applications of the Skyrme interaction in the published litera-

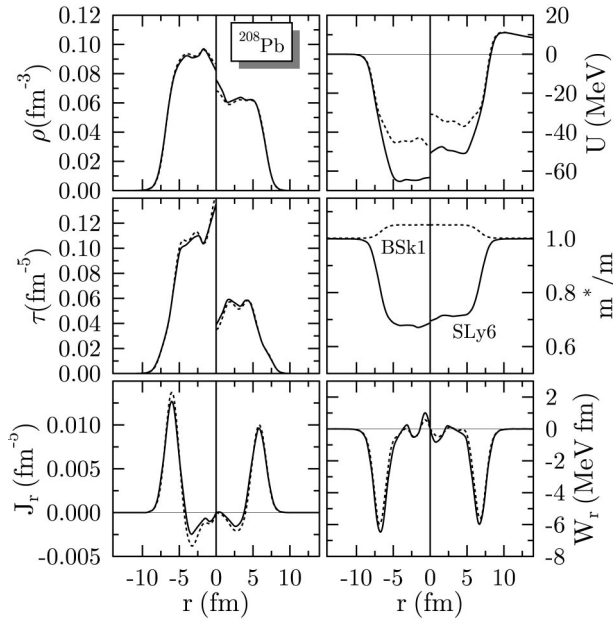


FIG. 1. Time-even densities and potentials in ^{208}Pb , for neutrons (left) and protons (right), as calculated with the Skyrme interactions: solid lines, SLy6; dotted lines, BSk1.

ture) are determined by the time-even fields B_q , U_q , and W_q only, because for these the time-odd fields vanish: $\mathbf{A}_q = \mathbf{C}_q = \mathbf{S}_q = 0$.

Figure 1 shows typical examples of the densities and potentials in ^{208}Pb . Both the spin-orbit current $J_{q,r}$ and the spin-orbit potential exhibit a peak at the nuclear surface. The densities obtained from SLy6 (Chabanat *et al.*, 1998) and BSk1 (Samyn *et al.*, 2002) are very similar, but there is a significant difference with regard to potentials. While SLy6 has a low effective mass of $m_0^*/m = 0.69$ in nuclear matter, the value for BSk1 is slightly larger than 1, leading to smaller kinetic energy. This is reflected in the depth of the potentials U_q , which are much shallower for BSk1 to obtain similar single-particle energies at the Fermi surface with both parametrizations.

c. Time-odd fields

The time-odd fields \mathbf{A}_q , \mathbf{C}_q , and \mathbf{S}_q contribute to the single-particle Hamiltonian, Eq. (52), only in situations where the intrinsic time-reversal symmetry is broken and Kramers degeneracy of single-particle levels is removed. One example is rotating nuclei where the cranking constraint $\omega \hat{J}_x$ violates time-reversal symmetry in the intrinsic frame. Other examples are odd- A and odd-odd nuclei, where the time-odd fields from the unpaired nucleon(s) induce dynamical core polarization. The time-odd fields also contribute to dynamics in time-dependent Hartree-Fock-Bogoliubov calculations and to various excitation modes calculated with the quasiparticle random-phase approximation.

d. Choices for the coupling constants

There are basically two concepts to motivate the Skyrme energy density \mathcal{E}_{Sk} :

- (i) \mathcal{E}_{Sk} is derived from the Hartree-Fock expectation value

$$\mathcal{E}_{\text{Sk}}^{\text{HF}} = \langle \text{HF} | \hat{v}_{\text{Sk}} | \text{HF} \rangle \quad (55)$$

of the zero-range momentum-dependent two-body force introduced by Skyrme (1956, 1959a),

$$\begin{aligned} \hat{v}_{\text{Sk}}(\mathbf{r}_{12}) = & t_0 (1 + x_0 \hat{P}_\sigma) \delta(\mathbf{r}_{12}) + \frac{1}{2} t_1 (1 + x_1 \hat{P}_\sigma) [\hat{\mathbf{k}}^{\dagger 2} \delta(\mathbf{r}_{12}) \\ & + \delta(\mathbf{r}_{12}) \hat{\mathbf{k}}^2] + t_2 (1 + x_2 \hat{P}_\sigma) \hat{\mathbf{k}}^\dagger \cdot \delta(\mathbf{r}_{12}) \hat{\mathbf{k}} \\ & + \frac{1}{6} t_3 (1 + x_3 \hat{P}_\sigma) \delta(\mathbf{r}_{12}) \rho^\alpha \left(\frac{\mathbf{r}_1 + \mathbf{r}_2}{2} \right) \\ & + i W_0 (\hat{\boldsymbol{\sigma}}_1 + \hat{\boldsymbol{\sigma}}_2) \cdot \hat{\mathbf{k}}^\dagger \delta(\mathbf{r}_{12}) \hat{\mathbf{k}}, \end{aligned} \quad (56)$$

with \hat{P}_σ , \mathbf{r}_{12} , and $\hat{\mathbf{k}}$ as introduced in Sec. II.A.1. Note that the $t_{0,1,2}$ terms in the Skyrme force, Eq. (56), correspond to the zero-range limit of a Gogny-type force up to second order in the derivatives (Vautherin and Brink, 1972). The calculation of the energy functional from Eq. (56) is presented by Engel *et al.* (1975); see Appendix A for the actual expressions for the coupling constants. When including pairing correlations, a strict approach calculates the energy functional from Hartree-Fock-Bogoliubov states, which then also gives a local pairing energy functional (Dobaczewski *et al.*, 1984). All Skyrme forces except SkP are well known to have unrealistic pairing properties. Therefore this strict approach is rarely followed, and only the particle-hole part of the energy functional is calculated from Eq. (55), i.e., the contributions to the pair energy are dropped.

- (ii) \mathcal{E}_{Sk} is parametrized directly without reference to an effective two-body force. The form of the Skyrme energy functional is obtained as a local-density approximation to the nuclear \mathcal{T} matrix (Negele and Vautherin, 1972, 1975); see Sec. I.D. It contains systematically all possible bilinear terms in the local densities and currents [Eq. (31)] up to second order in the derivatives, which are invariant with respect to parity, time-reversal, rotational, translational, and isospin transformations (Dobaczewski and Dudek, 1996). Some density dependence is added to the leading term in the expansion.

Choice (i) introduces many dependencies among the coupling constants, with the result that the isovector spin-orbit term and all time-odd terms are fixed. The 16 coupling constants of \mathcal{E}_{Sk} are then uniquely linked to the 10 parameters t_i , x_i , W_0 , and α of v_{Sk} (see Appendix A). These restrictions lead to some difficulties. For example, the usual parametrization of a three-body force, which was used in some early parametrizations to derive the density-dependent term, causes a spin instability in infinite nuclear matter (Chang, 1975) and finite nuclei (Stringari *et al.*, 1976), a problem which persists even in recent parametrizations (see also Sec. II.A.2.g below).

The consequences for spin-orbit splitting are discussed in Sec. II.A.2.e and the problem of tensor forces in Sec. II.A.2.f.

Choice (ii), on the other hand, is free of all these difficulties. The coupling constants of the energy functional not fixed by global symmetries are free parameters. This also nicely decouples the particle-hole and particle-particle (=pairing) channels of the effective interaction (see Fayans *et al.*, 2000). The price to be paid is that the additional coupling constants, i.e., $C_T^J = -C_T^{sT}$, C_T^s , and $C_T^{\Delta s}$, have to be adjusted to the data. Only a few applications have tried this so far. The simplest approach is to tentatively set the unknown couplings to zero, as done, for example, by Reinhard and Friedrich (1985), who include in their random-phase-approximation (RPA) calculations only those time-odd terms that are fixed by gauge invariance of the functional. Such a procedure is reasonable when describing natural parity excitations within the quasiparticle RPA, but it neglects the spin-spin terms, which are crucial for unnatural parity states. This, in turn, offers the possibility of adjusting the remaining coupling constants (see Bender, Dobaczewski, *et al.*, 2002).

e. Spin-orbit interaction

The two terms $\propto C_T^J$ and $\propto C_T^{\nabla J}$ contribute to the spin-orbit potential. For parametrizations that set $C_T^J=0$, as well as for spherical nuclei where the spin-orbit tensor \mathbf{J} always boils down to the spin-orbit current \mathbf{J} , the spin-orbit term in the single-particle Hamiltonian can be rewritten as

$$-\frac{i}{2}\{\mathbb{W}_q, \nabla\sigma\} \rightarrow -i\mathbf{W}_q \cdot \nabla \times \hat{\sigma} \quad (57)$$

where $\mathbf{W}_q = \delta E / \delta \mathbf{J}_q$ is now a local spin-orbit potential.

The Skyrme-force concept links C_T^J to the other Skyrme-force parameters, and it fixes the isospin structure of the genuine spin-orbit terms as $C_0^{\nabla J} = 3C_1^{\nabla J}$ (Bell and Skyrme, 1956; Skyrme, 1959b). The standard form of the relativistic mean-field model, as described in Sec. II.A.3, omits the exchange interactions and leads to values of $C_1^{\nabla J} \approx 0$ in the nonrelativistic limit. Lalazissis *et al.* (1994), Reinhard and Flocard (1995), and Sharma *et al.* (1995) find that this reduced isospin dependence is crucial for describing the isotopic shifts of the charge radii of Pb nuclei. The interpretation of the Skyrme interaction as an energy density functional endows the spin-orbit interaction with a more flexible isospin structure. This was exploited by Reinhard and Flocard (1995) to make two new Skyrme-type parametrizations; SkI3 and SkI4. These two forces differ from the standard Skyrme Hartree-Fock forces in the extrapolation of shell structure to exotic nuclei. Doubts about the necessity of this extension were raised by Onsi *et al.* (1997), Nayak and Pearson (1998), and Pearson (2001) for various reasons.

The spin-orbit interaction in the nonrelativistic limit of the standard relativistic mean field differs from the Skyrme energy functional not only in its isospin dependence, but also in its density dependence (see also Sec.

II.A.4). This additional degree of freedom was explored by Pearson and Farine (1994). Another form of density dependence was introduced by Pudliner *et al.* (1996). Inspired by shell-model calculations with realistic interactions for neutron drops, they introduced a density dependence to the spin-orbit term to get their Skyrme Hartree-Fock calculations for these highly speculative objects into agreement with other models, while leaving the properties of more stable nuclei nearly unchanged.

f. Tensor force

Most applications of the time-odd energy functional set $C_T^{\nabla s}=0$. The term it multiplies comes from a local two-body tensor force considered in the original papers of Skyrme (1956, 1959a) and discussed by Stancu *et al.* (1977), but omitted in all modern Skyrme parametrizations except for the SL1 force introduced by Liu *et al.* (1991). In the time-even part of the functional, a tensor force gives an additional contribution to the \mathbb{J}^2 term.

For spherical shapes, the \mathbb{J}^2 term contributes to the time-even energy density in the same way as the usually neglected tensor force. One might therefore argue that by including the tensor force one could counterbalance the unwanted \mathbb{J}^2 term exactly (Beiner *et al.*, 1975). This argument, however, applies neither to deformed shapes nor to time-odd fields. Although one might disagree with this rationale for neglecting the \mathbb{J}^2 terms, it is not easy to use C_T^J as a free parameter in the spirit of the energy-functional approach and to adjust it to spectral data. Only once in the published literature has there been an attempt to do so (Tondeur, 1983). Therefore setting $C_T^J=0$ is reasonable unless a unique way to adjust it is found. Among the forces which strictly enforce the Hartree-Fock expectation value for C_T^J are Z_σ (Friedrich and Reinhard, 1989), SkP (Dobaczewski *et al.*, 1984), the forces of Tondeur (Tondeur *et al.*, 1984), SLy5 and SLy7 (Chabanat *et al.*, 1998), and SkX (Brown, 1998). Most other parametrizations set $C_T^J=0$. The spin-tensor term also frequently triggers difficulties on the quasiparticle RPA level. Many numerical codes calculate the residual interaction strictly from Eq. (56), which violates self-consistency when employing forces with $C_T^J=0$ [see also the discussion of Bender, Dobaczewski, *et al.* (2002)].

g. Density dependence

All first-generation Skyrme interactions, like SI, SII introduced by Vautherin and Brink (1972), and SIII introduced by Beiner *et al.* (1975), use a power of density dependence $\alpha=1$, which is equivalent to a three-body delta force in the time-even functional (but not in its time-odd part). However, the power $\alpha=1$ yields too large an incompressibility K_∞ , a problem that is cured for values of α between 1/6 and 1/3 as they have been introduced, for example, with the forces SkM (Krivine *et al.*, 1980) and SkM* (Bartel *et al.*, 1982).

The simple generalization from 1 to α has been the most efficient so far. Many other generalizations have been tried, to correct this or that deficiency of the stan-

dard Skyrme functional. An alternative, in which the coupling constants also depend on the isospin density, is sometimes used (Aboussir *et al.*, 1995; Farine *et al.*, 1997). Krewald *et al.* (1977), Waroquier *et al.* (1983), and Liu *et al.* (1991) introduced additional three-body momentum-dependent forces. Waroquier *et al.* (1983) also added an admixture of the density-dependent two-body delta force and a three-body delta force. But none of these interactions has been used subsequently. Farine *et al.* (1997) add a density dependence to all momentum-dependent terms of the Skyrme force, Eq. (56). This idea was developed further by Farine *et al.* (2001) to generate a density dependence of the effective mass, enabling a good mass fit (that requires $m_0^*/m \approx 1$ at the nuclear surface) for the description of giant resonances, which call for $m_0^*/m \approx 0.8$ in the nuclear interior (Bohigas *et al.*, 1979; Chabanat *et al.*, 1997; see also Mahaux *et al.*, 1985). It is noteworthy that all generalizations of the density dependences published so far were formulated within the Hartree-Fock expectation-value approach to the Skyrme energy functional, which leads to numerous inter-relations between coupling constants and also adds density dependences in unwanted places.

h. Finite-range terms

The Skyrme Hartree-Fock method employs strictly point couplings, while the standard relativistic mean-field model has finite range through meson folding. The relativistic mean-field finite range differs from that of the Gogny force. It employs Yukawa folding (rather than Gaussian) and exchange terms are neglected. To a large extent, it plays the role of the gradient terms in the Skyrme Hartree-Fock method. Similarly, there is a variant of the Skyrme Hartree-Fock which merges the gradient term with the zero-range two-body force into a finite-range two-body coupling,

$$\int d^3r \rho_T^2(\mathbf{r}) \rightarrow \int d^3r \rho_T(\mathbf{r}) \bar{\rho}_T(\mathbf{r}), \quad (58)$$

with the folded density

$$\bar{\rho}_T(\mathbf{r}) = \int d^3r' \frac{e^{-|\mathbf{r}-\mathbf{r}'|/\mu}}{4\pi\mu^2|\mathbf{r}-\mathbf{r}'|} \rho_T(\mathbf{r}'), \quad (59)$$

where μ is a free parameter to be adjusted phenomenologically. Typical ranges of the Yukawa function are $0.3 \leq \mu \leq 0.5$ fm. The Yukawa folding, Eq. (59), has the technical advantage that it can be easily accomplished numerically by solving the Helmholtz equation $(-\Delta + \mu^2) \bar{\rho}_T(\mathbf{r}) = \mu^{-2} \rho_T(\mathbf{r})$. An early interaction constructed along these lines is the Bonche-Koonin-Negele force (Bonche *et al.*, 1976). It is a simplified version of the Skyrme functional, in which C_T^τ , $C_T^{\Delta\rho}$, C_T^J , $C_T^{\nabla J}$ and all time-odd coupling constants are set to zero. Complete Skyrme functionals with finite-range ρ_T^2 terms are used by Umar *et al.* (1989). The folded form has advantages in dynamical applications because folding smooths, while gradient terms stir up fluctuations.

i. The Fayans energy functional

The energy functional of Fayans *et al.* (2000) is constructed somewhat differently. While the Skyrme functional can be viewed as a systematic expansion in derivatives up to second order with a usually simple density dependence, the Fayans functional omits the terms containing derivatives except for the spin-orbit interaction, but employs a much more elaborate density dependence and folding for all remaining terms [including the density dependences, which prevents a mapping onto Eq. (48)]. This keeps the number of coupling constants around 10 as in the case of the Skyrme functional. No time-odd terms have been considered so far (although the functional is also used to calculate odd- A nuclei). The volume term contains a density dependence of the form $C_T^\rho[\rho] = C_T^\rho[0](1 - h_{1,T}^v \rho_0)/(1 + h_{2,T}^v \rho_0)$. As $C_T^\tau = 0$ the effective mass is everywhere $m_T^*/m = 1$. Instead of employing $C_T^{\Delta\rho} \rho_T \Delta \rho_T$ terms, the surface energy is modeled in analogy to Eq. (58), but includes a density dependence.

3. Relativistic mean-field models

Mean-field models for low-energy nuclear structure physics employing nonrelativistic kinematics are quite successful. This is at first not surprising, since the depth of the nuclear potential is below 100 MeV and much smaller than the nucleon rest mass of nearly 1 GeV. However, this depth is the result of the cancellation between much larger contributions and there are therefore good reasons to consider relativistic kinematics for the nucleon. One of the most obvious signatures of relativity is the large nuclear spin-orbit force. In a relativistic description, the spin-orbit interaction emerges naturally from the interplay between two strong and counteracting fields: a long-range attractive scalar field and a short-range repulsive vector field. These fields nearly cancel each other out in the calculation of the potential but add up for the spin-orbit interaction. Duerr (1956) had already shown by the 1950s how in a phenomenological relativistic theory the saturation properties of nuclear matter are reproduced and a spin-orbit interaction emerges naturally without any separate adjustable parameter. These properties are common to any relativistic model, although the mechanism leading to saturation or the way the spin-orbit interaction appears depend on the particular framework that is used.

Relativistic mean-field theories have been applied to nuclear matter and finite nuclei with remarkable success. The basic concept of these models is the same as for nonrelativistic mean-field approaches: the many-body state is built up as an independent particle or quasiparticle state from the single-particle wave functions, which are now four-component Dirac spinors. The motion of the nucleons is governed by the Dirac equation (Bjorken and Drell, 1964). The interaction, pointlike or through meson fields, is considered to be an effective interaction. There are several extensive reviews on the

relativistic mean-field method (see Reinhard, 1989; Serot, 1992; Ring, 1996), and we shall thus keep their presentation short.

There are many practical ways to define relativistic models for nuclear structure calculations. In nearly all cases the contribution from antiparticle states in the Fermi sea to the nucleon densities is neglected (the no-sea approximation). Another widely used approximation is the neglect of exchange (Fock) terms in the mean-field equations. The contribution of the exchange term is assumed to be absorbed into the effective coupling constants through the phenomenological fit of the model.

As in the case of nonrelativistic models, one has a choice between effective zero-range forces (point couplings) and effective finite-range interactions. In complete analogy to the Skyrme Hartree-Fock method, the single-particle potentials entering the Dirac equations of point-coupling approaches are functions of the various relativistic densities outlined in Sec. I.B.6. Much more often used, however, are finite-range models. Motivated by the idea of the nucleus as a system of interacting nucleons and mesons, the effective interaction is introduced through Klein-Gordon equations for the meson fields, which are coupled to the Dirac equations for the nucleons. These equations have to be solved self-consistently, with nucleon densities as source terms in the Klein-Gordon equations, and mesonic fields entering the Dirac equations. In finite-range models, one also has a choice in modeling the density dependence. This is done either through the nonlinearities of the meson fields, density-dependent couplings of nucleons and mesons, or a combination of both.

There is some confusion about the naming of the models. In a strict sense, all possible combinations of the above-mentioned approximations are relativistic mean-field models. Below, we shall use this label (as is often, but not always done in the literature) for the most widely used standard approach, the relativistic Hartree model with nonlinear finite-range meson fields. We shall concentrate here on this model, but give some references below to published work using other variants employing density-dependent couplings, relativistic Hartree-Fock models, and various brands of relativistic density-functional theory.

The relativistic mean-field method is usually formulated in terms of a hadronic Lagrangian. In the energy regime of nuclear structure, it may be assumed that the nucleons interact only through the exchange of the mesons with the lowest values of spin J and isospin T . Such an assumption is consistent with one-boson-exchange potentials fitted to nucleon-nucleon scattering at low energies (Erkelenz, 1974; Holinde, 1981; Machleidt *et al.*, 1987; Machleidt and Slaus, 2001). This view of the model, however, is not unique. In order to describe static nuclei, one has to specify a reference frame, and one can equally well formulate the model in terms of the corresponding energy density. This formulation makes the connection to the nonrelativistic models discussed above more apparent and will be chosen here. A detailed dis-

ussion of the Lagrangian can be found in several reviews of the relativistic mean-field method, including those of Serot and Walecka (1986), Reinhard (1989), Serot (1992), and Ring (1996).

Although the energy-functional approach relaxes the direct correspondence to hadronic physics, the fields are commonly denoted as the mesons whose quantum numbers they carry,

- σ field Φ_σ , J^π , $T=0^+$, 0, medium-range attraction;
- ω field Φ_ω^μ , $J^\pi T=1^-$, 0 short-range repulsion;
- ρ field Φ_ρ^μ , $J^\pi T=1^-$, 1, isospin channel.

The index μ is the standard index of a relativistic four-vector. There is no experimental evidence for a free σ meson, although the σ field is a crucial ingredient in relativistic mean-field models. This is a hint that we are dealing with effective fields in an effective Lagrangian. The lowest-mass and in many other respects most important π -meson field does not appear in the list. In fact, the π -meson field with $J^\pi=0^-$, $T=1$ cannot contribute on the Hartree level of standard relativistic mean-field models, because the pseudoscalar and pseudovector densities it couples to vanish for stationary states unless time-reversal invariance and parity are broken. It appears only in nuclear dynamics, or in the Hartree-Fock approximation via the exchange terms (Bouyssy *et al.*, 1987).

The standard relativistic mean-field energy functional is given by (setting $\hbar=1$ and $c=1$ as is usually done in relativistic theory)

$$E = \int d^3r \mathcal{E}_{\text{RMF}} + E_{\text{Coul}} + E_{\text{pair}} - E_{\text{cm}}, \quad (60)$$

$$\mathcal{E}_{\text{RMF}} = \mathcal{E}_{\text{nuc}} + \mathcal{E}_{\text{meson}} + \mathcal{E}_{\text{coupl}} + \mathcal{E}_{\text{nonl}}, \quad (61)$$

$$\mathcal{E}_{\text{nuc}} = \sum_{\alpha=1}^{\Omega} v_\alpha^2 \bar{\psi}_\alpha (-i \boldsymbol{\gamma} \cdot \nabla + m_B) \psi_\alpha, \quad (62)$$

$$\mathcal{E}_{\text{meson}} = \sum_{\mathcal{M}=\sigma,\omega,\rho} \frac{1}{2} \Phi_{\mathcal{M}} (-\Delta + m_{\mathcal{M}}) \Phi_{\mathcal{M}}, \quad (63)$$

$$\mathcal{E}_{\text{coupl}} = g_\sigma \Phi_\sigma \rho_{s0} + g_\omega \Phi_\omega^\mu \rho_{\mu 0} + g_\rho \Phi_\rho^\mu \rho_{\mu,1}, \quad (64)$$

$$\mathcal{E}_{\text{nonl}} = \frac{1}{3} b_2 \Phi_\sigma^3 + \frac{1}{4} b_3 \Phi_\sigma^4 + \frac{1}{4} c_3 (\Phi_{\omega,\mu} \Phi_\omega^\mu)^2, \quad (65)$$

where ρ_{sT} and $\rho_{\mu T}$ are the scalar and vector densities as introduced in Sec. I.B.6. The quantities g_σ , g_ω , g_ρ , m_σ , m_ω , m_ρ , b_2 , b_3 , and c_3 are parameters of the energy functional while the v_α^2 are BCS occupation probabilities, see Sec. I.B.4. Note that the spacelike components of the vector densities vanish for time-reversal-invariant systems. They correspond to the time-odd part of the Skyrme energy functional, while the scalar density and the zero component of the vector density correspond to the time-even part.

A functional with linear coupling terms Eq. (64) only allows us to give a qualitative description of the nuclei. However, essential nuclear properties such as incompressibility or surface properties cannot be reproduced

by such an ansatz. To do so requires nonlinear terms $\mathcal{E}_{\text{nonl}}$ which are usually parametrized as self-couplings of the meson fields. The most widely used and well-established form is a self-coupling of the σ field (Boguta and Bodmer, 1977). More recently, the self-coupling of the vector fields has been considered (Gmuca, 1992; Sugahara and Toki, 1994). The need for the latter and its particular advantage is not yet fully worked out. One ought to mention that this choice for the nonlinear form can lead to unstable conditions when solving the meson equations. A stabilized nonlinear functional has been proposed by Reinhard (1988) in connection with the parametrization PL-40.

The separation of the energy functional (61) into nucleonic and mesonic parts is not unique. In analogy to Eq. (58), the sum of the meson and coupling energy densities for each field can be rewritten as a folded bilinear term in local nucleonic densities, e.g., $\sim g_{\omega\rho\mu 0}\bar{\rho}_0^\mu$. In linear models the folding function is simply of Yukawa form [Eq. (59); see, for example, Ring (1996)], but it becomes more complicated for mesons with self-coupling.

While most applications use the standard approach outlined above, there are also numerous explorations of extensions of, or alternatives to, this model. As in the case of the Skyrme Hartree-Fock method, most of these studies are motivated by known deficiencies of the model in some particular detail. Within the standard relativistic mean-field approach, derivative (tensor) couplings of the vector fields are used by Rufa *et al.* (1988) and Bender *et al.* (1999), while Zimanyi and Moszkowski (1990) introduce derivative couplings of the scalar field.

Alternatives to nonlinear couplings in terms of density-dependent coupling constants have been suggested by several people (Brockmann and Toki, 1992; Haddad and Weigel, 1993; Ineichen *et al.*, 1996; Shen *et al.*, 1997; Cescato and Ring, 1998; Typel and Wolter, 1999). These models are often denoted as density-dependent relativistic mean-field (DDRMF) models. Relativistic Hartree-Fock models of nuclear matter and finite nuclei are described by Brockmann (1978), Blunden and Iqbal (1987), Bouyssy *et al.* (1987), Bernardos *et al.* (1993), and Von-Eiff, Haddad, and Weigel (1994). The role of the pion, which appears in the exchange term, is discussed in particular by Horowitz and Serot (1982). Relativistic density-functional theory for nuclei is analyzed by Speicher *et al.* (1991, 1993). A local-density approximation to the exchange terms in the linear relativistic mean-field model is discussed by Schmid *et al.* (1995a, 1995b). However, there is not yet a parametrization of a generalized Lagrangian that approaches the performance of the standard model.

All these models have in common finite-range meson fields. A point-coupling model, which has to be seen as the relativistic equivalent of the nonrelativistic Skyrme interaction, has been explored by Hoch and Manakos (1990), Nikolaus *et al.* (1992), Rusnak and Furnstahl

(1997), and Bürvenich, Madland, *et al.* (2002). It achieves a similar level of quality to that of the standard model.

4. Links between relativistic mean-field and Skyrme Hartree-Fock models

Like all self-consistent mean-field models, both the Skyrme Hartree-Fock (SHF) and the relativistic mean-field (RMF) schemes can be thought of as being derived from a local expansion of an underlying T matrix.

As discussed in Sec. I.D, the nonrelativistic SHF model expands the T matrix in terms of a zero-range effective force with gradient and kinetic corrections. The very involved density dependence of the T matrix is parametrized simply in terms of a power-law density dependence in the zero-range two-body interaction. The RMF method, on the other hand, parametrizes the T matrix in terms of meson fields with point coupling to the nucleons. The density dependence is described indirectly through a nonlinear self-coupling of the σ field. The spin-orbit coupling is automatically implied in the relativistic kinematics of the nucleons. At first glance, the two expansion lines, SHF and RMF, look very different. The differences are, however, not as large as one would expect. It is, in fact, possible to map the RMF model to a large extent onto the SHF model by using standard techniques of nonrelativistic expansion (Thies, 1986; Reinhard, 1989). As a first step, one eliminates the lower component of the Dirac wave functions for the nucleons. This yields the following v/c expansion for the scalar density in terms of nonrelativistic densities (isospin indices are omitted here):

$$\rho_s = \rho + \frac{1}{2m^*}(\tau - \mathbf{j}^2/\rho + \nabla \cdot \mathbf{J}). \quad (66)$$

Note that this expansion generates kinetic as well as spin-orbit terms. The zeroth component of the vector density directly becomes the normal density in the nonrelativistic limit. An independent expansion is required to map the finite range of the meson fields into a zero-range-plus-gradient correction as used in the SHF method. This can be written as an expansion of the meson propagator,

$$\frac{1}{-\Delta + m_{\mathcal{M}}^2} \simeq \frac{1}{m_{\mathcal{M}}^2} + \frac{\Delta}{m_{\mathcal{M}}^4}, \quad (67)$$

where $m_{\mathcal{M}}$ is the meson mass. This propagator is none other than the compact-operator formulation of the Yukawa folding [Eq. (59)] mentioned in connection with finite-range variants of SHF models. All together, we are dealing with a double expansion, one with respect to v/c and another one with respect to Δ/m^2 .

Now let us consider, *pars pro toto*, the scalar term in the coupling energy functional (64). After having eliminated the meson field we expand up to first order,

$$\rho_s \frac{g_\sigma^2}{m_\sigma^2 + \Delta} \rho_s \approx C_\sigma \rho^2 - \frac{C_\sigma}{m_\sigma^2} \rho \Delta \rho + \frac{C_\sigma}{2m^*} (\rho \tau - \mathbf{j}^2 + \rho \nabla \cdot \mathbf{J}), \quad (68)$$

where $C_\sigma = g_\sigma^2/m_\sigma^2$. The expansion for the vector mesons yields only the Δ/m^2 terms. These together produce precisely the same terms as are used in the SHF functional, Eqs. (48) and (49). The lowest order yields the zero-range force. The next order in Δ/m^2 yields the gradient corrections. The next order v/c yields the effective mass term and at the same time the spin-orbit force.

Thus far one can trace back the general structure of SHF terms and that of RMF ones. There are, however, differences in detail. The spin-orbit force comes mainly from the isoscalar spin-orbit current \mathbf{J}_0 while the isospin mix is different for SHF forces (Lalazissis *et al.*, 1994; Reinhard and Flocard, 1995; Sharma *et al.*, 1995). Moreover, the effective mass m^* in the denominator of Eq. (68) depends, in principle, on the density. We have thus obtained extra density dependence in kinetic and spin-orbit terms (Pearson and Farine, 1994), an effect which is absent from standard SHF models. Finally, we have already eliminated the tricky density dependence through the nonlinearity of the scalar field while eliminating the meson field at the starting point of the expansion. Density dependence is basically different for the two models. However, the differences are not appreciable for stable nuclei which all concentrate about the same equilibrium density.

The relation between RMF and SHF models is complicated by the fact that one needs a double expansion. There is an alternative to the RMF model which is formulated as nonlinear spinor theory employing zero-range coupling between the nucleonic currents (Nikolaus *et al.*, 1992). It has recently been shown that this relativistic point-coupling model performs as well as traditional SHF and RMF ones (Bürvenich, Madland, *et al.*, 2002). Such a model is then the ideal link for studying effects from the v/c and Δ/m^2 expansions separately. It has the further advantage that density dependence is mapped in a quite similar way to that in the SHF model.

5. The Coulomb interaction

The energy functionals that model the effective strong interaction have to be accompanied by an energy functional for the Coulomb interaction. The direct term of the Coulomb energy,

$$E_{\text{Coul}}^{\text{dir}} = \frac{e^2}{2} \iint d^3r d^3r' \frac{\rho_{\text{ch}}(\mathbf{r}) \rho_{\text{ch}}(\mathbf{r}')}{|\mathbf{r} - \mathbf{r}'|}, \quad (69)$$

is a functional of the local density. In most cases, the expression is simplified by employing the point proton density instead of the charge density, $\rho_{\text{ch}} \rightarrow \rho_p$. However, Tondeur *et al.* (1984; Tondeur *et al.*, 2000; Goriely *et al.*, 2001) use ρ_{ch} approximated by Gaussian folding with a finite proton size. Note that even more involved ap-

proximations are necessary to calculate the observable charge form factor; see Sec. V.A.2.

Very early SHF models and all relativistic mean-field forces employ the direct Coulomb term only. The exact Coulomb exchange term was used in the fit of the Gogny force and in subsequent spherical calculations. But it is very cumbersome to calculate, so approximations are usually invoked.

In the spirit of their local-density approximation, the exchange term is added to Skyrme interactions in the Slater approximation,

$$E_{\text{Coul}}^{\text{ex}} = -\frac{3}{4} e^2 \left(\frac{3}{\pi} \right)^{1/3} \int d^3r \rho_{\text{ch}}^{4/3}(\mathbf{r}). \quad (70)$$

The next-order term was studied by Titin-Schnaider and Quentin (1974) and found to be small. The difference between Eq. (70) and the exact Coulomb exchange term has been studied by Skalski (2001) in the framework of Skyrme interactions and by Anguiano *et al.* (2001a) in the framework of Gogny–Hartree-Fock-Bogoliubov methods. It mainly gives rise to a state-dependent shift of single-particle energies. There are hints from the study of displacement-energy systematics that the Slater exchange term has to be reduced (Brown *et al.*, 2000). The Nolen-Schiffer anomaly can be phenomenologically explained by either reducing the Coulomb exchange term or by introducing a charge-symmetry-breaking interaction. Brown (1998) considers this effect in the fit of SkX by scaling the Slater exchange term.

The Coulomb correlation energy has been studied by Bulgac and Shaginyan (1999a, 1999b). Its largest effect is in the nuclear surface, shifting single-particle energies, which affects the position of the calculated proton drip line and corrects mass differences of mirror nuclei.

There is also a contribution from the Coulomb interaction to the pairing interaction which emerges naturally when calculating the HFB expectation value of the two-body Coulomb potential. This is usually neglected. However, it was considered in the fit of Gogny forces. See Anguiano *et al.* (2001a) for a discussion.

The magnetic interaction, which gives a correction in situations with broken intrinsic time-reversal symmetry, is taken into account in some cranked relativistic Hartree-Bogoliubov calculations (Afanasjev *et al.*, 2000).

B. Pairing correlations

1. Pairing interactions

A first distinction has to be made concerning the isospin channel of pairing. As shown in Sec. I.B.5, the pairing density matrix contains contributions from $T=0$ as well as $T=1$. Pairing between like particles contributes to the $T=1$ channel only and is routinely used in mean-field calculations. Pairing between neutrons and protons contributes to both $T=1$ and $T=0$ pairing channels. Unlike like-particle $T=1$ pairing, which contributes to all nuclei, proton-neutron pairing probably plays a significant role for nuclei close to the $N=Z$ line only. It is

only recently that both pairing channels have been considered simultaneously (Terasaki *et al.*, 1998; Goodman, 1999). The complication introduced by the proton-neutron pairing interaction is that it can proceed either between states of different signatures, as for the like-particle pairing interaction, or between states of the same signature. Indeed, the latter possibility is not forbidden by the Pauli principle in this case, since the interacting particles have differing isospin. For this reason, a treatment of all the pairing channels requires breaking the signature symmetry. The study by Terasaki *et al.* (1998) has been, up to now, the only mean-field calculation (in our terminology) employing $T=0$ pairing. Here we follow the overwhelming majority of publications and consider only $T=1$ like-particle pairing correlations.

SHF and relativistic mean-field models require one to define a separate interaction to determine the pairing matrix elements. Let us recall that this is not the case for the Gogny interaction which is also well behaved for the like-particle $T=1$ pairing.

Several recent applications have shown that the use of a simple seniority interaction for the pairing is too crude [see, for example, work on superdeformed rotational bands (Terasaki *et al.*, 1995), on evolution of charge radii around magic numbers (Fayans, 1999; Fayans *et al.*, 2000; Tajima, Bonche, *et al.*, 1993), and on halo nuclei (Bertsch and Esbensen, 1991)]. Moreover, the HFB method reduces to the BCS method for a seniority interaction and the lack of localization (see Sec. I.B.2) thus makes the seniority force inappropriate for a study of nuclei that are far from stability. More sophisticated interactions have to be used. Two main ways of generalizing the seniority interaction have been investigated. In the first, the seniority interaction has been viewed as the first term of a multipole expansion of a more realistic interaction, and a quadrupole term has been added. This generalized pairing interaction has been used in mic-mac calculations (Satuła and Wyss, 1994) with a single-particle potential parametrized by a Woods-Saxon potential.

Nowadays, a widely used effective pairing interaction is a zero-range local force, often including a density dependence (Dobaczewski, Flocard, and Treiner, 1984; Krieger *et al.*, 1990; Tajima, Bonche, *et al.*, 1993; Terasaki *et al.*, 1995; Dobaczewski, Nazarewicz, Werner, *et al.*, 1996). This simple form of the interaction was introduced in the 1970s by Tondeur (1979). It is formally equivalent to a Skyrme interaction [Eq. (56)] with t_0 and t_3 terms only. A convenient way to write it as an energy functional is

$$E_{\text{pair}} = \sum_{q=p,n} \frac{V_q}{4} \int d^3r \left[1 - \left(\frac{\rho(\mathbf{r})}{\rho_c} \right)^\beta \right] \tilde{\rho}_q(\mathbf{r}) \tilde{\rho}_q^*(\mathbf{r}), \quad (71)$$

which corresponds to the density-dependent two-body pairing force,

$$v_{\text{pair}} = \frac{V_0}{2} (1 - \hat{P}_\sigma) \left[1 - \left(\frac{\rho(\mathbf{r}_1)}{\rho_c} \right)^\beta \right] \delta(\mathbf{r}_1 - \mathbf{r}_2). \quad (72)$$

Depending on the value of the switching density ρ_c , pairing is more active in the volume (“volume pairing,” $\rho_c \rightarrow \infty$) of the nucleus or on its surface (“surface pairing,” $\rho_c \approx \rho_{0,\text{eq}}$, where $\rho_{0,\text{eq}} = 0.16 \text{ fm}^{-3}$ is the saturation density of nuclear matter that approaches the density inside the nucleus). All pairing models smear out the occupation of single-particle levels close to the Fermi surface. Thus the dominant contribution often stems from the nuclear surface in coordinate space. A pure two-body force ($\rho_c = \infty$) keeps some sensitivity to the volume while a density dependence with $\rho_c \approx \rho_{0,\text{eq}}$ pushes the sensitivity towards the outer surface. A recent study by Dobaczewski, Nazarewicz, and Stoitsov (2002) seems to indicate that the density dependence is probably intermediate between these two extremes and is governed by values of ρ_c larger than the saturation density. The exponent β of the density dependence affects the appearance of neutron skins and halos (Dobaczewski, Nazarewicz, and Reinhard, 2001). It is difficult to fix using the present data. A widely used value is $\beta = 1$.

The pairing strengths $V_{p,n}$ are adjusted phenomenologically to reproduce the odd-even staggering of energies in selected chains of nuclei (see Sec. V.C). It is important to note that the strengths depend on the underlying mean-field force, particularly on its isoscalar effective mass. Low m_0^*/m produces low level density and requires larger pairing strengths. Moreover, the fits usually result in V_p slightly differently from V_n which breaks the isospin invariance of the pairing energy functional.

More complicated pairing interactions are sometimes used. Fayans (1999; Fayans *et al.*, 2000) adds several terms for density derivatives to a density-dependent interaction. A more ambitious attempt is the SkP parametrization of the Skyrme force (Dobaczewski, Flocard, and Treiner, 1984), which is specifically designed to use the same force [Eq. (56)] simultaneously in the mean-field and in the pairing channels of the HFB expectation value. In this way, the interaction is closer to the spirit of the Gogny interaction although it still requires an energy cutoff since the pairing does not converge as a function of the active space.

Significant progress has been made in the last few years (Kucharek and Ring, 1991; Ring, 1996; Serra *et al.*, 2000) in deriving a relativistic theory of pairing. An application to finite nuclei has been published just recently (Serra and Ring, 2002). In the spirit of most SHF calculations, a covariant point-coupling pairing interaction is used together with a standard relativistic mean-field force. In all other practical applications, the effective mean-field models use a nonrelativistic pairing formalism, often with the matrix elements of the Gogny force (Gonzalez-Llarena *et al.*, 1996). Note that, in other models, the pairing interaction is adjusted in conjunction with the mean-field interaction. The coupling constants of the pairing interaction depend on quantities governed by the mean field, like the density of single-particle states around the Fermi surface, which is related to the effective mass of the mean-field interaction. The consis-

tent use of a Gogny force in the pairing channel and relativistic Lagrangians has yet to be studied in detail.

2. Pairing-active space

Pairing interactions usually have strong matrix elements for very high-lying states. It is obvious that calculations using a seniority pairing interaction with constant matrix elements cannot converge at all. The same holds for zero-range interactions (Takahara *et al.*, 1994), while results using a finite-range interaction like the Gogny force converge, although very slowly, when increasing the pairing-active space of single-particle states, depending on the range of the interaction in momentum space (Grasso *et al.*, 2002). Thus, for all applications, pairing recipes need to be complemented with a prescribed cutoff. The situation is complicated by the fact that unbound single-particle states depend on the actual numerical representation, which prevents a mapping of cutoff recipes between expansion and grid methods. The box size in grid methods or the number of shells in a basis expansion adds an additional hidden cutoff to all applications (see also Sec. IV.A). In many cases, however, the choice of the actual cutoff is not too critical. The parameters of effective pairing interactions are fitted phenomenologically anyway. One simply has to do it in connection with a given cutoff. It is not clear, however, that a cutoff recipe has the same effect for all nuclei throughout the chart of nuclei.

Seniority pairing uses a band of single-particle energies around the Fermi surface. The bandwidth delivers the cutoff. Simple scaling rules allow us to tune the pairing strength to the actual bandwidth (Reinhard *et al.*, 1996).

Many recent applications consider pairing interactions as derived from zero-range forces [see Eq. (71)]. They are usually used in connection with a soft cutoff to avoid artifacts if single-particle states are crossing the cutoff line. To this end, one augments each state in the pairing-active space by a pairing weight factor w_n . The pair density, Eq. (33), is thus modified to $\bar{\rho}(\mathbf{r}) = -2\sum_{n>0} w_n u_n v_n |\psi_n(\mathbf{r})|^2$. The w_n are determined by a Fermi function in single-particle energies. This cutoff is applied either above the Fermi energy only (Bonche *et al.*, 1985; Krieger *et al.*, 1990) or above and below (Duguet *et al.*, 2001). The latter method allows us to use the same pairing strength for protons and neutrons. A fixed-width ϵ_{cut} of the Fermi function might be too rigid a recipe if one wants to cover a broad range of nuclei, particularly if one goes for exotic nuclei with their squeezed density of states. As an alternative, ϵ_{cut} might be determined in such a way that the distribution of w_n adds up to a given number of states (Bender, Rutz, *et al.*, 2000b).

A different approach has to be taken in connection with the HFB equations in the quasiparticle basis. To obtain the correct density matrices, one has to sum up from all the quasiparticle states corresponding to the bound particle states. Since these states have energies close to the depth of the potential well D , one has to set

the cutoff parameter at least as large as D , i.e., around 50 MeV (Dobaczewski, Flocard, and Treiner, 1984). This cutoff is so large that artifacts due to level crossing at the upper cutoff energy are negligible. There is, furthermore, a subtle difference between cutoff recipes in the BCS and HFB methods: they are formulated in terms of single-particle energies in BCS, but in terms of quasiparticle energies in HFB.

Let us note also that Bulgac (2002; Bulgac and Yu, 2002) has recently introduced a renormalization scheme for the HFB equations which allows us to avoid the divergence of a zero-range interaction as a function of the pairing-active space.

III. BEYOND THE STATIC MEAN-FIELD APPROACH

The static mean-field approach provides the lowest-order nuclear binding energy. It is well adapted to describing nuclear bulk properties throughout the chart of nuclei. To achieve a higher precision or to describe a larger set of data, one has to go beyond a strict mean-field approach and consider correlations. The most important correlation effects in nuclear structure stem from large-amplitude collective motion. Low-lying excited states are mixed into the calculated mean-field ground state which can be removed by configuration mixing, i.e., superposition of several mean-field states. This embraces nuclear surface vibrations related to low-lying excitation spectra and zero-energy modes (translation, rotation, etc.) related to the restoration of symmetries broken by the mean-field ground state. Both aspects will be discussed in this section. We start in Sec. III.A.1 with collective motion in general and come to the more specific case of symmetry restoration in Sec. III.B.

There are various concepts dealing with correlations. The one we follow here is the generator coordinate method, which relies on a superposition of mean-field states optimized variationally. This concept is closely related to the multiconfigurational Hartree-Fock method well known from atomic physics. There are also close links to the Monte Carlo shell model in nuclear physics, where often mean-field propagation is used to achieve appropriate importance sampling (Otsuka *et al.*, 2001). Alternative concepts are path integrals and diagrammatic methods. The path-integral methods still have links to the generator coordinate method, and both methods allow one to deal with large-amplitude collective motion. The diagrammatic techniques follow a different track. They are restricted to small amplitudes associated with collective correlations. In the regime of low-energy, relatively long-range correlations, one obtains the RPA correlations diagrammatically. For an overview and comparative discussion see Reinhard and Toepffer (1994).

There is a subtle conceptual problem when computing correlations. The energy functionals that we use are designed for SCMF calculations and supposedly embrace various correlation effects. Using them to compute correlations explicitly looks like double counting. However,

the procedure is still justified for correlations associated with low- or zero-energy states. These are strongly varying with shell effects and cannot be hidden in a smooth energy functional. Moreover they can be derived from a quasistatic sequence of mean-field states in the spirit of a Born-Oppenheimer approach. All considerations below belong to that class. The correlations from highly excited states, such as giant resonances, are in the dangerous regime of double counting. The problem is even worse for the short-range correlations.

A. Configuration mixing

1. Generator coordinate method

As has often been emphasized, collective and single-particle nuclear dynamics are intimately associated. The generator coordinate method was one of the first attempts to incorporate both seemingly contrary aspects into one single coherent quantum-mechanical formulation (Hill and Wheeler, 1953; Griffin and Wheeler, 1957). Early nuclear applications are found, for instance, in the work of Jancovici and Schiff (1964), Brink and Weiguny (1968), and Wong (1975). A review is given by Reinhard and Goeke (1987). The generator coordinate method has many attractive features. It is, formally at least, a simple and flexible variational method which extends the configuration-mixing formalism to the case of a continuous collective variable. In principle, it can address a wide range of collective phenomena. It accounts for long-range ground-state correlations and provides both excitation spectra and transition matrix elements to be compared with data. Moreover, all projection methods designed to restore broken symmetries are simply special forms of the generator coordinate method in which the weight functions are known *a priori*. The generator coordinate method has improved our understanding of the connection between phenomenological models of collective motion and microscopic descriptions such as Hartree-Fock (HF) or HF+BCS.

a. Review of the formalism

Given a family of N -body wave functions $|\Phi(q)\rangle$, depending on a collective variable q , the generator coordinate method (GCM) determines approximate eigenstates (hereafter called GCM states) of the Hamiltonian \hat{H} , having the form

$$|\Psi_k\rangle = \int dq |\Phi(q)\rangle f_k(q). \quad (73)$$

The weight functions f_k (where k is the index of the eigenstate of the Hamiltonian \hat{H}) are found by requiring that the expectation value E_k ,

$$E_k = \frac{\langle \Psi_k | \hat{H} | \Psi_k \rangle}{\langle \Psi_k | \Psi_k \rangle}, \quad (74)$$

be stationary with respect to an arbitrary variation δf_k . This prescription leads to the Hill-Wheeler integral equation (Hill and Wheeler, 1953),

$$\int dq' [\mathcal{H}(q, q') - E_k \mathcal{I}(q, q')] f_k(q') = 0, \quad (75)$$

in which the Hamiltonian kernel \mathcal{H} and the overlap kernel \mathcal{I} are defined as

$$\begin{aligned} \mathcal{H}(q, q') &= \langle \Phi(q) | \hat{H} | \Phi(q') \rangle, \\ \mathcal{I}(q, q') &= \langle \Phi(q) | \Phi(q') \rangle. \end{aligned} \quad (76)$$

In the same way, for any operator \hat{O} , we define the kernel \mathcal{O} by

$$\mathcal{O}(q, q') = \langle \Phi(q) | \hat{O} | \Phi(q') \rangle. \quad (77)$$

Since the weight functions f_k are not orthonormal, they cannot be interpreted as collective wave functions for the variable q . This role is assigned to the orthonormal set of functions g_k related to the f_k 's by the integral transform

$$g_k(q) = \int dq' \mathcal{I}^{1/2}(q, q') f_k(q'), \quad (78)$$

where $\mathcal{I}^{1/2}(q, q')$ is the Hermitean square root of the norm operator (see, for example, Reinhard and Goeke, 1987), and the matrix element of any operator \hat{O} between two GCM states can be expressed in terms of the g_k 's as

$$\langle \Psi_k | \hat{O} | \Psi_l \rangle = \int \int dq dq' g_k^*(q) \bar{\mathcal{O}}(q, q') g_l(q'), \quad (79)$$

with

$$\begin{aligned} \bar{\mathcal{O}}(q, q') &= \int \int dq'' dq''' \mathcal{I}^{1/2}(q, q'') \\ &\quad \times \mathcal{O}(q'', q''') \mathcal{I}^{1/2}(q''', q'). \end{aligned} \quad (80)$$

In particular, the GCM energies E_k and functions g_k are the eigenvalues and eigenvectors of the Hermitian integral operator with kernel $\tilde{\mathcal{H}}$,

$$\int dq' \tilde{\mathcal{H}}(q, q') g_k(q') = E_k g_k(q). \quad (81)$$

This is the starting point of the most commonly used method for solving the Hill-Wheeler equation.

In practical applications of the generator coordinate method, the family of states $|\Phi(q)\rangle$ is known for only a discrete set of values $\{q_i\}$, and Eqs. (73)–(81) transform into a discrete approximation to the GCM, where kernels become matrices and the integral equation a matrix equation.

b. Conservation of the nucleon numbers

Since the inclusion of pairing correlations is essential for a realistic description of heavy nuclei, BCS or HFB states appear as a natural choice for the GCM basis. However, such states are not eigenvectors of the nucleon number operators and have only expectation values of the operators \hat{N} and \hat{Z} equal to the neutron number N_0 and the proton number Z_0 . As a consequence, the solutions $|\Psi_k\rangle$ of the Hill-Wheeler equation (75) built from

BCS states are not eigenstates of \hat{N} and \hat{Z} . Furthermore, nothing guarantees that their average nucleon number values will be equal to N_0 and Z_0 . In fact, since the binding energy increases with the average particle number, one expects that an unconstrained variation of the weight functions f_k will generate a ground state (and first excited state) with an average number of neutrons and protons larger than N_0 and Z_0 , respectively. The correct average values of the particle numbers can be restored by means of two constraints involving the \hat{N} and \hat{Z} operators, using Lagrange multipliers λ_N and λ_Z .

c. Choice of the collective coordinate

Two families of choices can be made for the collective variable. The first category of applications of the generator coordinate method involves the restoration of broken symmetries. The family of the wave functions $|\Phi(q)\rangle$ is generated by the symmetry operations: rotation in coordinate space for angular momentum, rotation in gauge space for particle number, or parity transformation (in which case, the mixing is discrete). In these cases, the generating function $f_k(q)$ is determined *a priori* by the properties of the symmetry operator.

The second category concerns any kind of shape degree of freedom, in which case the collective space is generated by constrained mean-field calculations. The generating function is unknown and determined by diagonalization of the Hill-Wheeler equation (81). The constraint is chosen intuitively (quadrupole moment, octupole moment, cranking) in most cases. There exist systematic schemes to optimize the constraint variationally. Due to their derivation from the time-dependent mean-field approach, they are called adiabatic time-dependent Hartree-Fock (adiabatic TDHF) approaches (Baranger and Vénéroni, 1978; Goeke and Reinhard, 1978). For a review see Reinhard and Goeke (1987).

2. Gaussian overlap approximation

It is thanks to approximations of the generator coordinate method that one can make links between microscopic models based on mean-field wave functions and collective models. These approximations are based on the rapid decrease of the matrix elements between wave functions corresponding to different values of the collective variable. They have been extensively used to determine simple rotational and vibrational corrections to mean-field results.

a. Gaussian overlap kernel

In the Gaussian overlap approximation, the overlap kernel $\mathcal{I}(q, q')$, Eq. (96), is replaced by a Gaussian function of the form

$$\mathcal{I}(q, q') \approx \mathcal{I}_G(q, q') = \exp\left\{-\frac{1}{2}\left[\frac{(q-q')^2}{a(\bar{q})}\right]^2\right\}, \quad (82)$$

whose width a is in general a function of the average GCM coordinate $\bar{q} = (q + q')/2$.

b. Canonical collective variable

It is sometimes convenient to introduce another collective variable x in the Gaussian overlap approximation, defined in such a way that the overlap kernel, Eq. (82), becomes a Gaussian function with a constant width (Ring and Schuck, 1980), i.e.,

$$\mathcal{I}(q, q') \approx \mathcal{I}_G(q, q') = \exp\left\{-\frac{1}{2}[x(q) - x(q')]^2\right\}. \quad (83)$$

Both approximations, Eqs. (82) and (83), are equivalent up to terms of the fourth order in $q - q'$. The canonical variable x gives a measure of the distance between different wave functions in terms of the overlaps between them.

c. Gaussian overlap Hamiltonian kernel

Along with the quadratic approximation for the function $\log \mathcal{I}(x, x')$, Eq. (83), the Gaussian overlap approximation relies on the validity of an expansion quadratic in $(x - x')$ for the reduced Hamiltonian kernel $h(x, x')$,

$$\begin{aligned} h(x, x') &= \frac{\mathcal{H}(x, x')}{\mathcal{I}(x, x')} \approx h_G(x, x') \\ &= h_0(\bar{x}) - \frac{1}{2} h_2(\bar{x})(x - x')^2. \end{aligned} \quad (84)$$

The function $h_0(x)$ is equal to the Hartree-Fock energy along the collective path,

$$h_0(x) = h(x, x) = \mathcal{H}(x, x), \quad (85)$$

while the function $h_2(x)$ can be determined from the second derivatives of the reduced kernel (Reinhard and Goeke, 1987).

d. Collective Schrödinger equation

In the collective Schrödinger equation approximation, one introduces a collective Hamiltonian $\hat{\mathcal{H}}$ which is a second-order differential operator in the variable x :

$$\hat{\mathcal{H}} = -\frac{1}{2} \frac{d}{dx} B(x) \frac{d}{dx} + V(x). \quad (86)$$

The quantity $B(x)$ is the collective mass parameter and $V(x)$ is the collective potential energy. The collective Schrödinger equation is then written

$$\hat{\mathcal{H}} G_k = E_k G_k, \quad (87)$$

where $G(x)$ is the normalized collective wave function, i.e., $\int dx |G(x)|^2 = 1$. It is known that the collective potential $V(x)$ differs from the Hartree-Fock energy $h_0(x)$ by a quantity called the zero-point-motion correction. This should not be confused with trivial modifications of the potential term arising from a change of variable in the Schrödinger equation (87).

e. Relationship between the collective Schrödinger equation and the Gaussian overlap approximation

In most derivations which attempt a connection between the generator coordinate method and a Schrödinger equation, the Gaussian overlap approximation is introduced as an intermediate step. This is not surprising since, within the Gaussian overlap approximation, the Hill-Wheeler equation (75) is formally equivalent to the differential equation (87). A systematic study of this equivalence for one-dimensional problems has been made by Bonche *et al.* (1990a). More often, one introduces instead some approximation schemes (Girod and Gogny, 1976; Ring and Schuck, 1980; Reinhard and Goeke, 1987) based on Taylor expansions of the kernels. An alternative method based on the calculation of collective masses to the cranking approximation (Girod and Grammaticos, 1979) is frequently used to study the collective dynamics on top of potential energy surfaces calculated with the Gogny interaction (Girod *et al.*, 1989, 1992).

f. Extension of the generator coordinate method and the Gaussian overlap approximation

There are several refinements of this straightforward method. An appropriate treatment of dynamical features (associated with collective mass) is achieved by an extension to a two-parameter set of conjugate coordinates (q, p) . This allows the incorporation of a dynamical linear response and cranking masses into the approximation framework (Goeke and Reinhard, 1980).

As we have seen in the previous section, the Gaussian overlap approximation requires a collective coordinate of Cartesian-type spanning the interval $(-\infty, +\infty)$. However, there are many collective coordinates with different topology, such as the rotational angle which is defined on a unit sphere. For such cases, one can improve the performance of the approximation by properly implementing the topology of the collective coordinate into the model for the overlap (Reinhard, 1978; Gozdz *et al.*, 1985).

B. Symmetry restoration

Symmetries of the many-body state introduce relations between the single-particle wave functions, which obviously cannot be represented by a single independent-(quasi)particle state. A self-consistent mean-field wave function necessarily breaks several symmetries of the nuclear Hamiltonian. For example, translationally invariant SCMF wave functions can be constructed only from plane waves; a rotationally invari-

ant one must have spherical symmetry. As a consequence, an SCMF solution is degenerate with respect to the SCMF wave functions generated by the symmetry operation that is broken. One must superpose all these equivalent wave functions to restore the symmetry. These symmetry modes are a special case of collective motion. There is no restoring force for symmetry reasons. Thus they are associated with zero excitation energy and large-amplitude motion. Practically, they can be treated with the generator coordinate method, and the actual details are much simpler than in the general case because several features are determined by the given symmetry.

1. Particle-number projection

a. General treatment

BCS (or HFB) states are not eigenstates of the particle-number operator. They give the desired particle numbers N and Z only on average due to the constraints explained in Sec. I.B.2. Many-body states projected on good particle numbers (i.e., eigenstates of the particle-number operators \hat{Z} for protons and \hat{N} for neutrons) can be obtained from BCS or Bogoliubov wave functions with projection operators written as integrals over gauge angles,

$$\hat{P}_N = \frac{1}{2\pi} \int_0^{2\pi} d\phi_N e^{i\phi_N(\hat{N}-N)}, \quad (88)$$

where N stands here for the neutron number on which one projects. A similar expression holds for proton number Z . Altogether, one obtains an eigenstate $|\Phi(N, Z)\rangle$ of \hat{N} and \hat{Z} with N neutrons and Z protons by acting on any wave function $|\Psi\rangle$ which still spans a variety of particle numbers:

$$|\Phi(N, Z)\rangle = \hat{P}_N \hat{P}_Z |\Psi\rangle. \quad (89)$$

It can easily be checked that this operator extracts from $|\Psi\rangle$ a wave function with Z protons and N neutrons by writing the expansion of $|\Psi\rangle$ on a basis $|\Phi(N', Z')\rangle$ of wave functions with good neutron and proton numbers.

b. Variation before or after projection

Starting from an HFB wave function $|\Psi\rangle$ with mixed particle numbers, one can construct a wave function with well-defined particle numbers by acting with $\hat{P}_N \hat{P}_Z$ and calculating the resulting energy:

$$E_k = \frac{\langle \Phi(N, Z) | \hat{H} | \Phi(N, Z) \rangle}{\langle \Phi(N, Z) | \Phi(N, Z) \rangle}. \quad (90)$$

This procedure is called a projection after variation (PAV), since the HFB wave function is determined *a priori* by the resolution of the HFB equations. This is not satisfactory from a variational point of view because the PAV solution optimizes the mean field for a spread

of particle numbers, including adjacent nuclei. One optimizes, of course, the content of correct particle number by choosing $\langle \Psi | \hat{N} | \Psi \rangle = N$ and $\langle \Psi | \hat{Z} | \Psi \rangle = Z$ at least on the average, but with a nonzero dispersion $\langle \Psi | \hat{N}^2 | \Psi \rangle - N^2 > 0$. It is obviously an improvement to perform the variation of the projected HFB wave function. Such a calculation is called a variation after projection (VAP) calculation. See, for example, Egido and Ring (1982a, 1982b) and Sheikh and Ring (2000) for the general formalism and Anguiano *et al.* (2001b) for a recent application using the Gogny force. This distinction between PAV and VAP applies to any symmetry restoration discussed in this subsection.

The need for VAP is obvious in several practical applications where continuous trends with collective parameters are studied. Fast rotating nuclei are a clear example of the weakness of a mean-field description. Rotation tends to align the spin of the nucleons along the rotation axis and therefore to decrease the pairing correlations which favor pairs of nucleons with opposite spins (see, for example, de Voigt *et al.*, 1983; Szymanski, 1983; Casten, 1990). For a given angular frequency, the pairing breaks down, generating a sudden phase transition and sharp peaks in the the moment of inertia incompatible with the data. These sudden transitions are a particular feature of mean-field models, but are unrealistic in finite systems. To cure this deficiency while retaining the quality and the simplicity of a mean-field description, the best approach is VAP on correct particle number (Ring and Schuck, 1980; Anguiano *et al.*, 2001b).

c. The Lipkin-Nogami prescription

Full projection is difficult, the more so if used in connection with VAP. Thus one often employs approximate schemes for particle-number projection. A widely used scheme is the Lipkin-Nogami approach (Lipkin, 1960, 1961; Nogami, 1964; Pradhan *et al.*, 1973). The associated equations have been tested to provide a good numerical approximation of the VAP in situations where both the HFB and the BCS equations predict a collapse of the pairing correlations. [See the recent studies of model systems without rotation (Dobaczewski and Nazarewicz, 1992; Zheng *et al.*, 1992) and with rotation (Magierski *et al.*, 1993), and the references cited therein.]

The Lipkin-Nogami prescription amounts to modifying the energy E by adding the second-order Kamlah correction (Kamlah, 1968) to the energy,

$$E \rightarrow E - \lambda_2 \langle \Delta \hat{N}^2 \rangle, \quad (91)$$

where $\langle \Delta \hat{N}^2 \rangle = \langle \hat{N}^2 \rangle - \langle \hat{N} \rangle^2$. This Routhian has the same form as if a constraint on the dispersion in particle number had been introduced. However, the coefficient λ_2 is not a Lagrange multiplier, and one can show that it depends on the wave function and the Hamiltonian:

$$\lambda_2 = \frac{\langle \hat{H}(\Delta \hat{N}^2 - \langle \Delta \hat{N}^2 \rangle) \rangle - \langle \hat{H} \Delta \hat{N} \rangle \langle \Delta \hat{N}^3 \rangle / \langle \Delta \hat{N}^2 \rangle}{\langle \Delta \hat{N}^4 \rangle - \langle \Delta \hat{N}^2 \rangle^2 - \langle \Delta \hat{N}^3 \rangle^2 / \langle \Delta \hat{N}^2 \rangle}. \quad (92)$$

A consistent application of the Lipkin-Nogami prescription in connection with SCMF methods requires us to take the full effective interaction in the calculation of λ_2 (Bender, Rutz, *et al.*, 2000b; Valor *et al.*, 2000b). The modification of the HFB equations associated with the Lipkin-Nogami prescription is obtained by a restricted variation of $\lambda_2 \langle \Delta \hat{N}^2 \rangle$, namely, λ_2 is not varied although its value is calculated self-consistently using Eq. (92). For a thorough discussion of the Lipkin-Nogami method and other approximations to VAP see Flocard and Onishi (1997) and Balian *et al.* (1999).

2. Angular momentum projection

a. Principle of the method

Deformed mean-field states are not eigenstates of the total angular momentum. An eigenstate with eigenvalue J is obtained by projecting the mean-field wave function $|\Psi\rangle$:

$$|\Phi, JM\rangle = \frac{\sum_K g_K \hat{P}_{MK}^J |\Psi\rangle}{\sqrt{\sum_K |g_K|^2 \langle \Psi | \hat{P}_{KK}^J | \Psi \rangle}}, \quad (93)$$

where the projector is given by Ring and Schuck (1980):

$$\hat{P}_{MK}^J = \frac{2J+1}{8\pi^2} \int d\Omega D_{MK}^{J*}(\Omega) \hat{R}(\Omega), \quad (94)$$

where $\Omega \equiv (\alpha, \beta, \gamma)$ are the Euler angles and $\hat{R}(\Omega) \equiv e^{i\alpha \hat{J}_z} e^{i\beta \hat{J}_y} e^{i\gamma \hat{J}_z}$ is the rotation operator.

Wave functions with good angular momentum and particle numbers are obtained by restoration of symmetry on $|\Psi(q)\rangle$:

$$|\Phi, JMq\rangle = \frac{1}{\mathcal{N}} \sum_K g_K^J \hat{P}_{MK}^J \hat{P}_Z \hat{P}_N |\Psi(q)\rangle, \quad (95)$$

where \mathcal{N} is a normalization factor, \hat{P}_{MK}^J , \hat{P}_N , and \hat{P}_Z are, respectively, projectors onto angular momentum J with projection M along the laboratory z axis, neutron number N , and proton number Z . The operator \hat{P}_{MK}^J is not a projector in the mathematical sense (Ring and Schuck, 1980). It extracts from an intrinsic wave function the component with a projection K along the intrinsic z axis of the nucleus. Since K is not a good quantum number, all these components must be mixed and the coefficients g_K^J determined by a minimization of the energy.

Generalizing Eq. (76) to projected wave functions, one can define kernels for a projected generator coordinate calculation as

$$\begin{aligned} \mathcal{H}_{JM}(q, q') &= \langle \Phi JMq | \hat{H} | \Phi JMq' \rangle, \\ \mathcal{I}_{JM}(q, q') &= \langle \Phi JMq | \Phi JMq' \rangle. \end{aligned} \quad (96)$$

Since the Hamiltonian is rotationally invariant and conserves the number of particles, one has to restore the symmetries on only one of the two wave functions entering in each matrix element like Eq. (96). The kernels are obtained by integration on three Euler angles and two gauge angles of the matrix elements between rotated wave functions. There is a subtle problem with the density dependence of the interaction. It will be addressed in Sec. III.B.2.d below.

Solving the secular equation for the configuration mixing (96) amounts to a VAP in a many-body Hilbert space built on a limited set of states obtained for different values of the collective variables q' .

In the derivation above, it is assumed that the single-particle bases on which $|\Psi(q)\rangle$ and $|\Psi(q')\rangle$ are expanded are either complete or truncated in such a way that they span the same space. This property is not valid when orbitals are discretized on a three-dimensional mesh (Bonche *et al.*, 1990a) or expanded on different oscillator bases (Robledo, 1994). This problem can be solved by taking into account that the missing part of the expansion of the left states on the right basis includes empty states that do not affect the structure of the nucleus. These states are defined by the condition $v_\mu = 0$ and contribute neither to the overlap nor to the contractions (Valor, Heenen, and Bonche, 2000).

b. Calculation of multipole moments and transition probabilities

Besides the overlap and Hamiltonian kernels, restoration of rotational symmetry permits one to calculate spectroscopic quadrupole moments and transition probabilities directly in the laboratory frame of reference. Transition probabilities require the calculation of the matrix elements of a tensor of order L , \hat{T}_L^M , between projected states. Assuming axial symmetry, one has to take into account only the $K=0$ term. There are many applications using schematic interactions in reduced model spaces (see, for example, Hara *et al.*, 1982; Enami *et al.*, 2000, 2001). Recent applications for $E2$ transitions based on complete self-consistent models are those of Valor *et al.* (2000b) using Skyrme interactions and Rodriguez-Guzmán *et al.* (2000a, 2000b, 2000c, 2002) using the Gogny force. Sun *et al.* (1994) and Egido *et al.* (1992, 1996) have also applied this method for the calculation of $E3$ transition moments employing the Gogny force and collective wave functions obtained from the Gaussian overlap approximation of the generator coordinate method.

c. Density dependence of the effective interactions

The density-dependent term of the interaction must be generalized to calculate nondiagonal matrix elements. In the case of a density dependence equivalent to a three-body interaction, the Hamiltonians kernel can be expressed in terms of the mixed density (Bonche *et al.*, 1990a):

$$\rho(\mathbf{r}) = \sum_{\mu\nu\sigma} \langle a^+ b \rangle_{\mu\nu} \Phi_{l,\mu}^*(\mathbf{r}, \sigma) \Phi_{r,\nu}(\mathbf{r}, \sigma), \quad (97)$$

where the indices l (left) and r (right) refer to the mean-field single-particle states of the bra and the ket. They can correspond either to a collective variable like the quadrupole moment or to a rotation for symmetry restoration. The same dependence on the mixed density can also be chosen when there is no equivalence with a three-body interaction, i.e., for $\alpha \neq 1$ in the ansatz (50). The energy is then expressed as a functional of left and right wave functions similar to the mean-field functional. For spatial rotations, one can show that the mixed density depends only on the relative angles between the principal axes of both wave functions. Therefore, after integration on the Euler angles, the energy is real and does not depend on the orientation of the reference frame. One can thus restore symmetries on either the left or the right wave function.

d. Rotational correction as approximate projection

Applying a full angular momentum projection as described above is cumbersome. Various schemes for approximating the full projection have been proposed (see, for example, Villars, 1957; Kamlah, 1968; Scheid and Greiner, 1968; Fink *et al.*, 1972). A very simple approximation is provided by the rotational correction

$$E_{\text{rot}} = - \frac{\langle \mathbf{J}^2 \rangle}{2\mathcal{J}}, \quad (98)$$

where \mathcal{J} is the moment of inertia. This correction is employed in most deformation energy studies with the Gogny force, and also some recent studies with Skyrme forces done by Baran and Höhenberger (1995, 1996), or the recent Hartree-Fock mass formulas (Tondeur *et al.*, 2000; Goriely *et al.*, 2001; Samyn *et al.*, 2002). The recipe can be derived from Gaussian overlap approximation to rotational projection. It is valid for well-developed deformation, but fails for nuclei close to sphericity. An improved recipe can be drawn from a topologically corrected generator coordinate method; see Sec. III.A.2 and Reinhard (1978).

3. Center-of-mass projection

The mean field is localized in space. This violates translational invariance, which has to be restored by projection onto good center-of-mass momentum. And this is probably the most important case of symmetry breaking. Rotational projection is not needed for spherical nuclei. Particle-number projection is unnecessary for closed shells. But center-of-mass projection is compulsory under all conditions. It is thus desirable to develop particularly simple schemes for this case.

The projection of the mean-field state $|\Psi\rangle$ onto good center-of-mass momentum zero reads $|\Phi(\mathbf{P}_{\text{cm}}=0)\rangle = \int d^3R \exp[-(i/\hbar)\mathbf{R} \cdot \hat{\mathbf{P}}_{\text{cm}}] |\Psi\rangle$. VAP is preferable to PAV because VAP restores full Galilean invariance (Ring and Schuck, 1980). However, an exact projection is numerically expensive (Marcos *et al.*, 1983, 1984). It

turns out that the overlaps between translated wave functions fall off very quickly and that the Gaussian overlap approximation is particularly well adapted for that case. This allows us to derive a simple expression for a center-of-mass correction to the energy to second order in $\hat{\mathbf{P}}_{\text{cm}}$,

$$E_{\text{cm}} = -\frac{\langle \hat{\mathbf{P}}_{\text{cm}}^2 \rangle}{2mA}, \quad (99)$$

where $\hat{\mathbf{P}}_{\text{cm}} = \sum_k \hat{\mathbf{p}}_k$ is the sum of the single-particle momentum operators. The Gaussian overlap approximation improves with increasing mass number A . Results are fair for ^{16}O and quite good above $A \approx 40$ (Schmid and Reinhard, 1991). E_{cm} is positive and has to be subtracted from the energy functional to obtain the total binding energy. It describes the energy of states with spurious center-of-mass vibrations that are contained in the mean-field state. The same expression (99) is obtained by the introduction of “redundant coordinates” when going from the laboratory frame to center-of-mass and intrinsic coordinates; see Ring and Schuck (1980) and Dietrich (1996) for details. The center-of-mass correction decreases with A and vanishes for infinite nuclear matter. Since the total binding energy increases with A , the relative contribution of the center-of-mass correction to the total binding energy is largest for very small nuclei.

Few effective interactions have been adjusted with the center-of-mass correction [Eq. (99)] in the variational procedure, such as the Gogny forces or the Skyrme interactions SLy6 and SLy7 (Chabanat *et al.*, 1998). For Hartree-Fock states without pairing, E_{cm} contributes an additional term to the equations of motion but the Hartree-Fock equations can be solved as usual. For HFB states the mean field becomes state dependent, which complicates the solution of the mean-field equations for Skyrme forces. Therefore most applications avoid VAP or use simpler approximations.

An alternative is PAV, i.e., omitting the center-of-mass correction in the variational equations, but adding Eq. (99) *a posteriori* when calculating the binding energy. This is done, for example, for the Skyrme forces SkI1-SkI5 and the relativistic-mean field forces NL-Z, NL-Z2, PL-40, and TM2.

The simplest PAV scheme is to use a fixed formula for E_{cm} . Such a formula can be derived analytically for harmonic-oscillator states. With an oscillator constant taken from the Nilsson model, one obtains $E_{\text{cm}}^{\text{osc}} = -\frac{3}{4} 41 A^{-1/3}$ MeV. This is used for many relativistic mean-field forces like NL-SH, NL1, NL3, and TM1. Other forces in this family, like L1, use the approximation $E_{\text{cm}}^{\text{fit}} \approx -17.2 A^{-1/5}$ MeV, which is a fit to values of the full correction for selected nuclei calculated with the Skyrme interaction Z_{σ} .

An alternative that is often used for Skyrme forces is to consider the diagonal (direct) terms of Eq. (99) only. These can be expressed through the isoscalar local kinetic density τ_0 ,

$$E_{\text{cm}}^{\text{dir}} = \frac{1}{2mA} \sum_k v_k^2 p_k^2 = -\frac{\hbar^2}{2mA} \int dr \tau_0(\mathbf{r}). \quad (100)$$

The formula is usually applied with VAP. The contribution from the center-of-mass correction to the (nonrelativistic) equations of motion has the same structure as the kinetic term and leads to a renormalization of the nucleon mass $1/m \rightarrow (1/m)[1 - (1/A)]$. This scheme is used for most Skyrme interactions like SIII, SkM*, SkP, the Skyrme forces of Tondeur, and SLy4. The off-diagonal matrix elements of $\hat{\mathbf{P}}_{\text{cm}}^2$, however, have nearly the same size as the diagonal ones, but opposite sign. Therefore $E_{\text{cm}}^{\text{dir}}$ overestimates E_{cm} and exhibits an incorrect trend with respect to A . Butler *et al.* (1984) have suggested correcting for this by multiplying Eq. (100) by $f(A) = 2/(t + 1/3t)$, where $t = (\frac{3}{2}A)^{1/3}$.

When using $E_{\text{cm}}^{\text{dir}}$, $E_{\text{cm}}^{\text{osc}}$, or $E_{\text{cm}}^{\text{fit}}$ during the fit of an effective interaction, the difference between the “exact” value of Eq. (99) and the approximation is compensated by the force. This may induce in the forces an incorrect trend with respect to A which becomes visible in the nuclear matter properties. As a consequence, all forces using simple approximations for E_{cm} have significantly larger surface coefficients than those using the full correction. This leads to differences in the deformation energy which are particularly pronounced for superdeformed states and fission barriers (Bender, Rutz, *et al.*, 2000a).

When applied in VAP, Eq. (99) automatically corrects all observables. In all *a posteriori* correction schemes, a similar correction in the second order Gaussian overlap approximation needs to be applied to all other observables too. The effect on the charge density can be easily explained. The (localized) mean-field state contains spurious center-of-mass vibrations with a width $\Delta^2 r_{\text{cm}} = 1/(4\langle \hat{\mathbf{P}}_{\text{cm}}^2 \rangle) = 1/(8mA E_{\text{cm}})$. This means that the density distribution is folded by a Gaussian of that width and needs to be unfolded to access the intrinsic density [see Reinhard (1989, 1991) and Eq. (105)]. The recipe contains the center-of-mass energy which guarantees consistency with the energy correction.

C. Time-dependent mean-field approaches

1. Time-dependent Hartree-Fock (Bogoliubov)

Stationary mean-field models are tuned to describe ground-state properties, and that is what density-functional theory is designed for. The extension to a time-dependent mean-field theory is formally straightforward: a given mean-field state $|\Phi(t)\rangle$ at a certain instant of time t uniquely defines a one-body density matrix $\hat{\rho}(t)$, or generalized density matrix $\mathcal{R}(t)$, and with it the corresponding mean-field Hamiltonian (see Sec. I.B). This can be used to step to the next mean-field state by the self-consistent one-body Schrödinger equation,

$$i\hbar \frac{\partial}{\partial t} |\Phi(t)\rangle = \hat{\mathcal{H}}(t) |\Phi(t)\rangle. \quad (101)$$

The solution of this equation conserves the energy E if it is evaluated with the same expression from which $\hat{\mathcal{H}}$ was derived. This scheme is called time-dependent density-functional theory (TDDFT) in the realm of electronic density functionals (Runge and Gross, 1984). In nuclear dynamics, it is known as time-dependent Hartree-Fock (TDHF), or TDHFB in the case of pairing. The *ab initio* foundation of TDDFT is still a matter of debate (Gross *et al.*, 1994). Nonetheless, its practitioners are using it heavily for a large variety of applications. See, for example, Onida *et al.* (2002) or Calvayrac *et al.* (2000) for examples from metallic clusters. Similarly, there are applications of TDHF in nuclear and heavy-ion dynamics. See, for example, Kerman (1977), Negele (1982), and Abe *et al.* (1996) for discussions of general aspects of TDHF, Davies *et al.* (1985) for TDHF with Skyrme forces, and Cusson, Reinhard, Molitoris, *et al.* (1985) and Vretenar *et al.* (1993) for dynamics with the relativistic mean-field method. A thorough discussion of these large-scale applications goes beyond the scope of this review. We consider here limiting cases which allow us to compute nuclear excitation properties. The low-energy regime of surface vibrations and fission is reached by adiabatic TDHF (Baranger and Vénéroni, 1978). It is closely related to the generator coordinate method and the microscopic derivation of a Bohr Hamiltonian (Goeke and Reinhard, 1978; Reinhard and Goeke, 1987), which was discussed in Secs. III.A.1 and III.A.2. The other important limiting case is small-amplitude motion which accesses the regime of the nuclear giant resonances. It will be discussed in the next section. For more details about the various approaches, see Ripka and Porneuf (1975), Quentin and Flocard (1978), Goeke and Reinhard (1982), Balian and Vénéroni (1986, 1988, 1991), and Flocard (1989).

2. Quasiparticle random-phase approximation

The starting point for deriving the quasiparticle random-phase approximation (quasiparticle RPA) is the TDHFB equation (101). One considers small oscillations about the stationary mean-field ground state $|\Psi\rangle$. These are necessarily harmonic oscillations. The wave function $|\Phi_k\rangle$ of the excited states k can then be written in the form

$$|\Phi_k\rangle = (1 + \eta e^{-i\hbar\omega_k t} \hat{C}_k^+) |\Psi\rangle, \quad (102)$$

where \hat{C}_k^+ creates a superposition of two-quasiparticle states (one-particle/one-hole states in the case of TDHF) on top of the mean-field ground state $|\Psi\rangle$. The eigenfrequency of the eigenmode k is ω_k , while η is a small number. Inserting this ansatz into Eq. (101) and expanding up to order η^1 yields (Reinhard and Gambhir, 1992)

$$\hbar\omega_k \hat{C}_k^+ |\Psi\rangle = \left([\hat{\mathcal{H}}, \hat{C}_k^+] + \text{tr} \left\{ \frac{\delta \hat{\mathcal{H}}}{\delta \hat{\mathcal{R}}} [\hat{C}_k^+, \hat{\mathcal{R}}_\Psi] \right\} \right) |\Psi\rangle, \quad (103)$$

where $\hat{\mathcal{H}}$ is the HFB Hamiltonian, Eq. (12), $\hat{\mathcal{R}}_\Psi$ the generalized density matrix, Eq. (8c), corresponding to the mean-field ground state, and the trace is taken over $\partial/\partial \hat{\mathcal{R}}$ and the commutator. In case of TDHF without pairing, one has to replace $\hat{\mathcal{H}}$ by \hat{h} and $\hat{\mathcal{R}}$ by $\hat{\rho}$. The commutators in Eq. (103) select those two-quasiparticle or one-particle/one-hole states that contribute to a given excitation mode. The contribution from the effective interaction to the quasiparticle RPA equation, i.e., $\delta \hat{\mathcal{H}}/\delta \hat{\mathcal{R}}$ in the last term in Eq. (103), is usually called the residual interaction and determines the properties of the excited states. As $\hat{\mathcal{H}} = \delta \mathcal{E}/\delta \hat{\mathcal{R}}$, Eq. (12), this boils down to a second derivative of the energy functional (see, for example, Bertsch and Tsai, 1975; Reinhard, 1992b). Equation (103) is an eigenvalue equation for the mode k . This linearized TDDFT is called the random-phase approximation (RPA) due to its first derivation with diagrammatic techniques (Bohm and Pines, 1953). The RPA is the basic theory of nuclear excitations in the regime of giant resonances. There is a large body of literature on this topic and there exist many different notations for the RPA equations and techniques to solve them. See, for example, Rowe (1970), Bertsch and Tsai (1975), Ring and Schuck (1980), and Bertsch and Broglia (1994). We have chosen here the equations-of-motion technique of Rowe (1970), which provides the most compact formulation. The form is also suggestive as it resembles the commutator algebra of coupled harmonic oscillators. Further details about an actual numerical implementation of RPA in nuclei can be found in the articles of Bertsch (1991), Reinhard (1992b), and Reinhard and Gambhir (1992) or in the above-mentioned books. The generalization of the RPA which includes pairing, i.e., the quasiparticle RPA, has been much less often used. For recent examples see Engel *et al.* (1999), Auerbach *et al.* (2001), Hagino and Sagawa (2001), and Matsuo (2001).

One should take into account that the excitation energies of giant resonances reach the particle continuum. But most RPA calculations ignore that and discretize the continuum. There also exist schemes in which the continuum is treated correctly; see, for example, Shlomo and Bertsch (1975) and Cavinato *et al.* (1982).

The RPA calculations are usually very involved due to the large one-particle/one-hole spaces required. In the end, one is interested mostly in a few key data such as the peak position of a giant resonance. Thus there exist several approaches to simplifying RPA calculations for delivering just these few key quantities. A first step is a reduction to a fluid dynamics formulation in terms of local densities and currents. See, for example, Bertsch and Stricker (1976), Holzwarth and Eckart (1978), Stringari (1983), and Gleissl *et al.* (1990). Even simpler and sufficient for first surveys are sum-rule approaches (for a review, see Bohigas *et al.*, 1979).

There is an intriguing conceptual problem in connection with energy functionals. RPA tacitly assumes requantization of linearized TDHF and this requantization generates RPA correlations in the underlying

ground state; see, for example, Ring and Schuck (1980). On the other hand, the energy functional was constructed to incorporate the correlations already. Recomputation of the RPA correlation would mean double counting them. Moreover, the zero-range nature of the Skyrme force (and the short range of relativistic mean-field and Gogny forces) is badly tuned to that task. The correlation effects become very large and sometimes even diverge when computed in unlimited configuration space. Reasonably sized and pertinent correlations for radii have been obtained in RPA calculations using limited spaces of one-particle/one-hole states (Reinhard and Drechsel, 1979; Barranco and Broglia, 1985; Reinhard and Friedrich, 1985). The usual practice, however, is to ignore the RPA correlations (because they are supposed to be contained in the energy functional) and to consider only RPA excitations.

IV. TECHNICALITIES

A. Representations

The practical solution of the mean-field equations starts with an appropriate numerical representation of single-particle wave functions, densities, and fields. Two different schemes are used: basis expansions and grid techniques. Basis expansions usually employ harmonic-oscillator wave functions, for which there are powerful analytical methods to compute all conceivable matrix elements (Wong, 1970). For a recent detailed example of an application see Dobaczewski and Dudek (2000). The advantage of this scheme is that basis states are pre-sorted according to their approximate energy. This yields a compact representation. The technique is particularly advantageous if the nonlocal exchange operator is taken explicitly into account as is done for the Gogny force (Girod and Grammaticos, 1983). The disadvantage is that the oscillator basis is composed of tightly bound states which asymptotically decrease too rapidly. The expansion thus becomes very slowly converging if one has to describe weakly bound states or even continuum states, as is required for exotic nuclei. It is also very expensive to accommodate the extreme shapes which occur during fission. There are attempts to cure these defects. For example, a transformed oscillator basis can be tailored to accommodate the proper asymptotic behavior of the density (see Stoitsov *et al.*, 1998 for relativistic mean-field methods and Stoitsov *et al.*, 2000 for Skyrme Hartree-Fock applications). However, this generates a density-dependent basis.

The alternative to basis expansions are grid techniques in which the wave functions and fields are represented on a grid in coordinate space. Depending on the symmetry, this can be a radial 1D, an axial 2D, or a Cartesian 3D grid. The saturation properties of nuclear matter allow the use of equidistant grid points, which are particularly simple to handle. Coordinate-space grids are well suited for self-consistent mean-field models which employ local densities. The densities and potentials are given immediately on the grid without the need

to compute overlap matrix elements. This makes the coding simple and intuitive. Less simple is the representation of the kinetic energy. Various approximations can be chosen here: Fourier representation or finite-difference formulas at various orders. The Fourier technique is best suited to Cartesian 3D grids, where the fast Fourier transformation can be exploited either directly or via resummation in coordinate space (Baye and Heenen, 1986). It always yields the best possible approximation to momentum and the kinetic-energy operator. Finite differences exist at various orders of approximation. The optimum choice depends on the dimensionality. Higher orders are more efficient in 3D (Bonche *et al.*, 1985), while lower orders are preferable for 1D radial problems. For a discussion see Blum *et al.* (1992), and Reinhard (1991) for a detailed 1D Skyrme Hartree-Fock code. A further alternative for computing the kinetic energy is a representation using basis splines (Kegley *et al.*, 1996). This technique is advantageous in connection with nonequidistant grids and involved boundary conditions, of which finite elements are a special case. For an example in the relativistic mean-field model see Pöschl, Vretenar, and Ring (1997).

B. Algorithms

The actual solution of self-consistent mean-field equations can only proceed iteratively. Older schemes solve the mean-field equations for given potentials by diagonalization and update the mean-field potentials according to the new densities from the new wave functions. More efficient are direct iteration schemes. The simplest scheme is the gradient step downhill in the energy landscape of the Hilbert space of the single-particle wave functions. There are various options to improve the speed of this scheme: energy-selective step size (equivalent to preconditioning in numerical analysis; Reinhard and Cusson, 1982; Blum *et al.*, 1992) or the conjugate gradient step (Egido *et al.*, 1995).

Gradient techniques are not immediately applicable to the relativistic mean-field models because the solutions would search the minimum energy in the (forbidden) Fermi-sea states. A stable iteration can be achieved by mapping the Dirac equation onto an effective Schrödinger equation for the upper component of the Dirac wave function (Reinhard, 1989).

The HFB equation can be solved in any of the three bases introduced in Sec. I.B.2. Most codes proceed in the quasiparticle basis (see, for example, Dobaczewski *et al.*, 1984). A scheme well adapted to 3D grid techniques and to the use of different interactions in the mean-field and pairing channels relies on the use of a double basis, the Hartree-Fock and the canonical bases (Gall *et al.*, 1994; Terasaki *et al.*, 1996). An alternative choice is a basis composed of the natural orbitals, which is very efficient (Mühlhans *et al.*, 1984; Reinhard *et al.*, 1997) but requires a careful tuning of the iteration scheme (Tajima, 2000).

A particular problem is the computation of the long-range Coulomb potential. The issue is usually attacked

by solving the Poisson equation with similar iterative techniques to those mentioned above. Special care has to be taken in dealing with the long-range part. See, for example, Maruhn *et al.* (1976) and Lauritsch and Reinhard (1994). In the case of an oscillator expansion the Coulomb potential can be mapped onto a sum of Gaussian potentials, which is then solved with the standard techniques of the basis expansion.

Constraints also require special consideration. Constraints may drive the system towards an unstable solution as, for example, in the calculation of a fission barrier where the potential-energy surface has negative curvature. Such unstable (but physically interesting) regimes can be stabilized by iterative techniques (Cusson, Reinhard, Strayer, *et al.*, 1985). An alternative is to use a quadratic constraint (see Sec. I.B.3), which stabilizes any solution. No problem of that sort exists for cranking constraints, which still aim at a stable minimum in the cranked potential landscape. Additionally, constraints on multipole moments have to be damped at large distances, as there is always one direction in which the contribution from the constraint to the single-particle potential becomes negative as $r \rightarrow \infty$; see, for example, Rutz *et al.* (1995).

Further considerations must be taken into account for dynamical mean-field calculations. Various propagation techniques are used for full TDHF, and a large variety of solution schemes exist for RPA. We do not discuss them here because dynamics is not the main topic of this review.

V. PARAMETRIZATIONS

A. Observables

We present in this subsection the most prominent observables that are closely related to mean-field models, the bulk properties of finite nuclei, such as energy and density distribution, and the key features of nuclear matter. Both are used as phenomenological input to adjust effective forces, and the basic properties of the models are discussed in terms of these observables. Observables for pairing are a bit more involved and will be discussed separately in Sec. V.B. Other observables will be introduced as necessary in Sec. VI where results are discussed.

1. Energies

The total binding energy of a nucleus is the most immediate observable in self-consistent mean-field models. It is naturally provided by the numerical solution of the mean-field equations, but has to be complemented by corrections for spurious motion.

The single-particle energies ϵ_k are given by diagonalization of the single-particle Hamiltonian \hat{h} . However, their interpretation is not trivial. This will be discussed in Sec. VI.B.1.

2. Charge form factor and radii

The nuclear charge density is a useful observable for analyzing nuclear structure. It provides information about the nuclear shape and is determined by elastic electron scattering (Friedrich and Vögler, 1982). In order to compute the charge density from mean-field results, one has to take into account that the nucleons themselves have an intrinsic electromagnetic structure (Friar and Negele, 1975). Thus one needs to fold the proton and neutron densities in with the intrinsic charge density of the nucleons. We discuss this here in detail for the case of Skyrme Hartree-Fock methods. Folding becomes a simple product in Fourier space, i.e., in terms of form factors,

$$F_q(\mathbf{k}) = \int d^3r e^{i\mathbf{k}\cdot\mathbf{r}} \rho_q(\mathbf{r}), \quad (104)$$

where again $q \in \{p, n\}$. In fact, the form factor is closer to experiment than the charge density because it represents directly in Born approximation the amplitude for scattering at momentum transfer $\hbar\mathbf{k}$. It depends only on $k = |\mathbf{k}|$ for spherical systems, which we shall assume for what follows. The charge form factor is composed as

$$F_{\text{ch}}(k) = \sum_q (F_q G_{E,q} + F_{ls,q} G_M) \exp\left(\frac{\hbar^2 k^2}{8\langle \hat{\mathbf{P}}_{\text{cm}}^2 \rangle}\right), \quad (105)$$

where $F_{ls,q}$ is the form factor of $\nabla \cdot \mathbf{J}_q$ augmented by a factor $\mu_q/(4m^2)$, with μ_q being the magnetic moment of the nucleon. $G_{E,q}$ is the electric form factor, and G_M the magnetic form factor of the nucleons (assumed to be equal for both species). The exponential factor takes into account an unfolding of the spurious vibrations of the nuclear center of mass in harmonic approximation (see Sec. III.B.3). The nucleon form factors are taken from nucleon scattering data. For details see Appendix B.

Most of the information contained in the form factor at low momentum can be described by three parameters, the root-mean-square radius r_{rms} ,

$$r_{\text{rms}} = \sqrt{-\frac{3}{F_{\text{ch}}(0)} \lim_{k \rightarrow 0} \frac{d^2}{dk^2} F_{\text{ch}}(k)}, \quad (106)$$

the (first) diffraction radius,

$$R = \frac{4.493}{k_0^{(1)}}, \quad (107)$$

which is determined from the first zero of the form factor $F_{\text{ch}}(k_0^{(1)}) = 0$, and the surface thickness,

$$\sigma = \frac{2}{k_m} \ln\left(\frac{F_{\text{box}}(k_m)}{F_{\text{ch}}(k_m)}\right). \quad (108)$$

See Friedrich and Vögler (1982) for more details. The diffraction radius parametrizes the overall diffraction pattern, which is similar to that of a sphere of radius R . This is the so-called ‘‘box equivalent’’ radius. The actual nuclear form factor decreases faster than the box form factor F_{box} ,

$$F_{\text{box}}(k) = 3 \frac{j_1(k_m R)}{k_m R} \quad \text{with } k_m = 5.6/R \quad (109)$$

due to the finite surface thickness of nuclei, where j_1 is the spherical Bessel function. The Helm model assumes that the nuclear surface is obtained by folding the box distribution with a Gaussian, $\exp(-\frac{1}{2}q^2\sigma^2)$ (Helm, 1956). It allows us to determine the surface parameter σ by comparing the height of the first maximum of the box equivalent form factor and of the mean-field result F_{ch} . The Helm model establishes a fixed relation between these three key parameters of the nuclear charge distribution: $r_{\text{rms}}^2 = \frac{3}{5}R^2 + 3\sigma^2$. Deviations from the model appear mostly in the outer nuclear surface. This suggests the introduction of a nuclear halo parameter $\sqrt{\frac{3}{5}R^2 + 3\sigma^2} - r_{\text{rms}}$ which is found to be a relevant measure of the outer surface diffuseness (Mizutori *et al.*, 2000).

The calculation of the charge rms radius from the full charge form factor is very cumbersome for deformed nuclei. A simple approximation is provided by Bertozzi *et al.* (1972) and Chabanat *et al.* (1997):

$$r_{\text{rms}}^2 = \langle r^2 \rangle_p + r_p^2 + \frac{N}{Z} r_n^2 + \frac{1}{Z} \frac{\hbar}{mc} \sum_n v_n^2 \mu_{q,n} (\hat{\sigma} \cdot \hat{\ell})_n, \quad (110)$$

where $\langle r^2 \rangle_p$ is the mean-square radius of the point-proton distribution, and $r_p^2 = 0.74 \text{ fm}^2$ and $r_n^2 = -0.117 \text{ fm}^2$ are the charge mean-square radii of the free proton and neutron, respectively. The last term gives the contribution from the spin-orbit charge distribution, where $\mu_{q,n}$ is the magneton moment for the nucleon species of a given single-particle state n . Many applications simplify this further by considering the first two terms only and then using $r_p^2 = 0.64 \text{ fm}^2$.

A related quantity that is directly accessible by experiment and sometimes used in model fitting is the isotopic shift of charge mean-square radii $\delta r_{ms}(Z) = r_{\text{rms}}^2(Z) - r_{\text{rms}}^2(Z_0)$, i.e., the change of the mean-square radius relative to a reference nucleus with charge number Z_0 .

The charge distribution is mostly sensitive to the proton distribution. Useful complementary information is contained in the neutron distribution which, however, is not directly accessible in experiment. It couples predominantly to the strong interaction. Thus all sorts of medium corrections need to be taken into account (Batty *et al.*, 1989). One usually ends up with information on the neutron mean-square radius $\langle r^2 \rangle_n$. It can be easily computed theoretically from a given neutron distribution.

3. Nuclear matter

a. Infinite nuclear matter

Homogeneous infinite nuclear matter (INM) is a widely used model system for studying and characterizing effective interactions. It describes the leading contributions (volume terms) to nuclear properties, which are considered as useful pseudo-observables sometimes

used to adjust the parameters of effective interactions. The actual values of INM properties are given in Table III below. Most studies deal with the simplest case of symmetric INM where all densities of neutrons and protons with spin up and down are the same, i.e., $\rho_1 = \mathbf{s}_0 = \mathbf{s}_1 = 0$. The isoscalar density ρ_0 is then the only remaining degree of freedom. More general systems are asymmetric ($\rho_1 \neq 0$), polarized ($\mathbf{s}_0 \neq 0$), and spin-isospin polarized ($\mathbf{s}_1 \neq 0$) matter. The isotropy of polarized nuclear matter is broken, which leads to an axially deformed Fermi surface (Haensel and Dąbrowski, 1975; Dąbrowski and Haensel, 1976). A very detailed discussion of asymmetric INM in the Skyrme Hartree-Fock method is given by Chabanat *et al.* (1997). Infinite nuclear matter properties at large asymmetry are key ingredients for the description of neutron stars. See, for example, Haensel *et al.* (1989) and Chabanat *et al.* (1997) for a discussion at the mean-field level. A stability criterion for spin-isospin polarized neutron matter, derived by Kutschera and Wójcik (1994), has even been used by Chabanat *et al.* (1997, 1998) to constrain the parameters of the SLy x forces. Most works on polarized INM rely on the interpretation of the Skyrme functional as the Hartree-Fock expectation value of a two-body force. The more general energy-functional approach permits us to relax many dependencies among the properties of polarized and unpolarized INM; see Bender, Dobaczewski, *et al.* (2002).

The energy per particle $E/A = \mathcal{E}/\rho_0$, often called the equation of state, has its minimum $(E/A)_{\text{eq}} \approx -16 \text{ MeV}$ at saturation density $\rho_{0,\text{eq}} \approx 0.16 \text{ fm}^{-3}$. Further INM properties are connected to basic features of the excitations of finite nuclei. The incompressibility at the saturation point K_∞ is given by

$$K_\infty = 9 \rho_0^2 \left. \frac{\delta^2 \mathcal{E}}{\delta \rho_0^2 \rho_0} \right|_{\rho_{0,\text{eq}}}. \quad (111)$$

It corresponds to the curvature at the minimum and is related to breathing modes like the giant monopole resonance (Blaizot, 1980). From the theoretical side, K_∞ is determined by the density dependence of the effective interaction (Blaizot *et al.*, 1995; Friedrich and Reinhard, 1986; Chabanat *et al.*, 1997, 1998). An analysis of the breathing mode data has to take into account the interplay of the incompressibility with the surface and symmetry energy (Yoshida *et al.*, 1998) and with anharmonicity effects (Stocker and Chossy, 1998); see also Blaizot *et al.* (1995).

The symmetry energy coefficient is related to the isovector curvature at the saturation point by

$$a_{\text{sym}} = \frac{1}{2} \left. \frac{\delta^2 \mathcal{E}}{\delta \rho_1^2 \rho_0} \right|_{\rho_{0,\text{eq}}}. \quad (112)$$

Isoscalar and isovector effective masses are calculated from the single-particle energies ε_k in INM as $m^*(k) = k/(\partial_k \varepsilon)$. This yields, for nonrelativistic models,

$$\frac{\hbar^2}{2m_T^*} = \frac{\hbar^2}{2m} + \left. \frac{\delta \mathcal{E}}{\delta \tau_T \rho_0} \right|_{\rho_{0,\text{eq}}}, \quad (113)$$

and for relativistic models

$$m_T^* = \sqrt{(m + S_T)^2 + \hbar^2 k^2}, \quad (114)$$

with S_T denoting the scalar mean field. Note that m^* still depends on k in relativistic models. One usually refers to the value at $k=0$, while physically more relevant is the value at the Fermi surface k_F . Skyrme Hartree-Fock mass fits require isoscalar effective masses around $m_0^*/m \approx 1$, while giant isoscalar quadrupole resonances call for $m_0^*/m \approx 0.8$ (Bohigas *et al.*, 1979; Chabanat *et al.*, 1997). This conflict cannot be resolved within the standard energy functionals, but may possibly be resolved with the help of generalized density dependencies (Farine *et al.*, 1997, 2001).

The isovector effective mass is usually expressed as the enhancement factor of the Thomas-Reiche-Kuhn sum rule (Ring and Schuck, 1980), which reads

$$\kappa_{\text{TRK}} = \frac{m}{m_0^*} + \frac{1}{2} \frac{\delta}{\delta \rho_1} \frac{m}{m^*} \Big|_{\rho_{0,\text{eq}}} - 1 = \frac{m}{m_1^*} - 1, \quad (115)$$

where m_T^* are isoscalar and isovector effective masses in symmetric INM. This equation relates m_1^*/m to the isovector dipole giant resonance, but of course it also plays a role for ground-state properties. See the recent attempt by Pearson and Goriely (2001) to extract its value from a Skyrme Hartree-Fock mass fit. It has to be stressed that the meaning of the effective mass is slightly different in relativistic and nonrelativistic models (Mahaux *et al.*, 1985; Jaminon and Mahaux, 1990). The effective mass in the Dirac equation depends on momentum and cannot be simply identified with the nonrelativistic effective mass.

The present form of the effective interaction sometimes leads to strong dependencies between nuclear matter properties. See, for example, the analysis of the correlation between $\rho_{0,\text{eq}}$ and K_∞ by Tondeur *et al.* (1986) and of correlations between K_∞ , m_0^* , and the exponent α of the density dependence of the Skyrme interaction (Chabanat *et al.*, 1997). This and other deficiencies may be cured by generalized density dependencies, for which, however, conclusive answers have yet to come.

b. Semi-infinite nuclear matter

Surface properties can be studied in semi-infinite nuclear matter (SINM). This is not as trivial to compute as INM, because the density profile of the surface depends on the effective interaction. There are a few fully self-consistent calculations. See, for example that of Köhler (1976) using Skyrme interactions, Cote and Pearson (1978) for the Gogny force, and Von-Eiff, Stocker, *et al.* (1994) for the relativistic mean-field model. Most calculations invoke the simpler extended Thomas-Fermi approximation (Brack *et al.*, 1985), in which a semiclassical approximation for the energy is minimized with respect to a parametrization of the density profile. See Von-Eiff, Pearson, *et al.* (1994) for relativistic mean-field studies, and Centelles *et al.* (1998) for a comparison of

Skyrme Hartree-Fock and relativistic mean-field models for asymmetric SINM. Important SINM properties are the surface and surface asymmetry coefficients and the surface thickness. Note that values obtained from the extended Thomas-Fermi method differ significantly from those calculated self-consistently. While the latter quantify the actual mean-field models, the former are safer to compare with values from mic-mac models.

c. Relation to liquid-drop models

Nuclear matter properties are usually identified with the coefficients of the liquid-drop model, although the connection is not trivial (see, for example, Satpathy *et al.*, 1999). In its simplest form, the binding energy is given as

$$E_{\text{LDM}} = a_{\text{vol}}(1 + \kappa_{\text{vol}}I^2)A + a_{\text{surf}}(1 + \kappa_{\text{surf}}I^2)A^{2/3} + E_{\text{Coul}} + E_{\text{Pair}} + \dots \quad (116)$$

Refinements to the droplet model also take compressibility effects into account (Myers and Swiatecki, 1974; Myers, 1977). Modern versions include many corrections, such as finite-range effects on the surface term (Möller *et al.*, 1995). Often one identifies

$$a_{\text{vol}} = (E/A)_{\text{eq}}, \quad a_{\text{sym}} = a_{\text{vol}}\kappa_{\text{vol}}, \quad (117)$$

although a more consistent comparison with self-consistent models also requires droplet corrections to Eq. (116).

4. Stability

The variational principle guarantees that solution of an unconstrained mean-field calculation is an extremum for given symmetries, but it still might be a saddle point. The stability of a calculated state has to be checked *a posteriori*. This can be done by looking at the RPA excitations. A mean-field state is unstable as soon as one finds an imaginary excitation energy.

Sometimes such instabilities are even properties of the parametrization of the SCMF interactions. A first and simple check can be made for nuclear matter in terms of the Landau-Migdal parameters, which characterize the strength of the residual interaction for the basic excitation channels of INM. See Henning and Manakos (1987) for the relativistic mean-field method, Ventura *et al.* (1994) for Gogny forces, Bäckman *et al.* (1975), Chang (1975), Krewald *et al.* (1977), Liu *et al.* (1991), Van Giai and Sagawa (1981), and Waroquier *et al.* (1983) for two-body Skyrme forces, Eq. (56), and Bender, Dobaczewski, *et al.*, (2002) for Skyrme energy-density functionals, Eqs. (48) and (49). These two variants of the Skyrme Hartree-Fock method differ in the expressions for the Landau parameters in the spin channels. Stability in saturated INM, however, does not guarantee stability in finite nuclei, since their densities vary from center to surface. They also explore a large range of N/Z asymmetries.

5. Some words of caution

Effective energy-density functionals are designed for a pertinent description of the binding energy of a many-body system. The basic theorems of density-functional theory also state that the local density distribution is well described if one uses the “exact” energy functional (Hohenberg and Kohn, 1964; Kohn and Sham, 1965; Kohn, 1999). In practice, however, energy functionals are deduced at best by an additional local-density approximation. Thus the range of validity for the various observables is a point of concern. We shall sketch here briefly the known limitations and necessary corrections.

The binding energy should be the safest observable in density-functional theory. But the nuclear mean field breaks basic symmetries (translation, occasionally rotation, and particle number). These need to be restored (see Sec. III), and that creates corrections to the energy as well as to other observables. These are the minimum correlation effects which need to be taken into account. For spherical calculations the center-of-mass correction suffices (see Sec. III.B.3). Deformed calculations additionally call for angular momentum projection (see Sec. III.B.2), which, however, are only consistent if accompanied by the corresponding low-energy vibrational corrections (Reinhard, 1978).

The gross properties of the local density distribution $\rho(\mathbf{r})$ are usually reliable observables, while finer properties are not. The form factor $F(\mathbf{k})$, which is the Fourier transform of $\rho(\mathbf{r})$, allows a clear distinction. It is reliable for \mathbf{k} below the Fermi momentum and should be modified by short-range correlation effects for larger \mathbf{k} . This is hinted at by systematic deviations between mean-field models and experiment at large \mathbf{k} (Reinhard *et al.*, 1984) and corroborated by a systematic test of the local-density approximation (Reinhard, 1992a). Even so, all corrections to the energy have to be applied similarly to the density. See the example of a center-of-mass correction later on.

Single-particle energies do not belong to the guaranteed observables of density-functional theory, although they are often looked at in electronic systems as well as in nuclei. They are known to be plagued by a self-interaction error which can be removed by a self-interaction correction (Perdew and Zunger, 1981). A thorough discussion of self-interaction corrections in nuclei has yet to be done. Besides this open question, one has to think of the appropriate experimental approach. The analysis of single-particle energies from the spectra of adjacent odd nuclei is discussed in Sec. VI.B.1. More direct access may be given by fast separation processes, such as (e, e') or $(d, {}^3\text{He})$ reactions, combined with a careful analysis of final-state interactions. See, for example, Grabmayr *et al.* (1994).

Excitation energies go beyond the safe grounds of conventional density-functional theory. But modern developments of a time-dependent version suggest the optimistic view that these can be reliable observables. This view is supported by successes in the mean-field descrip-

tion of nuclear giant resonances, surface vibrations, and fission, as will be discussed in Sec. VI.

B. The pairing gap and odd-even staggering of masses

The most prominent observable for like-particle, $T = 1$, pairing correlations on the mean-field level is the odd-even staggering of nuclear masses, often identified with the pairing gap appearing in schematic models (Ring and Schuck, 1980). Reality is more complicated. The structure of odd nuclei differs from that of even nuclei in several respects. The unpaired nucleon’s contribution to all densities is not just half the contribution of a pair; it also breaks intrinsic time-reversal invariance. Owing to self-consistency, all other nucleons rearrange themselves to these changes, which adds a contribution from the mean field to odd-even staggering; see, for example, Rutz *et al.* (1999), Duguet *et al.* (2002a), and Sec. VI.B, where this is discussed in the context of single-particle energies.

There are several measures for odd-even staggering which are proposed in the literature. The only ones accessible by experiment and calculation are three-, four-, and five-point mass-difference formulas $\Delta_q^{(n)}$, $n = 3, 4, 5$ (Jensen and Miranda, 1986; Madland and Nix, 1988). Phenomenological fits to data are reviewed by Möller and Nix (1992).

Several studies have tried to disentangle the mean-field and pairing contributions to the $\Delta_q^{(n)}$. While this can be done in simple model systems (Dobaczewski, Magierski, *et al.*, 2001), it is impossible in full unrestricted HFB calculations (Duguet *et al.*, 2002b). This has consequences for the fit of pairing interactions. In most cases the unavoidable complications from the mean field in odd nuclei are simply neglected when adjusting the pairing strength. As they usually decrease the odd-even staggering, the pairing strength thus obtained will also be too small. This problem was examined by Rutz *et al.* (1999) in the framework of the relativistic mean-field model looking at global trends, and by Xu *et al.* (1999) with emphasis on rotational bands. The situation is complicated by the fact that the mean-field contribution is dominated by the time-odd part, which is not completely fixed in the Skyrme Hartree-Fock method and which was never carefully explored for Gogny or relativistic mean-field models. It can also be expected that correlations beyond the mean-field level, e.g., those discussed in Sec. VI.F.2, are different for even and odd nuclei, which again will affect the odd-even staggering of all observables.

Incorporating these complications in an effective manner, the Gogny force D1S was adjusted with a simplified description for odd nuclei but artificially reducing experimental pairing gaps by 300 keV. Another line is followed in the Hartree-Fock mass formula by Tondeur *et al.* (2000), which also employs a simplified description of odd nuclei and puts the remaining differences in the structure of even and odd nuclei into different pairing strengths for the two types of nuclei.

Note that all n -point formulas are peaked at magic numbers, just at the point where pairing breaks down. This spurious peak is caused by the discontinuity of the mean-field energy at shell closures (Bender, Rutz, *et al.*, 2000b; see also the extensive discussion of this effect for deformed nuclei on the Hartree-Fock level by Satuła *et al.*, 1998).

To compare theoretical models, simpler measures for pairing correlations can be used, which avoid the calculation of several nuclei. One criterion is the lowest quasiparticle energy in an odd nucleus. When using this, the HFB ground states of the fully paired odd- A nucleus should be used as reference state (Duguet *et al.*, 2002a). A measure that is also defined for even-even nuclei is the average matrix element of the pair potential (Dobaczewski *et al.*, 1984), which reads in the canonical basis $\langle v^2 \Delta \rangle_q = \sum_k v_k^2 \Delta_k / \sum_k v_k^2$. This puts too much weight on deeply bound states. An average that is more sensitive to states at the Fermi surface is provided by Sauvage-Letessier *et al.* (1981):

$$\langle uv \Delta \rangle_q = \frac{\sum_k u_k v_k \Delta_k}{\sum_k u_k v_k}. \quad (118)$$

The quantities u_k , v_k are the BCS occupation amplitudes, see Sect. I.B.4. See Bender, Rutz, *et al.* (2000b) and Duguet *et al.* (2002b) for a more detailed discussion. Pairing correlations also give significant corrections to other observables. These can be used to determine the parameters of more complicated pairing interactions, as was done by Fayens *et al.* (1994, 2000; Fayens and Zawischa, 1996) using isotopic shifts of mean-square charge radii. There is also the possibility of avoiding the calculation of odd-mass nuclei completely and adjusting the pairing functional solely to observables for even-even nuclei, e.g., to the dynamical moment of inertia \mathcal{J}_2 , as done by Duguet *et al.* (2001).

Measures for $T=0$ pairing are less well understood. The Wigner energy in nuclei close to the $N=Z$ line is usually associated with $T=0$ pair correlations (Satuła and Wyss, 1997), but there is still a lot of controversy about other unique signatures (Satuła *et al.*, 1997; Terasaki *et al.*, 1998; Satuła and Wyss, 2001a, 2001b). As $T=0$, pairing is neglected in all fits of mean-field models, its contribution to fitted nuclei with $N=Z$ like ^{16}O and ^{40}Ca is missing. This might cause some incorrect trends in the effective forces as the $T=0$ pairing effect has to be simulated by other terms in the effective interaction. To avoid this problem a correction for the Wigner energy as used in mic-mac models was introduced in the Hartree-Fock and HFB mass formulas by Tondeur *et al.* (2000) and Samyn *et al.* (2002).

C. Fit strategies

As argued above, the adjustment of nuclear effective energy functionals relies on fits to phenomenological input. There is a large variety of conceivable choices for

this input. As a general trend, early adjustments used less, and more basic, data, while more recent parametrizations include larger sets of information on finite nuclei and employ systematic least-squares fits to cope with the amount of data. Table I aims to summarize the phenomenological input for a selection of the most widely used forces at present, including the key references for each strategy. The case is a bit more involved for the family “SkI1-5, NL-Z2.” The underlying fitting strategy was initiated for the force Z_σ (Friedrich and Reinhard, 1986) and used for NL1 (Reinhard, Rufa, *et al.*, 1986), as well as NL-Z (Rufa *et al.*, 1988) and PL-40 (Reinhard, 1988). More data have been taken into account for the later fits of SkI1-5 (Reinhard and Flocard, 1995) and NL-Z2 (Bender, Rutz, *et al.*, 1999). This larger set is shown in the table.

The table is self-explanatory. Thus we shall skip a lengthy discussion of the differences in bias. For completeness, we mention here a few further families of forces and their fitting strategies. Amongst the earlier adjustments, there also exists a whole set of SkT1-9 forces developed by Tondeur *et al.* (1984), in which all forces share a common set of basic nuclear properties (E and r_{rms}), and a systematic variation of additional features has been added on top. A more recent alternative is the SkX force (Brown, 1998). The fits here again include bulk properties (E and r_{rms}) and, as a particular feature, detailed information on single-particle levels in various nuclei. The bias on single-particle energies is related to the aim of this force, namely, to provide self-consistent input for shell-model calculations. Very recently a new family of forces has shown up which relies on fits of binding energies for a huge selection of nuclei, including deformed ones. The aim is to develop Skyrme functionals which describe energies with the same high precision as the systematics fitted within mic-mac models. The family of forces MSk1-MSk7 uses BCS pairing in the fits (Tondeur *et al.*, 2000; Goriely *et al.*, 2001), while the most recent BSk1 employs HFB methods throughout (Samyn *et al.*, 2002). These forces demonstrate that it is very possible to reproduce binding energies with a root-mean square error of less than 0.8 MeV. However, one has to be aware that these forces may not describe other properties of nuclei so well.

The fitting strategies as listed in Table I show the bias on phenomenological data which went into the various forces. There are subtle differences at an even more basic level. These concern the various options which are open in Skyrme Hartree-Fock and relativistic mean-field models: choice of center-of-mass correction, choice of spin-orbit model, treatment of the Coulomb interaction, and the nucleon mass used in the calculations. Most of these options have been discussed in previous sections. Table II provides a summary for the selection of forces used in this review. See the text of the previous sections for discussion of other forces. Last but not least, one has to be aware of slightly different values for the Coulomb strength e^2 . A traditional choice is $e^2=1.44$ MeV fm. Some authors use more digits.

TABLE I. Compilation of phenomenological input for various parametrizations: E = binding energy, r = charge rms radius, R = charge diffraction radius, σ = charge surface thickness, δr^2 = isotopic shift of charge m.s. radius, r_n = neutron rms radius, INM = infinite nuclear matter properties as defined in Sec. V.A. The basic references are given in the heading lines together with the names of the corresponding forces.

Gogny D1, D1S (Dechargé and Gogny, 1980)	
E & r :	^{16}O , ^{90}Zr
$\ell \cdot s$	$^{16}\text{O}(1p_n, 1p_p)$
INM	equilibrium symmetric INM
Pairing	even-odd E in Sn isotopes (quenched)
SI-SVI (Beiner <i>et al.</i> , 1975)	
E :	^{16}O , ^{40}Ca , ^{48}Ca , ^{56}Ni , ^{90}Zr , ^{140}Ce , ^{208}Pb
r :	^{16}O , ^{40}Ca , ^{48}Ca , ^{56}Ni , ^{90}Zr , ^{140}Ce , ^{208}Pb
$\ell \cdot s$	$^{16}\text{O}(1p_n, 1p_p)$
	Additionally for SkM (Krivine <i>et al.</i> , 1980)
INM	K_∞ , a_{sym} (\leftrightarrow resonances in ^{208}Pb)
	Additionally for SkM* (Bartel <i>et al.</i> , 1982)
INM	a_{surf} (\leftrightarrow fission barriers)
SkP (Dobaczewski <i>et al.</i> , 1984)	
E :	^{16}O , ^{208}Pb
$\ell \cdot s$	differences E
INM	$(E/A)_{0,\text{eq}}$, $\rho_{0,\text{eq}}$, K_∞ , a_{sym} , κ_{TRK} , $m_0^*/m = 1$, $a_{\text{sym}}(\rho/2)$
Pairing	average gaps
SLy1-10 (Chabanat <i>et al.</i> , 1998)	
% E :	^{16}O , ^{40}Ca , ^{48}Ca , ^{56}Ni , ^{78}Ni , ^{132}Sn , ^{208}Pb
% r :	^{16}O , ^{40}Ca , ^{48}Ca , ^{56}Ni , ^{208}Pb
$\ell \cdot s$	$^{208}\text{Pb}(3p_n)$
INM	$(E/A)_{0,\text{eq}}$, $\rho_{0,\text{eq}}$, K_∞ , a_{sym} , κ_{TRK} , $E_0 S_{\text{neut}}$
SkI1-5, NL-Z2, (NL-Z, PL-40, NL1, Z_σ)	
% E :	^{16}O , ^{40}Ca , ^{48}Ca , ^{56}Ni , ^{58}Ni , ^{88}Sr , ^{90}Zr , ^{112}Sn , ^{120}Sn , ^{124}Sn , ^{132}Sn , ^{144}Gd , ^{208}Pb , ^{214}Pb
% R :	^{16}O , ^{40}Ca , ^{48}Ca , ^{58}Ni , ^{88}Sr , ^{90}Zr , ^{112}Sn , ^{120}Sn , ^{124}Sn , ^{208}Pb
% σ :	^{16}O , ^{40}Ca , ^{48}Ca , ^{90}Zr , ^{208}Pb
$\ell \cdot s$	$^{16}\text{O}(1p_n, 1p_p)$ (only SHF)
δr^2	^{214}Pb - ^{208}Pb (only SHF)
INM	κ_{TRK} (only SHF)
NL3 (Lalazissis <i>et al.</i> , 1997)	
E :	^{16}O , ^{40}Ca , ^{48}Ca , ^{58}Ni , ^{90}Zr , ^{116}Sn , ^{124}Sn , ^{132}Sn , ^{208}Pb , ^{214}Pb
r :	^{16}O , ^{40}Ca , ^{48}Ca , ^{58}Ni , ^{90}Zr , ^{116}Sn , ^{124}Sn , ^{208}Pb , ^{214}Pb
r_n :	^{40}Ca , ^{48}Ca , ^{58}Ni , ^{90}Zr , ^{116}Sn , ^{124}Sn , ^{208}Pb
INM	$(E/A)_{0,\text{eq}}$, $\rho_{0,\text{eq}}$, K_∞ , a_{sym}

TABLE II. The options used in the definition of the various forces from Table I (as well as the MSk1-7 and BSk1 family). For c.m. correction options see Sec. III.B.3. A δ indicates that the correction is included variationally. The asterisk in the case of MSk1-7 & BSk1 is a reminder that a correction for nondiagonal terms has been included; see Sec. III.B.3. For the Coulomb energies see Sec. II.A.5. ρ_p , proton density; ρ_C , charge density; LDA indicates that the Slater approximation to exchange was used. There are two options for the spin-orbit field. The first column indicates whether the J_T^2 term [see Eq. (48)] is taken into account. The second column indicates whether the isovector term of the spin-orbit force is considered as a separate degree of freedom. Conventional Skyrme forces are identified by $3C_1^{\text{vj}} = C_0^{\text{vj}}$ in Eq. (48). The entity “var” means that various options (“yes” and “no”) have been used within the family of forces. Numerical values are given in nuclear units, energies in MeV, and lengths in fm.

Force	$\frac{\hbar^2}{2m}$	E_{cm}	Coulomb		$\ell \cdot \mathbf{s}$	
			$E_{\text{Coul}}^{(\text{dir})}$	$E_{\text{Coul}}^{(\text{ex})}$	J_T^2	$T=1$
D1,D1S		$\delta \frac{\langle \hat{p}_{\text{cm}}^2 \rangle}{2mA}$	ρ_p	exact	–	no
SI, . . . ,SkM*	20.73	$\delta \frac{\langle \sum_i \hat{p}_i^2 \rangle}{2mA}$	ρ_p	LDA	no	no
SkP	20.73	$\delta \frac{\langle \sum_i \hat{p}_i^2 \rangle}{2mA}$	ρ_p	LDA	yes	no
SLy1-10	20.73553	var	ρ_p	LDA	var	var
SkI1-5	20.7525	$\frac{\langle \hat{P}_{\text{cm}}^2 \rangle}{2mA}$	ρ_p	LDA	no	var
MSk1 . . . BSk1	20.7505 20.7219	$\delta \frac{\langle \sum_i \hat{p}_i^2 \rangle}{2mA}, *$	ρ_C	LDA	yes	no
Force	mc^2	E_{cm}	$E_{\text{Coul}}^{(\text{dir})}$	$E_{\text{Coul}}^{(\text{ex})}$		
NL1	939.0	$\frac{30.75}{A^{1/3}}$	ρ_p	none		
NL-Z, NL-Z2	938.9	$\frac{\langle \hat{P}_{\text{cm}}^2 \rangle}{2mA}$	ρ_p	none		
NL3	939.0	$\frac{30.75}{A^{1/3}}$	ρ_p	none		

D. Global results

1. Nuclear matter properties

Key features of symmetric nuclear matter are summarized in Table III. A few comments are in order. The relativistic mean-field method tends to larger volume energy coefficients a_{vol} than the nonrelativistic models. Even more pronounced is the difference in saturation density $\rho_{0,\text{eq}}$. The relativistic mean-field method delivers much lower values than Skyrme Hartree-Fock models (the SIII interaction does not count here, as it does not perform well for radii.) Both discrepancies are larger than the estimated extrapolation errors from least-squares fits. We encounter here a deep-rooted difference between the two models which has yet to be understood. There are also large and systematic differences concerning the effective mass m_0^*/m and the sum-rule enhance-

ment factor κ_{TRK} . The relativistic mean-field model uses very small m_0^*/m and large κ_{TRK} . It should be remembered, however, that the effective mass from this model has a different meaning from that in nonrelativistic models (see Sec. V.A.3).

The isoscalar effective mass is directly related to the giant quadrupole resonance, and $m_0^*/m \approx 0.8$ is required for a proper reproduction (see Sec. VI.F.3). The sum-rule enhancement is not so easily fixed. It is related to the giant dipole resonance. But the relativistic mean-field model with large κ_{TRK} and also large κ_{sym} yields similar resonance energies to the Skyrme Hartree-Fock, with both quantities being smaller (see Sec. VI.F.3). It is to be noted that the features of the (finite-range) relativistic mean-field model also persist for the point-coupling model PC-F1 (Bürvenich, Madland, *et al.*, 2002). The differences are thus due to relativistic kinematics and not due to the finite range of the interaction.

TABLE III. Nuclear matter properties according to the liquid-drop model formula, Eq. (116): $\rho_{0,\text{eq}}$, saturation density; K_∞ , incompressibility modulus; m_0^*/m , isoscalar effective mass; κ_{TRK} , sum-rule enhancement factor. The second line for the relativistic mean-field forces shows m_0^*/m and κ_{TRK} at the Fermi surface k_F rather than at $k=0$. Not all values are predictions of the forces as some infinite nuclear matter properties might have been constrained during the fit.

Force	a_{vol} (MeV)	κ_{vol}	a_{surf} (MeV)	κ_{surf}	$\rho_{0,\text{eq}}$ (fm^{-3})	K_∞	m_0^*/m	κ_{TRK}
SIII	-15.93	1.77	17.0	3.22	0.145	356	0.76	0.53
SkM*	-15.86	1.89	17.6	2.01	0.161	218	0.79	0.54
SkT6	-16.07	1.86	18.1	2.61	0.161	237	1.00	0.00
SkP	-16.03	1.87	18.0	2.74	0.163	202	1.00	0.35
SLy6	-15.92	2.01	17.4	1.55	0.159	230	0.69	0.25
SkI4	-15.92	1.85	17.3	1.45	0.160	248	0.65	0.25
BSk1	-15.80	1.76	16.7	1.45	0.157	231	1.05	-0.05
D1S	-16.02	-	19.0	-	0.160	209	0.67	-
NL3	-16.24	2.30	18.5	1.39	0.148	272	0.59	0.68
-	-	-	-	-	-	-	0.65	0.53
NL-Z2	-16.07	2.43	17.7	1.34	0.151	172	0.58	0.72
-	-	-	-	-	-	-	0.64	0.55
PC-F1	-16.17	2.34	-	-	0.151	270	0.61	-
-	-	-	-	-	-	-	0.67	-

The differences in the surface energy coefficient a_{surf} look small but make a crucial difference for the shape of deformation potential-energy surfaces. A smaller a_{surf} tends to allow shape transitions more easily. There are large differences in the incompressibility modulus K_∞ . This is well known and much discussed. Experimental access is provided by the monopole resonance (see Sec. VI.F.3).

Pure neutron matter constitutes the extreme end of isotopic trends and is relevant for astrophysical applications (Pethick and Ravenhall, 1995). Predictions for the equation of state of neutron matter are compared in Fig. 2. There is a broad span of predictions from Skyrme interactions. The data are simply not very well fixed by finite-nuclei information. But the SLy6 interaction demonstrates that neutron data can easily be accommodated

by Skyrme forces (Chabanat *et al.*, 1997). The situation is different for the relativistic mean-field interactions. The shape of the curve is quite different from those of the Skyrme Hartree-Fock forces and from the Friedmann and Pandharipande results. There is no way to fit these neutron matter pseudodata with standard relativistic mean-field functionals. Extensions of the models are needed, e.g., nonlinearities of the vector fields (Oyamatsu *et al.*, 1998) or density-dependent coupling constants (Typel and Wolter, 1999).

2. Average quality of bulk observables

As outlined in Sec. V.C, the various parametrizations of the models have been adjusted, often to very different sets of experimental data. Even if it does not do justice to all parametrizations, it is instructive to compare them with respect to a common quality measure. Table IV shows the relative rms errors on the binding energies and the three parameters describing the charge form factor (see Sec. V.A.2), computed for the set of data used to adjust the Skyrme interactions SkI1-6 and the relativistic mean-field force NL-Z2 (see Table I). All parametrizations reproduce the binding energies well. Systematic differences appear for the charge form factor. As expected, those data which are explicitly fitted are described better. This suggests that mean-field interactions have enough versatility to describe charge form factors, but their predictions are not completely constrained by the other ground-state data. There is a systematic difference between Skyrme interactions and relativistic mean-field forces. Within the standard relativistic mean-field model (represented here by the NL3 and NL-Z2 parametrizations) all three key quantities of the charge form factor are not simultaneously well described. This seems to be a deficiency of the current

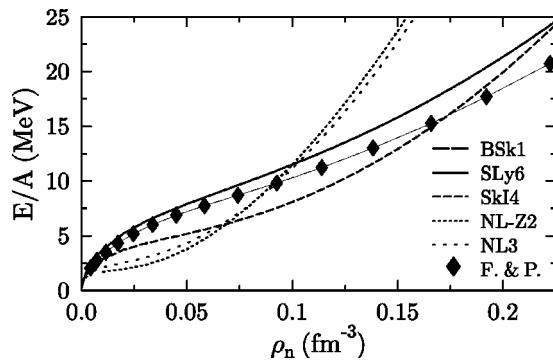


FIG. 2. Energy per particle in pure neutron matter (at zero temperature) calculated with the effective interactions as indicated: Filled diamonds connected by a thin solid line denote results from a variational many-body calculation (Friedmann and Pandharipande, 1981) which are widely used as reference data for neutron matter.

TABLE IV. Relative error $\delta O = (O_{\text{calc}} - O_{\text{expt}})/O_{\text{expt}}$ calculated for δE , the experimental binding energy; δR , charge diffraction radius; $\delta\sigma$, charge surface thickness; and δr , charge rms radius in %. The experimental data included are those taken from the fits of the SkI1-5 and NL-Z2 interactions (see Table I) Numbers in italics indicate data that were also included in the force fitting, while numbers in roman type show “predictions.”

Force	δE	δR	$\delta\sigma$	δr
SIII	<i>0.38</i>	2.84	4.8	<i>1.20</i>
SkM*	<i>0.38</i>	0.36	4.9	<i>0.34</i>
SLy6	<i>0.24</i>	0.69	5.3	<i>0.44</i>
SkI4	<i>0.33</i>	<i>0.44</i>	1.8	0.64
MSk7	<i>0.27</i>	1.12	2.5	0.57
NL-Z2	<i>0.22</i>	<i>0.92</i>	1.8	1.18
NL3	<i>0.34</i>	0.88	5.5	<i>0.85</i>
PC-F1	<i>0.27</i>	<i>0.48</i>	<i>1.4</i>	<i>0.50</i>

standard finite-range model. The relativistic point-coupling model PC-F1 (Bürvenich, Madland, *et al.*, 2002) performs as well as the nonrelativistic Skyrme interactions in that respect.

VI. APPLICATIONS

We shall now compare results obtained with the various models presented here for a broad selection of observables. We have chosen a few representative parametrizations for each model, i.e., the Skyrme interactions SLy4 or SLy6 (Chabanat *et al.*, 1998), the Skyrme interaction with generalized spin-orbit interaction SkI3 (Reinhard and Flocard, 1995), the Skyrme-HFB mass fit BSk1 (Samyn *et al.*, 2002), the Gogny force D1S (Berger *et al.*, 1984), and the relativistic mean-field parametrizations NL3 (Lalazissis *et al.*, 1997) and NL-Z2 (Bender, Rutz, *et al.*, 1999). We omit a comparison of the various choices for pairing models and forces, but give references wherever it is known that results are sensitive to details of pairing.

A. Binding energies

A detailed look at the reproduction of binding energies is given in Fig. 3. The performance is very good for the fitted nuclei (see Table I), setting a typical error margin of about ± 2 MeV. The force BSk1 with its extreme

bias on energies performs visibly better than all others here. The errors for nonfitted nuclei usually also stay within the typical error bands. SkI3 is sometimes an exception. The reason is that this force produces deformed nuclei more easily than the other forces and that we have compared only spherical calculations in this figure. Another feature is noteworthy: the errors are not distributed statistically but show a pronounced trend to underbinding in the midshell regions. This is either an effect of underestimated pairing interaction or of missing correlation energy. Note that trends visible in Fig. 3 cannot be trivially related to the nuclear matter properties that enter the liquid-drop modal formula (116). The problem is that binding energies are overlaid with strong shell fluctuations. The comparison becomes more instructive if one subtracts the shell correction energy, Eq. (36), before looking for trends, as was done by Kleban *et al.* (2002) for the Gogny force. Complete mass tables have been published by Goriely *et al.* (2001) for the Skyrme interaction MSk7 and Lalazissis, Raman, and Ring (1999) for the relativistic mean-field force NL3. For the recent mass fit MSk7, the rms error of 0.738 MeV for all currently known binding energies reaches nearly the quality of the best current mic-mac models. This value is quite close to the lower limit for the rms error in a mean-field approach estimated by Bohigas and Leboeuf (2002).

Figure 4 extends the comparison to the available superheavy elements. It is gratifying to see that the extrapolations work very well for the selection of (recent) forces shown here. A systematic difference between relativistic mean-field and Skyrme Hartree-Fock interactions develops where the latter tend to underbinding. This is probably related to the significant binding differences seen in Table III. When the binding is plotted versus mass number A , one obtains flat curves for all Skyrme Hartree-Fock forces, while there is a small but visible slope for the relativistic mean-field forces that points to an unresolved isoscalar trend. When plotted versus the relative neutron excess I , all forces (perhaps with the exception of BSk1) show slopes that point to unresolved trends in the isovector channel. This is true even for modern forces like NL3 or SLy6 fitted with bias on good isovector properties. However, one has to be careful with that interpretation since the range of known masses in I is rather small, and wrong trends in the “macroscopic part” of the models interfere with local

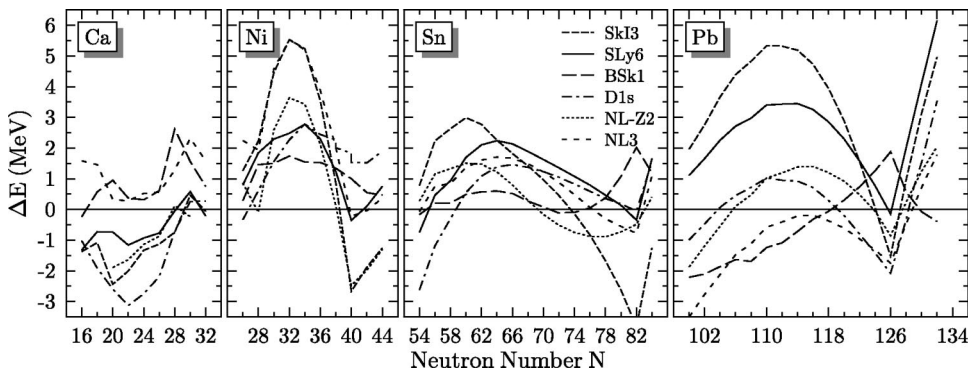


FIG. 3. Error on the total binding energy for the isotopic chains and forces indicated. Positive ΔE denote underbound nuclei with respect to the experiment; negative ΔE correspond to overbound nuclei. Results were obtained from spherical mean-field calculations.

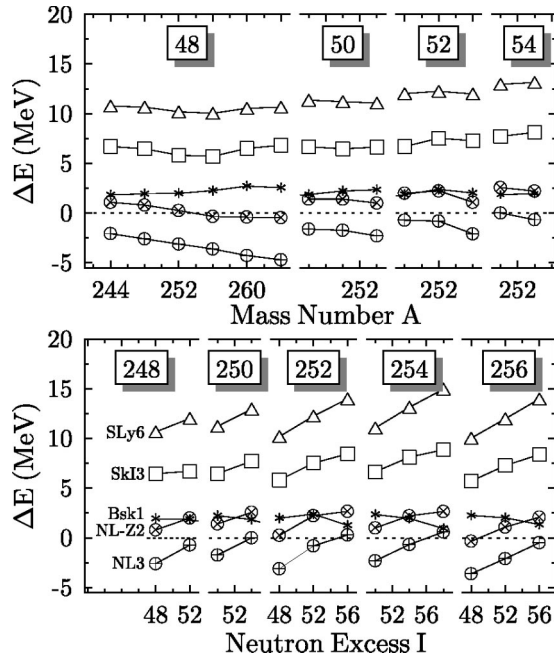


FIG. 4. Error on the binding energy ΔE for the heaviest nuclei where the mass is known. To separate trends in the isoscalar and isovector channels of the effective interactions, ΔE is plotted in the upper panel against total mass number $A = N + Z$ for chains of nuclei with the same neutron excess $I = N - Z$, and vice versa in the lower panel. The calculations include quadrupole axial deformations. Calculations are taken from Bender (2001), Bürvenich *et al.* (1998), and Samyn *et al.* (2002).

kinks of the shell structure, as found in Fig. 3 around all shell closures.

A magnifying glass is provided by energy differences, such as the two-neutron separation energy

$$S_{2n}(Z, N) = E(Z, N) - E(Z, N - 2). \quad (119)$$

Figure 5 shows the evolution of S_{2n} along the chain of Sn isotopes. All forces agree nicely with data in the regime of stable nuclei. Significant differences develop

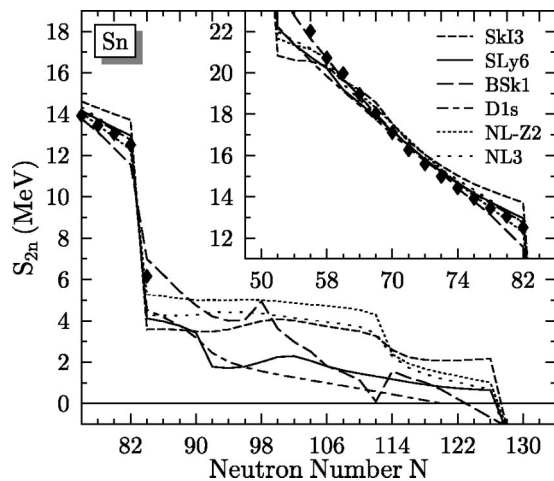


FIG. 5. Two-neutron separation energy S_{2n} for the chain of tin isotopes. The inset on the upper right shows results for $N \leq 82$.

from ^{132}Sn on. One reason for this is that the jump in the S_{2n} at the shell closure is predicted differently. This jump is a typical shell effect, and the results indicate that the various forces, although similar in bulk properties, have different detailed shell structure. This can also be seen from the small jumps following for larger N . They are predicted at different N and with different amplitudes. One would have expected that the trends in long isotopic chains would reflect the isovector properties of the effective interactions, e.g., a_{sym} as given in Table III. Figure 5 demonstrates that these are overlaid by shell structure. More direct access to isovector forces is provided by the neutron skin (see Sec. VI.C.2).

B. Shell structure

Global trends of nuclear observables are relatively well described by the analogy between nuclei and droplets. However, shell effects are crucial for almost all observables. For example, the existence of superheavy nuclei relies only on shell effects. In this section, we discuss those observables most directly related to shell structure, namely, the nuclear level scheme and shell closures.

1. Single-particle energies

Experimental information on single-particle energies of even-even nuclei is drawn from the single-nucleon removal energies into or out of the low-lying excited states of adjacent odd- A nuclei. Identification of an even nucleus with calculated single-particle energies works only if the modifications of the mean fields induced by the extra nucleon (or hole) are small. Looking at single-particle spectra around doubly magic nuclei permits us to limit the modifications on the mean field to polarization effects. The magnitude of these effects has been investigated by Rutz *et al.* (1998) for doubly magic nuclei within the relativistic mean-field method. Figure 6 shows the example of proton states in ^{208}Pb . The last column gives the experimental removal energies relative to the doubly magic nucleus, i.e., $S_p(^{208}\text{Pb}) = E(^{208}\text{Pb}) - E(^{207}\text{Tl})$ for hole states and $S_p(^{209}\text{Pb}) = E(^{209}\text{Bi}) - E(^{208}\text{Pb})$ for particle states. The $9/2^-$ single-particle state corresponds to the ground state of ^{209}Bi and the $1/2^+$ to the ^{207}Tl ground state. All levels above the $9/2^-$ or below the $1/2^+$ state correspond to excited configurations of ^{209}Bi or ^{207}Tl , respectively. The other columns of Fig. 6 show relativistic mean-field results. The first column shows the eigenvalues of the single-particle Hamiltonian in ^{208}Pb . Columns 2 through 4 are drawn from one-proton removal energies as in the experimental data. They correspond to various stages of refinement as explained in the caption. Each polarization effect contributes in a similar way, while all together build up a substantial shift of the “single-particle energies” of the order of 0.5 MeV for ^{208}Pb . The effect is even larger for lighter nuclei. The direction of the shift will be in opposite for particle and hole states. The $9/2^- - 1/2^+$ gap is strongly affected by polarization. Single-particle energies on an absolute scale [as used, for example, in the fits

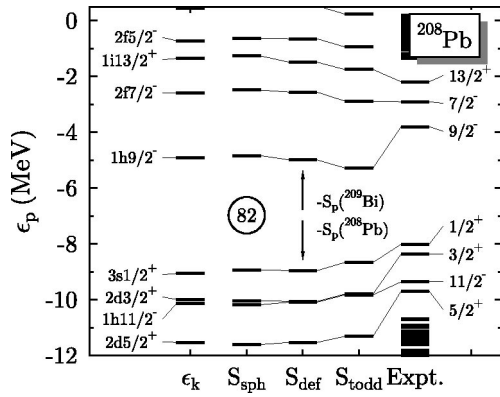


FIG. 6. Proton spectra of ^{208}Pb calculated with the relativistic mean-field model and the force PL-40. Column 1 shows the ϵ_k spectrum of the eigenvalues of the mean-field Hamiltonian for ^{208}Pb . Columns 2–4 show the one-proton separation energies S_p from and to the adjacent nuclei as indicated. Column 2 results from spherical calculations of the odd nuclei, column 3 from axially symmetric deformed calculations with time-reversal invariance, and column 4 from deformed calculations allowing for broken time-reversal symmetry. The last column shows the experimental values calculated from excitation energies taken from Kinsey *et al.* (1997) and masses given by Audi and Wapstra (1995). Data taken from Rutz *et al.* (1998).

of the Skyrme parametrization SkX by Brown (1998)] are not reliable either. However, the relative energies amongst the particle states and the hole states, taken separately, are more robust. Thus information on energy differences can be taken from the experimental spectra of odd nuclei and safely compared with differences of ϵ_k . For example, spin-orbit splittings are a robust observable as long as they do not cross the shell gap. Similar results were obtained by Bernard and Van Giai (1980) with a Skyrme interaction using linear response theory in the particle-core coupling model [see also Hamamoto (1974) and Mahaux *et al.* (1985)].

The upper part of Fig. 7 shows neutron spectra for ^{208}Pb obtained with a representative set of interactions. All forces predict the same ordering of hole levels, in agreement with data with the exception of the $2f_{5/2^-}$, which is generally too low and is predicted differently by the various interactions. It is known that the average level density at the Fermi surface scales with the effective mass as $g_q(\epsilon_{Fq}) \approx (3/4)N_q 2m_q^*/(\hbar k_{Fq})^2$, where N_q is the particle number, m_q^* the effective mass, and k_{Fq} the Fermi momentum for a given nucleon species. One can indeed see in Fig. 7 a correlation between m_0^*/m (see Table III) and the $9/2^- - 1/2^+$ gap. However, there is no clear relation to the density of states amongst the hole or particle states.

The lower part of Fig. 7 shows neutron spectra in the doubly magic ^{132}Sn . The pattern looks at first glance very similar to that of ^{208}Pb . All forces predict similar level orderings, which are, however, in disagreement with the experimental data. The experimental ground state of ^{131}Sn has spin $3/2^+$ while all mean-field models, Skyrme Hartree-Fock, Gogny, and relativistic mean-field, predict spin $11/2^-$. The origin of this discrepancy is

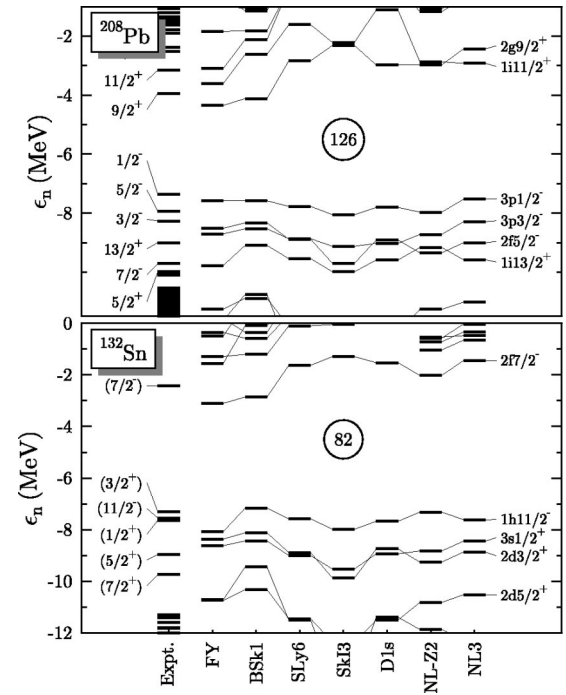


FIG. 7. Eigenvalues ϵ_n of the single-particle Hamiltonian for neutrons in ^{208}Pb (upper panel) and ^{132}Sn (lower panel) calculated with the Skyrme forces BSk1, SLy6, and SkI3, the Gogny force D1S, and the relativistic mean-field forces NL3 and NL-Z2. Results obtained with the folded Yukawa model (FY) used in mic-mac models are shown for comparison. Experimental values as in Fig. 6.

not clear. It may be related to a peculiarity of the high l states, which affects their average position or their spin-orbit splitting.

Moving away from magic shells, the structure of odd nuclei is also affected by changes in the pairing field due to the unpaired nucleon and by the breaking of time-reversal invariance (Duguet *et al.*, 2002a, 2002b). All these effects have to be taken into account. The impact of ground-state correlations is discussed in Sec. VI.F.2.

The spectra of superheavy nuclei are particularly sensitive to subtle details of the shell structure. The level density increases with mass number A , and small differences between the forces are magnified in this mass region. Figure 8 shows as an example the proton spectra in $^{292}120$. Different parametrizations predict different shell closures, $Z=114$, 120, or 126 (see Rutz *et al.*, 1997; Kruppa *et al.*, 2000). These differences are caused by changes in the spin-orbit splitting of the $2f$ shell and the development of “semibubble” shapes around $^{292}120$ (see Bender, Rutz, *et al.*, 1999; Dechargé *et al.*, 1999).

The spin-orbit splitting predictions made for stable nuclei with the same interactions are compared with the data in Fig. 9. The splittings in ^{16}O are included in the fit of most Skyrme Hartree-Fock forces and are well reproduced. Note, however, that the splittings are not included for SLy6 and BSk1 without noticeable loss of quality. Large differences show up for heavier nuclei. The relativistic mean-field interactions agree nicely with the data, which is remarkable in view of the fact that the

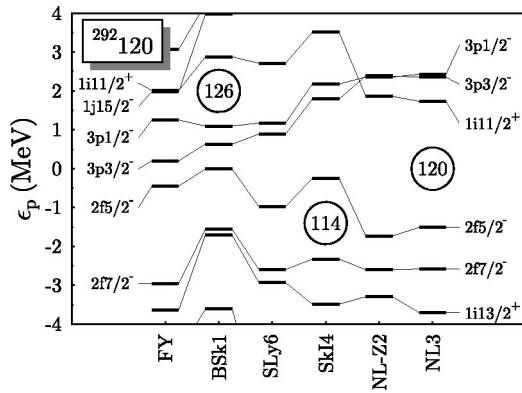


FIG. 8. Proton spectra of $^{292}_{120}\text{172}$ at spherical shape. The numbers in circles indicate the (magic) proton numbers corresponding to the gap. Data taken from Bender *et al.* (1999).

spin-orbit force needs no adjustment at all in this method. The Skyrme Hartree-Fock forces show larger deviations, even for SkI3, which is tailored to map the isospin mix of the spin-orbit force from the standard relativistic mean-field model. The reasons for this weakness are still under investigation. At the present stage, one has to be aware that these uncertainties plague detailed predictions for the level scheme of superheavy elements.

2. Signatures for shell closures

When discussing the stability of shell closures far from stability, one needs signatures to identify them. The first indications of shell closures were derived from isotopic and mass abundances as well as from the number of stable isotones (Göppert-Mayer, 1948). The findings could be related to the systematics of binding energies. Around the stability line, shell closures are associated with a jump in nucleon separation energies (see Fig. 5), which reflects the large change in the Fermi energy when crossing the gap in the single-particle spectrum at a magic number (see Sec. VI.B.1). This suggests that a

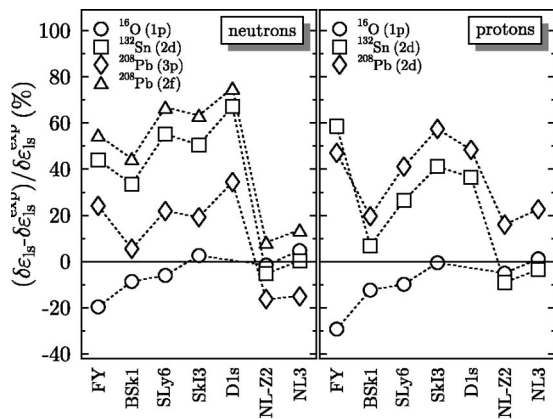


FIG. 9. The relative error on spin-orbit splittings in several doubly magic nuclei as indicated for a variety of forces. Data taken from Bender *et al.* (1999).

simple signature of shell closures is the two-nucleon shell gap, which for neutrons is given by

$$\begin{aligned} \delta_{2n}(Z, N) &= S_{2n}(Z, N+2) - S_{2n}(Z, N) \\ &= E(Z, N-2) - 2E(Z, N) + E(Z, N+2), \end{aligned} \quad (120)$$

and similarly for protons. This signature is usually simple to compute and also to determine experimentally from mass tables. However, there is a possible pitfall. This quantity represents a signature of shell closure only if no dramatic rearrangements of the mean field take place between the three adjacent nuclei. That is not always the case in exotic nuclei (see, for example, Bender, Cornelius, *et al.*, 2002) and the discussion of shell quenching in Sec. VI.B.3.

Another measure for shell effects is the shell-correction energy δE_{shell} [see Eq. (36)], which quantifies the “bunchyness” of the ϵ_k . It is large and negative at shell closures because the discrete sum has a particularly low value there while the smoothed expression extends over the shell gap. The δE_{shell} measures the deviation of the actual level density at the Fermi energy from the averaged level density. The separation of the binding energy [Eq. (36)] into a smooth part and δE_{shell} provides a powerful tool for analyzing all phenomena related to quantal shell effects, like the stabilization of superheavy nuclei or the structure of fission barriers of heavy nuclei. Nonetheless it is a purely theoretical measure without experimental access.

Both criteria, the two-nucleon shell gap and the shell-correction energy, yield well distinguished peaks at shell closures along and near the valley of stability, as can be deduced from Fig. 5. The situation becomes less clear in the region of superheavy nuclei, as illustrated in Fig. 10. The two-proton shell gap δ_{2p} has shrunk to at most 2 MeV at the shell closures $Z=120$, (124), and 126. The shell-correction energy has minima at some proton numbers, but they are broad and soft, predicting substantial stabilization by shell effects in a large area around the shell closures. The stabilized region is even broader because deformation effects (not included in the calculations for Fig. 10) also enhance the stabilization. The concept of magicity thus dissolves (for details see Bender, Nazarewicz, and Reinhard, 2001).

There is one further experimental signature for magic numbers: the excitation energy of vibrational states and the associated electric transition rates. The gap in the single-particle spectrum sets the scale for the lowest excitations. Peaks in the systematics of the lowest 2^+ states in even-even nuclei reflect the stiffness of the potential-energy surface, which is largest in closed-shell nuclei (see also Fig. 21 below). Compared to binding-energy differences, the data on vibrational states have the advantage that they do not mix information from different nuclei. The disadvantage is on the theoretical side. Reliable computations of excitation spectra are not easy (see Sec. VI.F).

3. Shell quenching

The weakening or “quenching” of spherical shell closures when going away from the valley of stability to

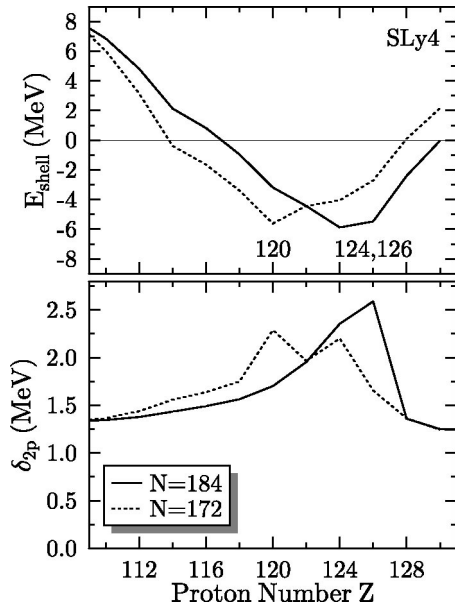


FIG. 10. Signatures for (spherical) proton shell closures along two isotonic chains of superheavy elements ($N=184$ and $N=172$), computed for spherical configurations with the SLy4 interaction. Upper panel: shell correction energy (36). Lower panel: two-proton shell gap $\delta_{2p} = E(Z-2, N) - 2E(Z, N) + E(Z+2, N)$. Data taken from Kruppa *et al.* (2000) and Rutz *et al.* (1997).

weakly bound nuclei is a phenomenon of great current interest. It is now well established for neutron-rich $N=20$ and $N=28$ isotones, and there are first hints that it may apply for the $N=50$ and $N=82$ shells (see the compilation of data by Kautzsch *et al.*, 2000). Shell quenching in neutron-rich systems has far-reaching consequences for astrophysics, as it influences the r -process path (Chen *et al.*, 1995; Pfeiffer *et al.*, 1996).

The actual sequence of magic numbers in neutron-rich nuclei is strongly affected by various nonstandard features: an increased diffuseness of the neutron density, the closeness of the particle continuum (Dobaczewski *et al.*, 1994), and changes in the spin-orbit splitting (Von-Eiff *et al.*, 1995; Lalazissis *et al.*, 1998a). For whatever reason, one finds an increased destabilization of the spherical shape for light neutron-rich $N=28$ isotones which can even lead to a stable quadrupole deformation; see, for example, Lalazissis, Vretenar, Ring, Stoitsov, and Robledo (1999); Werner *et al.* (1994); Terasaki *et al.* (1997a); Reinhard *et al.* (1999); Peru *et al.* (2000), and the example discussed in Sec. VI.D.2.

However, there are cases where the signatures for shell quenching are ambiguous. One has to distinguish between real shell quenching, in which the spectrum of ϵ_k is quenched, and the disappearance of certain indirect signatures for shell closures which might be independent of the underlying shell structure of magic nuclei. An example is the neutron-deficient Pb isotopes. The $Z=82$ shell gap in the single-proton spectra ϵ_k is predicted to be stable by all mean-field models, while recent mass measurements show a significant quenching of the two-proton shell gap $\delta_{2p} = E(Z+2, N) - 2E(Z, N) + E(Z$

$-2, N)$. The discrepancy is resolved when considering the deformation softness of Hg and Po isotopes. The additional deformation energy of Po and Hg reduces δ_{2p} and thus masks the spherical $Z=82$ shell effect for Pb. The deformation effect remains at the level of pure mean-field models (Bender, Cornelius, *et al.*, 2002). It is often accompanied by deformation softness whose quantitative description requires configuration mixing. See, for example, Bonche *et al.* (1990a, 1991) and Chasman *et al.* (2001) for examples from the neutron-deficient Pb region.

4. Proton emitters

The properties of proton-rich nuclei around the drip line differ in many respects from those of their neutron-rich counterparts. The smaller asymmetry and the stabilizing Coulomb potential hinder large proton skins and prevent the formation of proton halos. The proton drip line has been reached experimentally up to large charge number, and there is now a wealth of available data. An interesting phenomenon in proton-rich nuclei is the occurrence of proton emitters. Nuclei that are unstable with respect to the emission of a proton may have sizable lifetimes due to the large Coulomb barrier (Åberg *et al.*, 1997), and a large number of proton emitters are known experimentally (Woods and Davids, 1997). The description of unbound nuclei by mean-field methods is a challenge. In principle standard mean-field equations do not converge when the Fermi level is in the continuum (see Sec. I.B.2), although this feature can sometimes be neglected due to the large Coulomb barrier, as done in some recent relativistic mean-field calculations (Lalazissis *et al.*, 1999a, 1999b). A more satisfactory approach is to use mathematical tools to generalize the mean-field equation for positive Fermi energy. This has been done using the complex scaling method for spherical Skyrme calculations without pairing correlations (Kruppa *et al.*, 1997) and with them (Kruppa *et al.*, 2001).

C. Observables of the density distribution

1. Systematics of charge radii

A detailed comparison of the charge radii obtained with several models is given in Fig. 11. More extensive plots may be found in the articles of Pomorski *et al.* (1997) for the relativistic mean-field method, Kleban *et al.* (2002) for Gogny forces, and Buchinger *et al.* (2001) for Skyrme Hartree-Fock forces. The agreement with experimental data is generally very good. The relativistic mean-field interaction NL-Z2 tends to show the largest deviations, which hints again at the problem of covering all at once the key features of the charge form factor with finite-range meson fields (see also Sec. V.D.2). For the Ca isotopes all forces show a significant deviation from the data in the isotopic trends. This clearly points to an effect of ground-state correlations. See the semiphenomenological discussions of Barranco

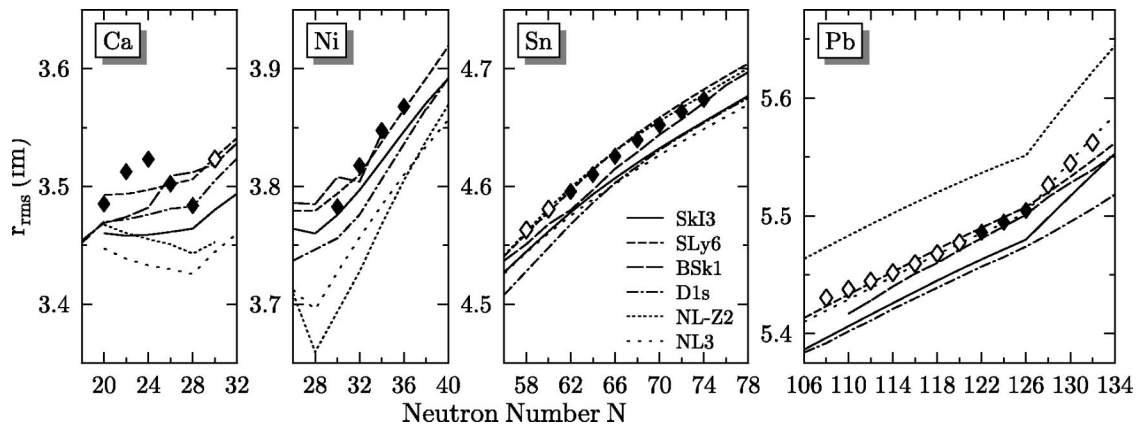


FIG. 11. Comparison of rms radii of the charge distributions from spherical mean-field calculations. Experimental data are taken from Nadjakov *et al.* (1994). Filled diamonds denote results from direct radius measurements, while open diamonds are obtained from measurements of isotopic shifts.

and Broglia (1985) and Caurier *et al.* (2001) for an analysis using shell-model calculations.

There is also a significant deviation in the trends for Pb isotopes. The experimental trend exhibits a kink at the doubly magic ^{208}Pb . The relativistic mean-field calculations reproduce this nicely, while the radii obtained with most Skyrme Hartree-Fock forces crosses $N=126$ without any kink. It is argued by Reinhard and Flocard (1995) and Sharma *et al.* (1995) that this hints at a difference in isovector spin-orbit force. The mismatch has been cured by extending the spin-orbit force in the Skyrme parametrization (see Sec. II.A.2) in the forces SkI3 and SkI4, which better reproduce this kink at ^{208}Pb . This is a nice example of how a comparison between different models has improved our understanding of each model. However, the case is not yet settled, as there exist arguments that the kink could equally well be due to a density-dependent pairing interaction like that in Eq. (71) (see Fayans *et al.*, 2000 and Tajima, Flocard, *et al.*, 1993).

As for energies, looking at differences between radii in an isotopic chain, i.e., isotopic shifts, often makes effects more visible.

From the experimental side, isotopic shifts can be measured directly and with high precision by laser spectroscopy. This technique also allows us to deal with unstable isotopes. Thus there exists a rich pool of data and a large body of literature; for a review see Otten (1989). Amongst the prominent effects in this regime is the huge even-odd staggering in proton-rich Hg isotopes which can be related to a prolate-oblate shape isomerism (Bengtsson *et al.*, 1987). The effect is qualitatively provided by all mean-field models although quantitative predictions about the transition point differ (Reinhard, Reiss, *et al.*, 2000). Most data on isotope shifts give indirect information about collective ground-state correlations (Reinhard and Drechsel, 1979; see also the above example of Ca isotopes). These correlations have been considered in early microscopic generator coordinate calculations using the Gaussian overlap approximation

(Girod and Reinhard, 1982a). A more recent example will be given in connection with low-energy excitations in Fig. 21.

2. Neutron radii

Neutron radii would provide very valuable information complementing the rich pool of data from charge radii. Unfortunately, their experimental determination has so far been model dependent because the strong interaction is involved (Batty *et al.*, 1989). There is hope that a clean tool will be available soon from parity-violating electron-nucleus scattering experiments (Vretenar, Lalazissis, and Ring, 2000; Horowitz *et al.*, 2001). Reliable data on neutron radii will improve models in several respects. For example, there is a close connection between the equation of state of neutron matter and the neutron rms radius of ^{208}Pb . See Brown (2000) for the Skyrme Hartree-Fock method and Typel and Brown (2001) for the relativistic mean-field model.

Other interesting phenomena related to the neutron density are the presence of neutron skins (Hamamoto and Zhang, 1995; Dobaczewski, Nazarewicz, and Werner, 1996; Lalazissis *et al.*, 1998b) or of neutron halos (Sagawa, 1992; Hansen *et al.*, 1995; Tanihata, 1996) far from β stability. Their description takes advantage of the variational principle that self-consistently optimizes the density profile (separately for neutrons and protons), a feature that is absent in mic-mac approaches and limits their use for neutron-rich systems.

One can establish a direct relation between isovector forces and the neutron skin, defined as the difference between neutron and proton radii (Reinhard, 1999; Sagawa, 2002). Figure 12 shows the skin in Sn isotopes predicted by various forces. It hints that larger skins are produced by forces with large symmetry energy and smaller skins by those with low a_{sym} . More thorough variations of a_{sym} confirm that there is a unique relation between skin and asymmetry energy within the current standard form of the Skyrme Hartree-Fock interactions

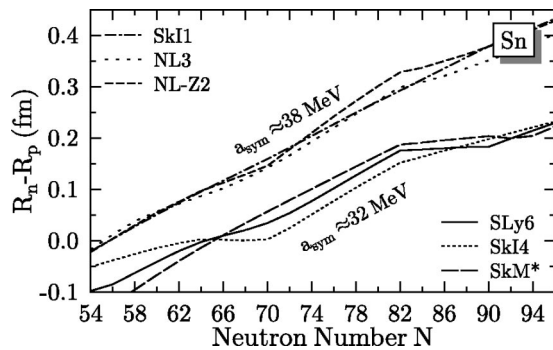


FIG. 12. Neutron skin $R_n - R_p$ along the chain of Sn isotopes. Results are shown for two groups of forces, one with low and one with high asymmetry energy.

(Reinhard, 1999). The effect is particularly pronounced for neutron-rich exotic nuclei.

Nuclei that exhibit experimentally a neutron halo are light neutron-rich nuclei, like ^{11}Li and ^{14}Be . The presence of a halo is due to the very weak binding of the outermost neutron. There is no consensus in the literature on how to define and parametrize halos. A simple and robust measure can be obtained from a combination of rms radius, diffraction radius, and surface thickness, quantifying the deviation from the Helm model (see Sec. V.A.2; for a thorough discussion see Mizutori *et al.*, 2000).

A reliable description of neutron halos requires careful modeling. Experimental data are available so far only for small systems, in which the number of nucleons is not large enough to justify a pure mean-field approach (see, for example, Barranco *et al.*, 2001). Pairing plays a crucial role for halo nuclei (Bertsch and Esbensen, 1991); see also the pairing antihalo effect discussed by Bennaceur *et al.* (2000) and the sensitivity to model details of the density dependence of the pairing interaction, as discussed by Dobaczewski, Nazarewicz, and Reinhard (2001). A careful description of the coupling to loosely bound or even continuum states is unavoidable and requires the HFB method, otherwise artifacts from BCS pairing might produce spurious halos (see discussions by Dobaczewski *et al.*, 1984; Dobaczewski, Nazarewicz, and Werner, 1996; Grasso *et al.*, 2001). There have been several HFB studies using Skyrme interactions (Mizutori *et al.*, 2000), Gogny forces (Nerlo-Pomorska *et al.*, 2000), and relativistic mean-field Lagrangians (Pöschl, Vretenar, Lulazissis, and Ring, 1997; Meng and Ring, 1998; Stoitsov *et al.*, 1998).

D. Deformation

Nuclei with closed or nearly closed shells are well described by a mean field with spherical symmetry. Far from closed shells, the incomplete filling of a shell triggers deformation and one has to allow the mean-field potential to be deformed. This necessity is illustrated, for instance, by the appearance of rotational bands and the sequence of vibrational states in the low-energy spectrum of many nuclei (Casten, 1990). Deformation is related to shell filling and is, in principle, a nuclear Jahn-

Teller effect (Reinhard and Otten, 1984; Nazarewicz, 1993). In fact, we encounter a dynamical Jahn-Teller effect as the pairing interaction tends to restore spherical shapes.

There are several ways to access deformation experimentally. Direct information can be obtained by Coulomb excitation cross sections, from measurements of lifetimes or of static quadrupole moments. Indirect evidence can be deduced through rotational and vibrational spectra. The rms deformation in the intrinsic system of reference of the nucleus can be related to quadrupole transition moments. At the mean-field level of approximation, a measure for deformation is given by multipole moments of the ground-state density. To compare deformations across different system sizes, it is better to deal with dimensionless multipole deformations defined as

$$\beta_\ell = \frac{4\pi}{3AR_0^\ell} \langle r^\ell Y_{\ell 0} \rangle \quad \text{with } R_0 = 1.2 A^{1/3} \text{ fm}, \quad (121)$$

where $Y_{\ell 0}$ is the spherical harmonic. Note that these β_ℓ are computed from the expectation values of the actual densities and need to be distinguished from the generating moments used in the multipole expansion of the nuclear shape in mic-mac models (Hasse and Myers, 1988). Note also that self-consistent calculations produce deformed ground states by straightforward variation. The potential-energy surfaces for collective motion are computed by constraint Hartree-Fock calculations, in which one or two (usually isoscalar) multipole moments are fixed. Except for these constraints, the self-consistency optimizes all other multipole moments for protons and neutrons. This is to be contrasted with mic-mac models, which need to parametrize a large number of higher multipole moments and which, in particular, assume that protons and neutrons have the same deformation. The consequences of this assumption were explored by Berger and Pomorski (2000), and shown to enhance fission barriers by about 1 MeV for actinides.

There is a world of test cases for nuclear deformation and a large variety of related phenomena, which are reviewed, for example, by Åberg *et al.* (1990) and Nazarewicz and Ragnarsson (1996). We shall sketch a few selected examples in the subsequent sections.

1. Medium-mass nuclei

Particularly interesting are isotopic chains along which one observes a transition from spherical to deformed shapes. A typical example is given by the isotopes of Gd above the neutron shell at $N=82$. This chain has been studied by Baran and Höhenberger (1996) with Skyrme interactions and by Blum *et al.* (1989) with the relativistic mean-field method.

Figure 13 shows the potential-energy surfaces for the chain of Gd isotopes at and above ^{146}Gd together with the systematics of the ground-state deformations. The potential-energy surfaces illustrate nicely the transition from a spherical to a well-deformed minimum, with vibrationally soft intermediate nuclei. Although the de-

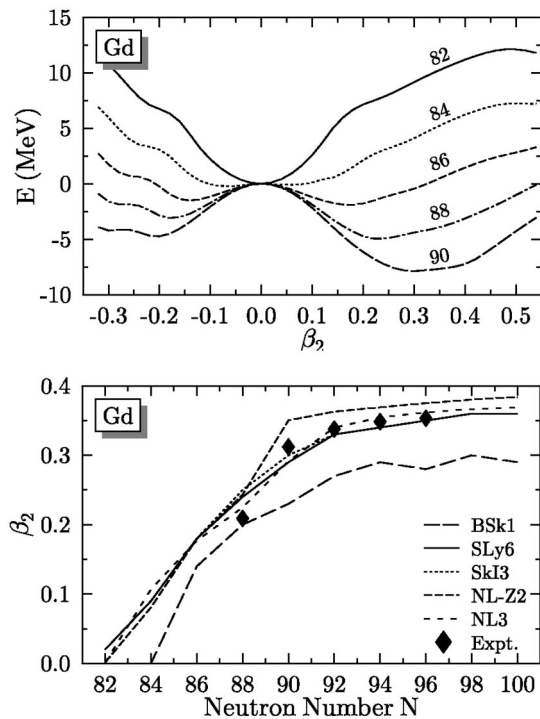


FIG. 13. Transition from spherical to deformed shapes in the chain of Gd isotopes. Upper panel: HF+BCS potential-energy surfaces calculated with the SLy6 interaction for neutron numbers ranging from 82 to 90. Lower panel: Ground-state deformation of Gd isotopes for several forces. Pairing is treated with the BCS method except for BSk1 for which the HFB method is used. Experimental values are taken from Raman *et al.* (2001).

scription of these intermediate isotopes requires one, in principle, to take into account fluctuations of shapes, one can discuss the evolution of shapes by looking only to the minima of the potential-energy surfaces. The lower panel shows how these deformations are predicted by different forces. The shape transition from $N=82$ to $N=90$ is similarly obtained by all the forces, but the way the transition takes place shows significant differences. In particular, the deformation obtained by the BSk1 interaction is systematically lower. A possible source for this difference may be its larger effective mass (see Table III). The deviation from the experimental deformation could be a hint that this large m_0^*/m is inappropriate. However, there are several other possible sources for this discrepancy, mainly the pairing correlations and the approximate rotational correction that is incorporated in BSk1. A conclusive answer has yet to be found.

2. Shell quenching in light nuclei

Due to the small number of nucleons, the mean-field approximation is less valid for light nuclei than it is for heavy ones. Fluctuations beyond the mean field play a larger role and there is stronger competition between spherical- and deformed-shell effects. For this reason, the phenomenon of shape coexistence [see Heyde *et al.*

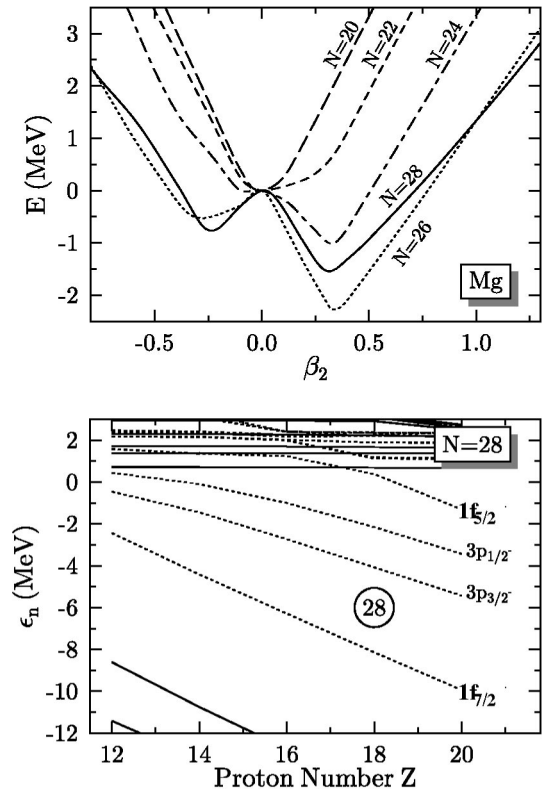


FIG. 14. Disappearance of the spherical $N=28$ shell in neutron-rich nuclei. Upper panel: Deformation energy of neutron-rich Mg isotopes computed with the HFB method and the SLy6 interaction. Lower panel: neutron single-particle energies ϵ_n at spherical shape for the $N=28$ isotones. Solid lines denote states with positive parity, dotted lines states with negative parity.

(1983) and Wood *et al.* (1992) for reviews] is even more abundant here than it is in heavy nuclei (Reinhard *et al.*, 1999).

The Mg isotopes are a good example of the problems encountered in a mean-field description of light nuclei. They extend over three supposedly magic neutron numbers ($N=8, 20$, and 28). On the other hand, $Z=12$ corresponds to a deformed-shell effect and the stable isotope ^{24}Mg is a good example of a nucleus with deformed ground state. Figure 14 illustrates the situation for the heavy isotopes, ^{32}Mg up to ^{40}Mg . The upper panel shows the potential-energy surfaces for quadrupole deformation relative to the energy of the spherical configuration.

Let us first discuss the case of ^{32}Mg . It corresponds to a magic neutron number $N=20$ and its ground state is predicted to be spherical, though with a rather soft potential-energy surface. This result is in contradiction with the experimental spectrum of ^{32}Mg : its first 2^+ state is at low excitation energy and has a strong $B(E2)$ transition probability to the ground state. The deformation deduced from the experimental data is around $\beta_2=0.5$. No effective interaction predicts a deformation like that for ^{32}Mg (Terasaki *et al.*, 1997a; Rodríguez-Guzmán *et al.*, 2000a); mean-field calculations give at most a potential-energy surface presenting an excited shallow

minimum or an inflexion point at a β_2 value around 0.5. For this reason, it is generally assumed that vibrational and rotational corrections have to be included to describe nuclei in this mass region. A typical vibrational zero-point energy here would be around 3 MeV and this corresponds to fluctuations $\Delta\beta_2 \sim \pm 0.4$. We shall come back to this point in Sec. VI.F.2. The softness of the potential-energy surfaces increases for $N=22$, and a deformed minimum appears for $N=24$. The deformation energy increases further for $N=26$, and the next magic number, $N=28$, by no means restores sphericity.

This tendency to deformation for nuclei far from stability may be related to the shell quenching that is likely to appear towards drip lines (see also Sec. VI.B.3). The effect is demonstrated in the lower panel of Fig. 14, showing the evolution of neutron levels along the $N=28$ chain as a function of the number of protons. The $N=28$ gap shrinks when going from ${}^{48}\text{Ca}_{28}$ towards the neutron drip line (at spherical shape, the next nucleus ${}^{38}_{10}\text{Ne}_{28}$ has a positive neutron Fermi energy). Already for $Z=16$, the gap at $N=28$ is too small to counterbalance the deformation induced by the nonmagic proton number $Z=16$ and to drive the nucleus to spherical symmetry (as is the case for $N=20$).

3. Fission barriers

Fission has been one of the major motivations for developing models of nuclear collective motion (Bohr and Wheeler, 1939; Hill and Wheeler, 1953). It is also a critical test case for mean-field models as a microscopic picture of collectivity (see, for example, Sec. III.A.1). On the experimental side, there exists a large pool of information on fission barriers deduced by model analysis from spontaneous and induced fission (Specht, 1974; Bjørnholm and Lynn, 1980). On the theoretical side, fission barriers are often used as a benchmark for mean-field models (Bartel *et al.*, 1982; Berger *et al.*, 1984), as they probe the surface tension of the parametrizations (see also Tondeur, 1985; Bender *et al.*, 2000a).

The fission paths are special collective paths which evolve from the ground-state deformation to the outer barrier and then slide asymptotically down the Coulomb valley. As with any collective path, they are represented by a succession of deformed mean-field states $\{|\Phi_q\rangle\}$. An unambiguous self-consistent definition of the path is given by the adiabatic TDHF equations (Baranger and Vénérioni, 1978; Goeke and Reinhard, 1978). Most practical calculations use quadrupole constrained mean-field calculations (Flocard *et al.*, 1973) as an intuitive approximation. Furthermore, correlation corrections play a role in fission. The zero-point energies for vibration and rotation modify the barriers by about 2 MeV (Reinhard and Goeke, 1979, 1987). The way pairing correlations are described also has a critical influence, since the path connects minima with low level density and barriers with high level density.

Fission paths explore many shape degrees of freedom including triaxiality and reflection-asymmetric shapes. There are usually two (or more) separate valleys in the

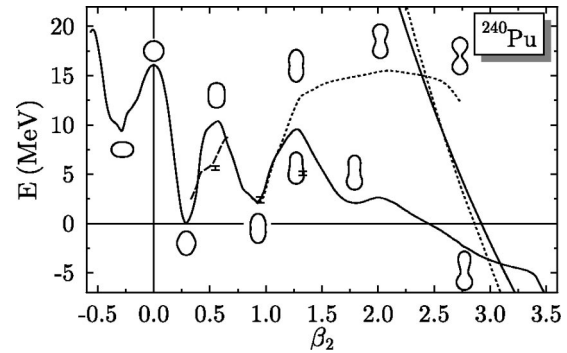


FIG. 15. Paths in the deformation energy landscape of ${}^{240}\text{Pu}$ calculated with the SkI4 interaction. The solid line corresponds to axial quadrupole and octupole (reflection asymmetric) constraints, the dashed line to triaxial quadrupole constraints, the dotted line to axial quadrupole constraint only. The two steep lines correspond to the symmetric (dotted line) and asymmetric (solid line) fusion paths. Shapes along the paths are indicated by the density contours at $\rho_0 = 0.07 \text{ fm}^{-3}$. From Bender (1998).

multidimensional landscape (see, for example, Berger *et al.*, 1984). A typical example is given by the distinction of fusion and fission paths which differ in their hexadecapole moment. An additional difficulty arises from the fact that separate valleys found in a calculation might be an artifact from an overly restricted symmetry (e.g., axial) and merge if computed more generally (e.g., triaxially); see the example given by Bender, Rutz, *et al.* (1998). Finally, it might not be sufficient to compute only the potential-energy surfaces along the fission path. Strong variations in the collective masses can cause the fission path to deviate from the minimum-potential line (see, for example, Giannoni and Quentin, 1980a, 1980b). It is clear that fission studies are a very complex task and many technical improvements are still required.

As a test case, we consider the fission barrier of ${}^{240}\text{Pu}$, which has been the traditional benchmark for the performance of mean-field models. The description of the double-humped fission barrier of actinides was one of the first prominent successes of the shell-correction method. It also became one of the first applications of constrained self-consistent calculations with Skyrme interactions (Flocard *et al.*, 1974), the Gogny force (Berger *et al.*, 1984), and the relativistic mean-field method (Blum *et al.*, 1994; Rutz *et al.*, 1995).

Figure 15 shows as a typical example the potential-energy surfaces for ${}^{240}\text{Pu}$ computed with the SkI4 interaction. The oscillations of the surfaces are due to shell fluctuations, while the liquid-drop-model energy would give one broad smooth barrier. The actual size of the shell effects depends strongly on the shapes that are involved in the calculation. Relaxing symmetries often decreases the barriers, as can be seen from the axial and triaxial paths at the first barrier and the (axial) reflection-symmetric and reflection-asymmetric paths at the second barrier. The paths with steep slopes at large β_2 correspond to symmetric and asymmetric entrance channels for fusion. The two approaching nuclei have to

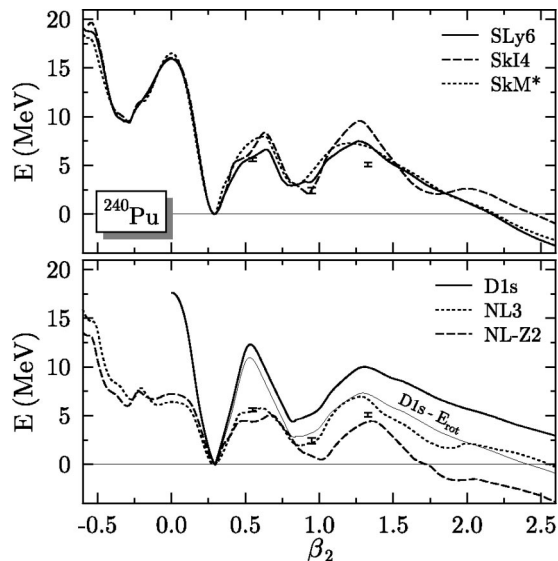


FIG. 16. Deformation energy along the fission path of ^{240}Pu calculated with the mean-field forces as indicated. Shapes are triaxial and reflection symmetric at the first barrier around $\beta_2 \approx 0.6$; they are axial and reflection asymmetric at the second barrier, which is located around $\beta_2 \sim 1.3$.

overcome the barrier between the fusion path and the fission path before this can form a neck and fuse. This happens only for smaller deformations. Note that both paths are connected in a landscape of varying hexadecapole moment, which is not constrained in the calculation here. The points with error bars, which are drawn at arbitrary deformations, indicate the empirical barriers and minima. The mean-field result overestimates the barriers a bit. Vibrational and rotational corrections will probably help to come closer to the data.

Figure 16 shows the potential-energy surfaces of ^{240}Pu for a variety of forces. The typical pattern of a double-humped barrier is reproduced by every mean-field model. There are quantitative differences in the barrier height and depth of the second minimum. The Gogny force D1S produces rather high barriers. The relativistic mean-field forces, on the other hand, predict low barriers and a low second minimum, while all Skyrme Hartree-Fock forces fall in between. These differences between the interactions are even more pronounced for superheavy elements around $Z \approx 116$, where Skyrme forces strongly stabilize against fission, while the relativistic mean-field forces show only shallow barriers, which increase again towards the next shell closures (Ćwiok *et al.*, 1996; Bender, Rutz, *et al.*, 1998; Berger *et al.*, 2001). However, the comparison is a bit touchy for the Gogny force D1S. One has to remember that this force has been adjusted on the fission barrier of ^{240}Pu to include a correction for rotation. Therefore, we also show in Fig. 16 the potential-energy surfaces for D1S where the rotational correction has been taken into account. This comes closer to the data. A similar correction should then be applied to all other forces as well. In fact, several other zero-point corrections also had to be included. These are not yet available for the relativistic

mean-field model. At present the most consistent way is to compare just the uncorrected potential-energy surfaces, as is done in Fig. 16.

4. Superdeformed states and fission isomers

Fission isomers are a special case of superdeformed minima which appear very often in heavy elements. There are some experimental data on the absolute excitation energies of superdeformed minima at zero spin. These provide information on the magnitude of shell effects in the second well. A test of several Skyrme interactions (Heenen *et al.*, 1998; Takahara *et al.*, 1998) has shown that they reproduce particle separation energies within a well much better than absolute excitation energies. This suggests that configuration mixing (for examples, see Bonche *et al.*, 1989, 1990a, 1990b, 1991, 1994, 1996) and symmetry restoration or at least dynamical zero-point energy corrections (see Girod and Reinhard, 1982b; Delaroche *et al.*, 1989, 1994; Deloncle *et al.*, 1989; Libert *et al.*, 1999) have to be taken into account. However, the experimental data have up to now been too limited to permit conclusive studies.

Transition probabilities from fission isomers to the ground state have been measured experimentally for $^{236,8}\text{U}$. Their determination by a generator-coordinate-method calculation including mean-field states in the two wells allows us to test the topology of the barrier because quantum tunneling is extremely sensitive to the height and thickness of the barrier (Chinn *et al.*, 1992; Krieger *et al.*, 1994, 1996). Theoretical lifetimes agree with experimental ones within two orders of magnitude, which gives us some confidence in the ability of mean-field calculations to describe the topology of the first barrier correctly.

5. Octupole deformation

Observation of negative-parity states at very low excitation energies was the first evidence that nuclei might have a shape that is reflection asymmetric, such as a pear shape. Extensive investigations have led to the conclusion that these shapes are not as stable as quadrupole deformations. Butler and Nazarewicz have given both a short introduction to the subject (1991) and an extensive review (1996). There are now a few examples of nuclei exhibiting negative-parity bands at low excitation energy, which can be related to intrinsic shapes with parity-breaking multipole moments. Examples are ^{20}Ne and nuclei around ^{146}Ba and ^{222}Th . Octupole instability was first analyzed in terms of shell effects within the framework of mic-mac models (Leander *et al.*, 1982; Nazarewicz *et al.*, 1984). Soon after the pioneering calculations of ^{222}Ra with the Skyrme interaction SIII by Bonche *et al.* (1986), the intrinsic octupole deformation of Ra isotopes was investigated by Robledo *et al.* (1987) with the Gogny interaction D1S. It was found that octupole deformations do not yield a large gain in energies. Depending on the interaction, one obtains either a shallow minimum or a very flat octupole potential-energy surface. Thus one needs configuration mixing and parity

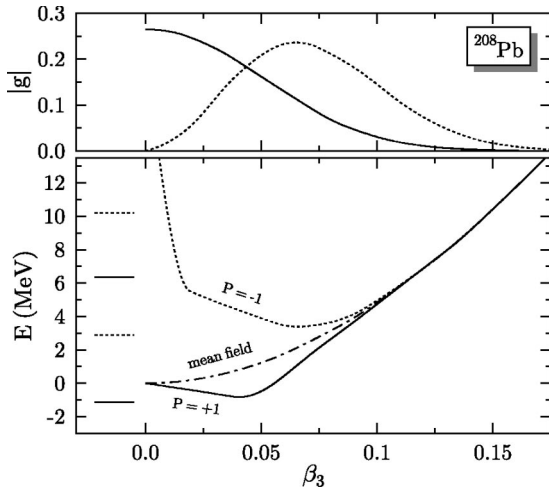


FIG. 17. Octupole deformation properties in ^{208}Pb computed with SLy4. The lower panel shows the potential-energy surfaces from mean-field and parity projected calculations as indicated. The upper panel shows the collective wave functions $g_k(\beta_3)$, Eq. (78), for ground state and first excitation. Data taken from Heenen, Valor, Bender, Bonche, and Flocard (2001).

projection. This was first done in the framework of a collective Schrödinger equation approximation to the generator-coordinate method (see Sec. III.A.2.d) with either adiabatic TDHF or generator-coordinate method masses (Robledo *et al.*, 1988; Egido and Robledo, 1989, 1990, 1992). Full parity projection after variation was subsequently performed for studies of octupole ground-state correlations in several regions of the nuclear chart with the Gogny interaction by Egido and Robledo (1991) and with the Skyrme interaction including configuration mixing by the generator coordinate method by Skalski, Heenen, and Bonche (1993) and Heenen, Skalski, *et al.* (1994). Good agreement with the experimental data was obtained, in particular for $E1$ transition probabilities determined with the Gogny interaction. Symmetry-unrestricted Skyrme HFB calculations of $N = Z$ nuclei from ^{64}Ge to ^{84}Mo (Yamagami *et al.*, 2001) have demonstrated the extreme softness of these nuclei against nonaxial octupole deformations in several excited states.

Figure 17 illustrates for the case of ^{208}Pb (Heenen, Valor, Bender, *et al.*, 2001) how octupole deformations develop due to the inclusion of correlations. The mean-field potential-energy surface of ^{208}Pb is flat as a function of octupole deformations and presents a minimum at spherical shape. When projecting on parity for each value of the octupole moment, one obtains a different potential-energy surface for each parity. Since there is no energy gain by projection for the spherical configuration, a shallow well develops for the positive parity, with a minimum for a small, nonzero value of the octupole moment. The minimum of the curve projected on negative parity appears for a much larger octupole deformation. The generator-coordinate method mixes mean-field states corresponding to different octupole moments. This yields a spectrum of states. The energy

difference between the first states of both parities is rather close to the energy difference between the minima of the wells of both parity. One must note that the positive-parity wave function has a maximum value in the spherical shape and spreads approximately like a Gaussian over octupole deformations. Conversely, the maximum of the lowest GCM state of negative parity corresponds to the minimum of the potential-energy surface with negative parity.

The ground-state shapes of Ra and Th isotopes have been investigated within the relativistic mean-field method by Rutz *et al.* (1995). Several studies have also been devoted to the investigation of octupole deformations in the superdeformed well of nuclei in the Hg-Pb mass region. There is indeed experimental evidence (Wilson *et al.*, 1996) that some superdeformed rotational bands are generated by the rotation of reflection-asymmetric intrinsic states. Parity projected calculations of octupole deformations in the superdeformed well in ^{194}Pb were investigated by Bonche *et al.* (1991). A coupled quadrupole-octupole generator-coordinate-method study of ^{194}Pb , including all the quadrupole deformations from the spherical ground state to the superdeformed intrinsic state, was performed by Meyer *et al.* (1995). This enabled these authors to determine octupole-phonon states in both wells. The nonaxial octupole modes were calculated by Skalski, Heenen, Bonche, Flocard, and Meyer (1993), showing, in contrast to non-self-consistent calculations, that nonaxial modes are not energetically favored. The same formalism was used by Heenen and Skalski (1996) to describe the coupling between the octupole and isovector dipole modes in the normally deformed nucleus ^{152}Sm and in the superdeformed ^{190}Hg . They showed that the low-energy states of negative parity are well described without the inclusion of the dipole degree of freedom. Inclusion of isovector dipole deformations permits a satisfactory description of the giant dipole resonance simultaneously with the low energy octupole excitations.

Reflection-asymmetric shapes have been much less studied for rotating nuclei. A symmetry-unrestricted cranked Skyrme Hartree-Fock calculation of high-spin states in ^{32}S was performed by Yamagami and Matsuyanagi (2000), who showed that nonaxial deformations of Y_{31} type play a role above spin 5. The transition to octupole deformations at high spin for $N=88$ isotopes around ^{144}Ba is discussed by Garrote *et al.* (1997, 1998) in a cranking approach using the Gogny interaction.

E. Q_α values in superheavy elements

Superheavy elements have attracted much interest in the past and continue to do so. This interest is motivated by the general interest in extending the table of elements up to the limits of stability and finding new shell closures. Superheavy elements provide a testing ground for nuclear models as they probe the interplay of the collective effects triggered by the strong repulsive Coulomb field and details of the stabilizing shell structure.

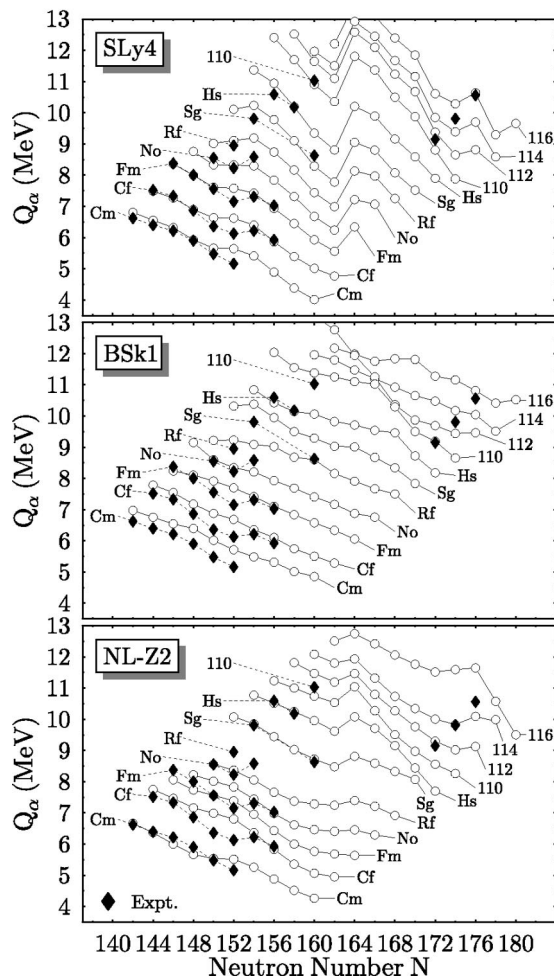


FIG. 18. Q_α values of even-even superheavy elements as predicted by self-consistent mean-field models. Experimental values are taken from Audi and Wapstra (1995), Hofmann *et al.* (2000), and Oganessian *et al.* (2001); SLy4 values are from Cwiok *et al.* (1999), NL-Z2 values are from Bender (2000); and BSk1 values are from Samyn *et al.* (2002). Experimental values at the upper right corner are for $Z = 116, 114,$ and 112 .

Experimental data on superheavy nuclei are still sparse (Hofmann, 1998; Armbruster, 2000; Hofmann and Münzenberg, 2000); in most cases the only available observable is the α -decay energy release $Q_\alpha(N, Z) = E(N, Z) - E(N-2, Z-2) - E(2, 2)$, which is a differential observable similar to the two-nucleon separation energies, Eq. (119). Figure 18 compares calculated and experimental systematics of Q_α in the regime of the heaviest observed elements. Large gaps between the curves and kinks within the curves are related to deformed proton and neutron shells, respectively. All forces reproduce the overall pattern of the Q_α , but there are differences among the forces in the shift between experimental and calculated curves for a given Z , as well as in the appearance or position of kinks in the trends with respect to N . Keep in mind that BSk1 with its large m_0^*/m has the smoothest trends, even smoother than the data. The parametrizations differ in their predictions for the next spherical shell closures (see Fig. 8).

On the basis of the currently available data for Q_α (for even nuclei), none of the parametrizations is to be preferred, although we see clear differences among them.

Figure 18 covers a transition from well-deformed nuclei at the lower end up to transitional nuclei close to the next shell closures (Cwiok *et al.*, 1996; Bürvenich *et al.*, 1998), which is reflected in an increased softness of the deformation energy surfaces with increased Z . The heaviest nuclei shown cannot be safely described on the mean-field level; including long-range correlations will alter the systematics of Q_α similarly to the findings for S_{2n} discussed in Sec. VI.F.2.

Results in Fig. 18 are for even nuclei only. There are more data for odd nuclei, but their modeling is as involved as the calculation of separation energies discussed in Sec. VI.B.1. It is by no means guaranteed that experimental data refer to transitions between the lowest quasiparticle states. Selected decay chains are investigated by Cwiok *et al.* (1999) and Bender (2000).

F. Excitations

1. Rotational bands

The 1990s saw a significant breakthrough for mean-field methods in the calculation of rotational bands in several regions of the nuclear chart, in particular for nuclei in which superdeformed rotational bands have been detected experimentally (Garett *et al.*, 1986; Nolan and Twin, 1988; Janssens and Khoo, 1991; Baktash *et al.*, 1995). Before that time, mean-field calculations were performed either with simple interactions in a restricted space (see, for instance, Egido *et al.*, 1980a, 1980b) or within a pure Hartree-Fock framework (Passler and Mosel, 1976; Fleckner *et al.*, 1979; Bonche *et al.*, 1987). A major numerical difficulty in handling rotating nuclei is that time-reversal invariance is broken, with the consequence that one cannot treat pairing correlations in the BCS approximation. But pairing correlations are inevitably needed because superdeformed bands have been detected down to very low spin. This is particularly true around $A \approx 190$, where the moment of inertia of the bands varies strongly as a function of spin, a clear sign of varying pairing correlations.

All the variants of the mean-field methods discussed here have now been applied to the study of superdeformed bands and usually have shown surprisingly good agreement with the experimental data. Recent references include studies of superdeformed bands in the $A \approx 190$ mass region with the Skyrme Hartree-Fock-Bogoliubov method (Terasaki *et al.*, 1995, 1997b), with the Gogny force (Girod *et al.*, 1994; Valor *et al.*, 2000a, 2000b), and with the relativistic mean-field method (Afanasjev and Ring, 2000; Afanasjev *et al.*, 2000). Very recently, rotational bands were detected in ^{252}No (Reiter *et al.*, 2000) and there are experiments underway to measure bands in superheavy odd- A isotopes. This will provide a unique opportunity to test the quasiparticle spectra of the pairing correlations in very heavy nuclei and the validity of mean-field interactions for extrapola-

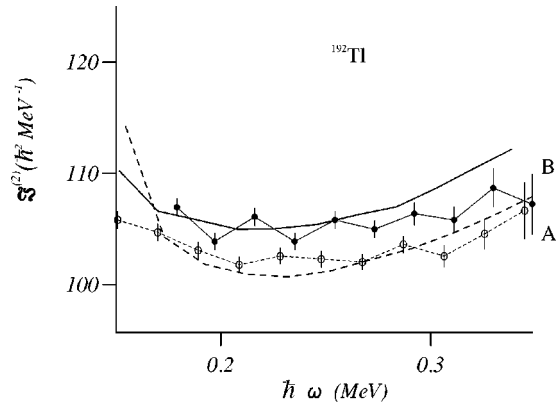


FIG. 19. Dynamical moment of inertia $\mathcal{J}^{(2)}$, which is equal to the second derivative of the energy with respect to the rotational frequency ω , for two rotational bands in ^{192}Tl calculated with density-dependent pairing and the SLy4 interaction (Heenen and Janssens, 1998). Experimental data are taken from Han and Wu (1999).

tion to superheavy nuclei. Up to now, Skyrme Hartree-Fock-Bogoliubov calculations (Duguet *et al.*, 2001) and calculations with the Gogny interaction (Egido and Robledo, 2000) nicely reproduce the experimental data.

The study of rotational bands extending up to very high spins has shown the necessity of treating pairing correlations beyond the HFB method. Indeed, at this level of approximation, pairing correlations collapse abruptly as a function of the rotational frequency, leading to an unphysical phase transition (Gall *et al.*, 1994). The best way to cure this deficiency would be to perform a variation after projection (VAP) on particle numbers. Up to now, all applications have used an approximate VAP by means of the Lipkin-Nogami method which has proven sufficient to avoid an abrupt pairing collapse.

Besides the nice reproduction of moments of inertia of even nuclei, calculations of the large number of one- and two-quasiparticle bands that have been detected have increased our confidence in the quasiparticle spectra predicted by the mean-field interactions. Figure 19 compares two bands calculated with the SLy4 Skyrme force with the data for an odd-odd isotope ^{192}Tl . These bands correspond to two different one-quasiparticle excitations on an even vacuum. The agreement between data and theory is very nice; in particular, the relative magnitudes of the moments of inertia is well reproduced. Several similar results have allowed us to assign the excited bands to specific quasiparticle excitations.

The study of rotational bands has also initiated investigations of the importance of time-odd terms in Skyrme interactions (Dobaczewski and Dudek, 1995), and of time-odd fields in relativistic Lagrangians (Afnasjev and Ring, 2000). Rotational bands might be the appropriate tool to constrain these time-odd components (Bender, Dobaczewski, *et al.*, 2002). However, more systematic studies remain to be done.

Recent progress in realistic shell-model calculations allows the calculation of medium-mass nuclei by these methods. Thus medium-mass nuclei are a good place to compare mean-field and shell-model calculations. Cau-

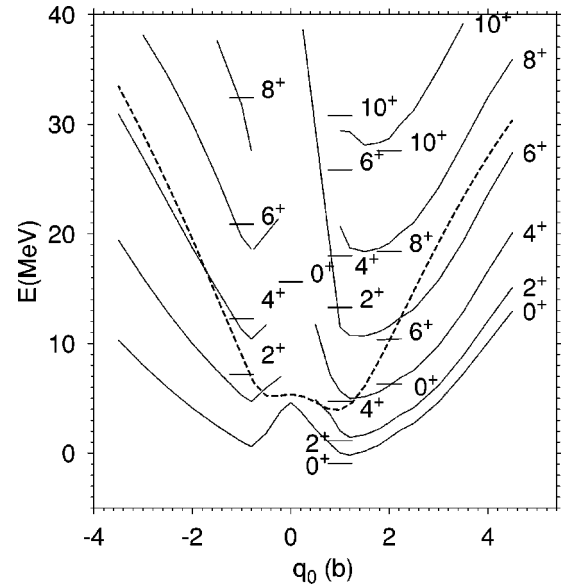


FIG. 20. Projected potential-energy surfaces of ^{24}Mg for angular momentum $J=0$ to 10, as a function of the axial quadrupole moment q_0 of the state that is projected. The dashed curve is the mean-field result. The first three energies obtained for each J in the configuration-mixing calculation are represented by horizontal bars centered at the value of q_0 where the respective collective wave functions have their largest value. Taken from Valor, Heenen, and Bonche (2000).

rier *et al.* (1995) have compared spherical shell-model calculations with cranked HFB using the Gogny interaction for ^{48}Cr . The rotational band of this nucleus is known up to spin 16. It shows a backbend which is reproduced by both calculations. However, the mean-field moment of inertia is too large, while the shell-model result agrees with the experimental data. This hints at a deficiency in the treatment of pairing correlations. In particular, no neutron-proton $T=0$ pairing is taken into account in the mean-field calculations.

2. Low-energy spectra

a. Light nuclei

We have seen in Sec. VI.D.2 that the description of light nuclei requires the introduction of correlations beyond a mean-field approach. Let us look first at the effect of these correlations for the stable nucleus ^{24}Mg , which is well deformed in its ground state. The axial quadrupole potential-energy surfaces presented in Fig. 20 (obtained with SLy4 and a density-dependent delta pairing) show a mean-field minimum for a quadrupole moment around 2 b. Potential-energy surfaces for angular momenta values ranging from 0 to 10 are obtained by projecting the mean-field wave functions for each quadrupole moment onto good angular momentum and particle numbers. As expected from the usual estimates of zero-point energy motion, the restoration of each mode brings a gain of energy of around 2 MeV. The mean-field wave function corresponding to the minimum of the $J=0$ projected curve has a quadrupole moment slightly

larger than the minimum of the intrinsic curve. The position of this minimum does not vary significantly with angular momentum. Configuration mixing with respect to the quadrupole moment of the mean-field states still brings a small gain in energy, but much smaller than the restoration of symmetry. As expected for a vibrational correlation as well, it slightly decreases the mean quadrupole moment of the mixing and brings it back to the value of the intrinsic curve. Thanks to the symmetry restoration, transition probabilities between the different states can be calculated directly in the laboratory frame of reference and compared to the experimental data without having to introduce approximations.

Calculations along these lines have been done for several light nuclei. Many of these studies focus on the phenomenon of shape coexistence (see Heyde *et al.*, 1983 and Wood *et al.*, 1992 for reviews) or on the evolution of the $N=20$ and $N=28$ shell closures in neutron-rich nuclei. Some of the calculations rely on the Bohr Hamiltonian approximation of the generator-coordinate method [see, for example, Reinhard *et al.* (1999), who use Skyrme interactions or Peru *et al.* (2000), who use the Gogny force]. Configuration-mixing calculations of angular momentum projected wave functions using the Gogny force have been performed for some Mg and Si isotopes (Rodríguez-Guzmán *et al.*, 2000a) and for a possible superdeformed band in ^{32}S (Rodríguez-Guzmán *et al.*, 2000c). The quadrupole collectivity has been investigated with the same model for $N \approx 20$ nuclei by Rodríguez-Guzmán *et al.* (2000b), and $N \approx 28$ nuclei by Rodríguez-Guzmán *et al.* (2002). Finally, a configuration mixing of many-body states with different quadrupole moments, projected onto angular momentum and particle number, has been performed for ^{32}S with a Skyrme interaction and a density-dependent delta pairing force by Heenen, Valor, and Bonche (2001).

In all these applications, the correlations beyond the mean field provided by the symmetry restorations and the configuration mixing significantly improve the agreement with experimental data. They also confirm the result based on simpler models that magic numbers like $N=28$ are not preserved far from stability. These first explorations demonstrate the need for correlations and better mean-field models in light nuclei.

b. Deformation effects in medium-mass nuclei

The light Sr isotopes are a good example of nuclei whose shape varies rapidly with changing neutron number. ^{88}Sr is a spherical nucleus, due to the neutron shell closure at $N=50$, while ^{78}Sr is strongly deformed. The potential-energy surfaces of the intermediate isotopes are extremely soft against triaxial quadrupole deformations, with several minima of very different shapes but similar energies. This prevents a meaningful comparison of the charge radii with experiment. Although the minima have similar energies, their radii are quite different. Such a deficiency can be corrected by performing a configuration mixing by the generator-coordinate method. This has been done by Heenen, Bonche, *et al.* (1993). The mean-field wave functions for a grid of tri-

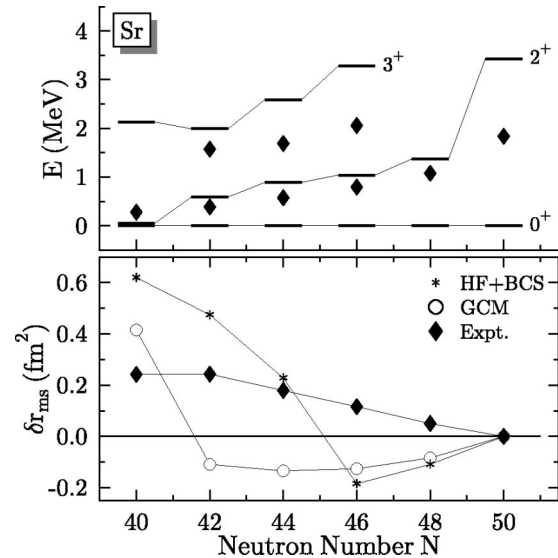


FIG. 21. Isotopic shifts (bottom) and excitation energies of the first 2^+ and 3^+ states (top) for light Sr isotopes. The theoretical results are obtained from HF+BCS+LN calculations with the Skyrme force SIII and a schematic seniority pairing interaction, and from generator-coordinate method calculations on triaxial quadrupole mean-field wave functions projected on particle number (Heenen *et al.*, 1993). Experimental values for δr_{ms} are taken from Buchinger *et al.* (1990), while excitation energies are taken from Kinsey *et al.* (1997).

axial quadrupole moments were generated by Hartree-Fock+BCS+Lipkin-Nogami (HF+BCX+LN) calculations with the SIII Skyrme interaction and a seniority pairing. They were mixed by a generator-coordinate method calculation after particle-number projection. Partial restoration of angular momentum was also performed by mixing the six possible orientations of the principle axes of the nucleus along the axes of the intrinsic frame of reference. Results are shown in Fig. 21 for the excitation energies of the lowest 2^+ and 3^+ states obtained after the approximate angular momentum projection, and for the isotopic shifts. The decrease in the excitation energy of the first 2^+ from $N=50$ to $N=40$ is a consequence of the gradual appearance of deformations. It agrees qualitatively with experiment. The isotopic shifts are greatly affected by the mixing of configurations. The ambiguities of the mean-field calculation are removed thanks to configuration mixing. However, the increase of the isotopic shift with decreasing neutron number is not reproduced for the intermediate isotopes. An exact restoration of angular momentum would favor an increase of deformations and its lack is probably the major source of discrepancy in the present example.

c. Ground-state correlations and mass systematics

Figure 22 shows, together with the experimental data, the two-neutron separation energies calculated around ^{68}Ni (Reinhard, Bender, *et al.*, 2000) and around ^{208}Pb (Heenen, Valor, Bender, Bonche, and Flocard, 2001) with the SkI4 and SLy4 parametrizations, respectively. In both cases, the mean-field results are obtained from

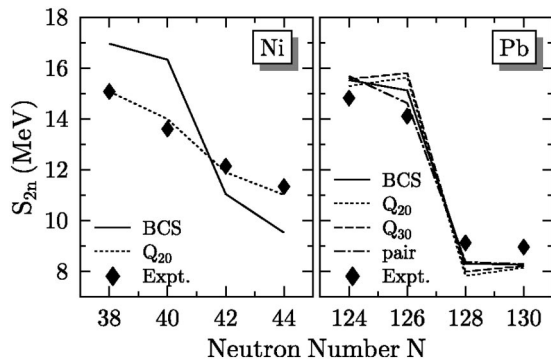


FIG. 22. Influence of ground-state correlations on the S_{2n} around ^{68}Ni (left panel) and ^{208}Pb (right panel). Q_{20} , Q_{30} , and “pair” denote quadrupole, octupole, and pair vibrations, respectively. Data taken from Reinhard, Bender, *et al.* (2000) (^{68}Ni) and Heenen, Valor, Bender, Bonche, and Flocard (2001) (^{208}Pb).

Skyrme-HF+BCS+LN calculations employing a density-dependent delta force. Correlations beyond the mean field are included in both cases, for Ni with the Gaussian overlap approximation of the generator-coordinate method and for Pb with particle-number projected generator-coordinate method calculations. The inclusion of quadrupole correlations in the Ni case significantly modifies the mean-field S_{2n} and brings them close to the experimental data. For Pb isotopes, several collective variables have been explored but none of them allows us to obtain the same quality of agreement with the data as that for Ni. The mode that most strongly affects the Pb results is pairing vibration. The difference between Ni and Pb is probably related to their different “magicity”: the $N=126$ gap in ^{208}Pb is much larger than the $N=40$ gap in ^{68}Ni , which means that collective quadrupole vibrations are much softer in ^{68}Ni than in ^{208}Pb .

3. Giant resonances

An important characteristic of nuclear excitation spectra is the presence of giant resonances (Speth and van der Woude, 1981; Goeke and Speth, 1982; Speth and Wambach 1991; van der Woude, 1991; Bertsch and Broglia, 1994; Bortignon *et al.*, 1998). This mode appears in almost any multipolarity and isospin channel. The most prominent resonances are the isovector dipole, which is in lowest order a collective oscillation of the proton against the neutron density, the isoscalar monopole, which is a radial vibration of the nucleus as a whole (“breathing mode”), and the isoscalar quadrupole, which corresponds to small collective quadrupole oscillations. These modes show up in an energy range of 10–30 MeV, where a large fraction of the multipole sum rules are exhausted. They explore only small-amplitude oscillations around the nuclear ground state and are thus ideally suited for a description in terms of the RPA.

There is a long-standing history of microscopic calculations of giant resonances. Several of them rely on phenomenologically adjusted model potentials with effec-

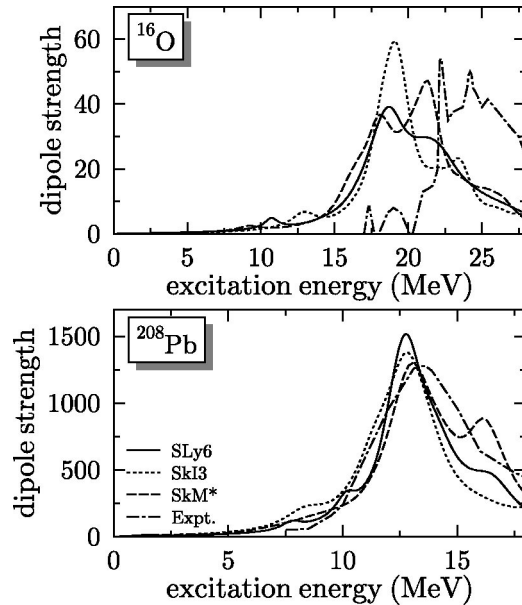


FIG. 23. Random-phase approximation results for the dipole strength distributions in ^{16}O (upper panel) and ^{208}Pb (lower panel) for various forces indicated. The discrete RPA spectra have been folded with a Lorentzian of width 1 MeV to account roughly for escape width and collisional broadening. Experimental photoneutron cross sections are taken from Dietrich and Bermann (1988).

tive residual interactions, for reviews see Goeke and Speth (1982) and Speth and Wambach (1991). There is also a large body of RPA calculations based on self-consistent mean-field models with Skyrme interactions [for recent compilations see Colo *et al.* (1995) and Reinhard (1999)], and the Gogny force (Blaziot *et al.*, 1976; Blaziot and Gogny, 1977). The first RPA results based on the relativistic mean-field approach were published recently (Vretenar, Wandelt, and Ring 2000; Ma *et al.*, 2001; Ring *et al.*, 2001; Vretenar *et al.*, 2001a, 2001b, 2002). We shall give here a brief overview of the three most important resonances: the isoscalar monopole ($L=0$, $T=0$), the isovector dipole ($L=1$, $T=1$), and the isoscalar quadrupole ($L=2$, $T=0$).

In Fig. 23, the dipole strength distribution in ^{16}O and in ^{208}Pb , calculated with three different Skyrme forces, is compared to photoneutron experiments. The resonance in ^{208}Pb shows a nicely dominating peak, in experiment as well as in calculations. In fact, this peak is strongly fragmented by interference with one-particle/one-hole states (Landau fragmentation), but the coupling to other modes (escape width and nucleon-nucleon collisions) smooths the detailed structure in such a way that one broad peak remains visible. A thorough treatment of all contributions to the width goes beyond the RPA (Bertsch *et al.*, 1983). For ^{208}Pb the Landau fragmentation (included in the RPA) is the dominant contribution (about 2/3) while the escape (included in the continuum RPA) and collisional widths are responsible for about 1/3 of the width (Reinhard, Yadav, and Toepffer, 1986). All three theoretical results for ^{208}Pb are close to the experimental curve. The picture looks quite differ-

TABLE V. The peak positions of the most important giant resonances in ^{208}Pb computed with the RPA for various forces and compared with experimental values. All energies are given in MeV.

	$L=1, T=1$	$L=2, T=0$	$L=0, T=0$
Expt.	13.6	11.2	14.2
SIII	14.1	12.0	17.5
SkM*	13.0	11.6	14.0
SkP	12.5	10.3	13.2
SLy6	12.8	12.5	14.5
SkI3	12.7	13.7	15.3
SkI4	12.7	13.0	15.1
MSk5	11.4	10.3	14.1
SkT6	14.5	12.4	9.9
NL3	12.9	11.3	13.8

ent for a light nucleus such as ^{16}O . The lower density of one-particle/one-hole states leaves a detailed fragmentation pattern apparent in the smoothed strengths, in qualitative agreement with the data. All forces systematically produce too low a resonance energy. This leads to the conclusion that the A dependence of the asymmetry energy is underestimated by present-day mean-field interactions, although the precise reasons for this mismatch are not yet fully understood.

We confine further considerations to the safe case of ^{208}Pb . Here, all major giant resonances show a clear single-peak structure and comparisons can be made on the grounds of peak positions. This introduces a small ambiguity in comparison with the experimental data. Figure 23 shows that the spectral distribution is asymmetric. Thus the position of the maximum depends slightly on the folding width of the Lorentzian used on the discrete RPA results. We have to assume an uncertainty of about ± 0.5 MeV for the resonance energy.

Table V shows results for the three major resonances computed with a broad selection of forces. We see that most forces perform very well for the dipole resonance. The interaction MSk5, which has been exclusively adjusted to all known masses, is the only one to underestimate the energy of the resonance significantly. The position of the dipole resonance is determined by bulk parameters: the symmetry energy coefficient a_{sym} , the sum-rule enhancement factor κ_{TKR} , and the density dependence of the symmetry energy coefficient $\partial_{\rho}a_{\text{sym}}$. The resonance energy increases with increasing κ_{TKR} , while it decreases with increasing a_{sym} ; cf. Table III. The latter trend is unexpected. It stems from a strong link to $\partial_{\rho}a_{\text{sym}}$ in the ground-state fits (Reinhard, 1999). The various influences on the peak position inhibit direct access to a_{sym} by these data.

The results for the isoscalar quadrupole resonance gather nicely around the experimental value. It is well known that the resonance position is uniquely related to the isoscalar effective mass (Brack *et al.*, 1985). Standard Skyrme Hartree-Fock parametrizations with $m_0^*/m = 0.8$ fit the resonance best (Reinhard, 1999). It is clear that parametrizations with $m_0^*/m = 1$ (here SkP and

MSk5) yield values that are too low while forces with low effective mass (SkI3, SkI4, SLy6) predict resonance energies that are too large. See also Sec. V.A.3.

The position of the isoscalar monopole resonance is closely related to the incompressibility (Blaizot, 1980; Blaizot *et al.*, 1995). The far too high value obtained from the early parametrizations, e.g., SIII, was one of the motivations for extending the model by allowing $\alpha < 1$ in the exponent of the density dependence [see Eq. (50) and Krivine *et al.* (1980)]. The more recent forces perform fairly well for this component. Note that the monopole resonance has not been fitted but comes out as a prediction from the force. Nuclear surface properties and trends with respect to mass number also carry a lot of (indirect) information on the incompressibility. These seem to go in the right direction once α has been allowed to take on values less than 1.

In sum, we see that there is a world of valuable information in the resonance excitation spectra, even more when taking into account isotopic trends and trends in system size. Other modes carry further information, which has yet to be thoroughly examined.

The extrapolation of giant resonance properties to nuclei far from stability has been extensively discussed by Hamamoto *et al.* (1997a, 1997b, 1997c, 1998) using Skyrme interactions (see also Sagawa and Esbensen, 2001).

4. Excitations of unnatural parity and β decay

The previous section dealt with giant resonances of natural parity. Here we look briefly at excitations with unnatural parity, i.e., $J^{\pi} = 0^{-}, 1^{+}, 2^{-}$, etc., which are still in the early stages of exploration. The dominant isoscalar modes have magnetic dipole ($M1$) structure and spin and orbital current contributions. Orbital $M1$ strength is related to the nuclear scissors mode which has been observed by Bohle *et al.* (1984; see Iudice, 1997 for more details). The most prominent isovector mode is the Gamov-Teller spin-isospin resonance which is observed in charge-exchange reactions (for reviews, see Gaarde *et al.*, 1981; Osterfeld, 1991, 1992). Most calculations discuss strength distributions or simply the peak energies of the corresponding giant resonances obtained in quasiparticle RPA. Only models based on Skyrme interactions have been used so far.

There are two possible choices for \mathcal{E}_{odd} in the Skyrme interaction (see Sec. II.A.2), which differ significantly when modeling unnatural parity states. RPA calculations using the two-body Skyrme force, Eq. (55), are reported by Auerbach and Klein (1984), Hamamoto (1999), Hamamoto and Sagawa (2000), and Suzuki and Sagawa (2000) for $M1$ strength and by Colo *et al.* (1994), Hamamoto and Sagawa (1993), Van Giai and Sagawa (1981), Sagawa *et al.* (1995), and Suzuki and Sagawa (2000) for Gamov-Teller resonances (though the calculations are not always done in a fully self-consistent way; see, Bender, Dobaczewski, *et al.*, 2002). One finds a large scattering of predictions among the various Skyrme in-

teractions; some parametrizations are even unstable with respect to certain spin-excitation modes. This led to the parametrization SGII of Van Giai and Sagawa (1981) tailored for this particular purpose. To understand this deficiency of Skyrme interactions, one has to remember that the dominant contribution from the residual interaction (see Sec. III.C.2) to unnatural parity states stems from the time-odd part \mathcal{E}_{odd} of the effective interaction, Eq. (49). Within the two-body Skyrme force framework, the coupling constants of the time-odd terms determined from Eq. (55) are a function of the time-even ones [see also Eq. (A1)]. The resulting dependence of \mathcal{E}_{odd} on $\mathcal{E}_{\text{even}}$ imposes, for example, a relation between Gamov-Teller properties and the isobaric analog state discussed by Colo *et al.* (1994, 1995). It seems that Eq. (55) does not offer enough versatility to describe the usual bulk properties and the Gamov-Teller response data at the same time. Furthermore, the usual fitting strategies do not constrain \mathcal{E}_{odd} as it does not contribute to the ground states of even-even nuclei and gives a small correction only when calculating odd- A nuclei or rotating nuclei (see Secs. II.A.2, VI.B.1, and VI.F.1). Excitation modes with unnatural parity deliver the only available data that are dominated by \mathcal{E}_{odd} . The energy-functional framework for the Skyrme interaction offers the freedom to adjust \mathcal{E}_{odd} to $M1$ or Gamov-Teller data without affecting $\mathcal{E}_{\text{even}}$. When constructing a time-odd Skyrme energy functional for Gamov-Teller studies, the simplest approach is to use only the isovector spin-spin term $\mathcal{E}_{\text{odd}} \sim s_{1t_3}^2$ (note that only the off-diagonal $t_3 = \pm 1$ terms contribute here). This is equivalent to a Landau-Migdal s -wave interaction with strength g'_0 (Bertsch, 1981). An attempt to adjust all the relevant parameters of the time-odd Skyrme energy functional to Gamov-Teller response data was undertaken by Bender, Dobaczewski, *et al.* (2002), who found that the available data do not uniquely determine all coupling constants.

Nothing is known about the performance of those mean-field models that do not have any freedom in their time-odd part, i.e., the Gogny force or the standard relativistic mean field (in the standard Lagrangian there are neither mesons nor couplings nor exchange terms which directly access the spin distribution).

Some applications use an even simpler separable schematic residual interaction, e.g., $v = \kappa_{\text{GT}} \hat{\sigma} \cdot \hat{\sigma}' \hat{\tau} \cdot \hat{\tau}'$ for Gamov-Teller studies. The coupling constant κ_{GT} has to be a function of A . Examples are the study of $M1$ resonances by Sarriguren *et al.* (1997) and the Gamov-Teller and β -decay studies of deformed nuclei by Sarriguren *et al.* (2001). Although in both cases the coupling constant κ is estimated from the Landau parameters of the two-body Skyrme force, the quality of this approximation to a fully self-consistent calculation is unclear. This is because the schematic interaction thus obtained is not equivalent to the Landau interaction (Gaarde *et al.*, 1981), nor is the Landau interaction in infinite nuclear matter equivalent to the original Skyrme interaction in finite nuclei (Bender, Dobaczewski, *et al.*, 2002).

It is to be noted that for a complete description of Gamov-Teller properties the strength distribution re-

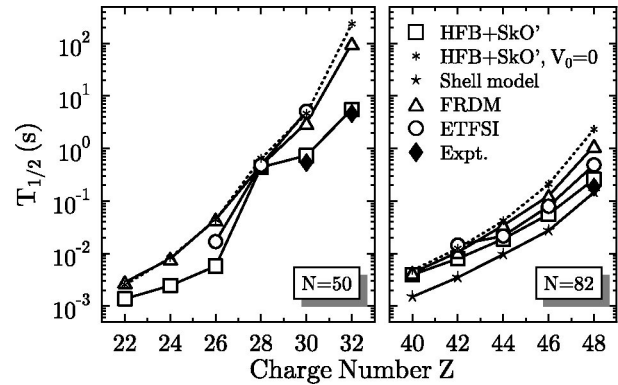


FIG. 24. Predictions for the half-lives of closed neutron-shell nuclei along the r -process path from quasiparticle RPA calculations. \square , HFB+SkO' results are shown with $T=0$ pairing; $*$, (HFB+SkO', $V_0=0$) without $T=0$ pairing. Data taken from Engel *et al.* (1999) and Martínez-Pinedo and Langanke (1999) (shell model).

quires us to take into account intrinsic degrees of freedom of the nucleon (see Sagawa and Van Giai, 1982) for a generalized model including Δ -hole excitations (see also Towner, 1987).

The low-energy tail of the Gamov-Teller strength distribution is explored by β^- decay. The key observable here is the decay rate, which is computed from the matrix element of $\hat{\sigma}\hat{\tau}$ augmented by a kinematic factor for the outgoing (e^- , $\bar{\nu}_e$) pair, which is very sensitive to the energy release Q_β . The modeling of β decay is complicated by the fact that proton-neutron $T=0$ pairing also contributes. The $T=0$ pairing interaction redistributes the low-energy tail of the Gamov-Teller strength distribution (therefore it can be safely neglected in Gamov-Teller resonance studies) that determines the β transition rates. Owing to the lack of other data, the $T=0$ pairing strength is fitted to β -decay data and so introduces an adjustable parameter into the modeling. Very few calculations consider proton-neutron pairing, as does the β^- -decay calculation of Borzov *et al.* (1996) for nuclei around ^{132}Sn based on the Fayans energy functional, using a phenomenological spin-spin residual interaction, or the study of neutron-rich nuclei by Engel *et al.* (1999) in which the same Skyrme force SkO' is used everywhere for the particle-hole channel. Typical results are shown in Fig. 24. Including $T=0$ pairing shortens half-lives by a factor of 2 to 5 times that of models without $T=0$ pairing. The shorter half-lives alter predictions for the abundance distribution of r -process elements and for the time it takes to synthesize them.

VII. CONCLUSIONS AND OUTLOOK

We have reviewed self-consistent models for nuclear structure and low-energy excitations. The formal basis is in every case the Hartree-Fock-Bogoliubov scheme. The actual models differ in their ansatz for parametrizing the effective forces or the energy-density functionals. The three most widely used forms have been considered: the Gogny force, the Skyrme energy functional, and the

relativistic mean-field model. In each case parametrizations exist which provide an excellent description of nuclear bulk properties. More than that, one can also accommodate very well excitation properties such as fission, vibrational states, rotations, and various giant resonances. Of course, differences in performance show up when looking at more subtle observables and when extrapolating far into the realm of exotic nuclei. This points to weaknesses in the existing models. At the same time, it provides interesting and helpful hints for further developments and a deeper understanding of the models. Thus the assessment is mixed. On the one hand, self-consistent mean-field models have reached a high descriptive and predictive power in many respects. On the other hand, there are many open problems calling for further investigation. Probably the most important next step is a proper and highly efficient inclusion of ground-state correlations. The precision of the mean-field description has reached such a high level that correlation effects can no longer be neglected. On the other hand, thanks to experimental progress related to the construction of exotic-beam facilities, many new data on nuclei far from stability should be available. They will constitute a great challenge for self-consistent mean-field methods and should allow us to specify more precisely the key ingredient of these models: the effective interaction.

ACKNOWLEDGMENTS

The authors thank the many colleagues who have helped with advice and with material for this article, J. Bartel, J.-F. Berger, P. Bonche, M. Brack, T. Bürvenich, J. Dobaczewski, S. Goriely, J. A. Maruhn, W. Nazarewicz, and D. Vretenar. This work has been supported in part by Bundesministerium für Bildung und Forschung (BMBF), Project No. 06 ER 808, and the PAI-P5-07 of the Belgian Office for Scientific Policy. M.B. acknowledges support through a European Community Marie Curie Fellowship.

APPENDIX A: ENERGY-DENSITY FUNCTIONAL FROM THE TWO-BODY SKYRME FORCE

Calculating the Hartree-Fock expectation value $\langle \text{HF} | \hat{v}_{\text{Sk}} | \text{HF} \rangle$ of the standard Skyrme force [Eq. (56)] yields the energy functionals (48) and (49) with coupling constants given by

$$C_0^{\rho} = \frac{3}{8} t_0 + \frac{3}{48} t_3 \rho_0^{\alpha}, \quad (\text{A1})$$

$$\begin{aligned} C_1^{\rho} &= -\frac{1}{4} t_0 (\frac{1}{2} + x_0) - \frac{1}{24} t_3 (\frac{1}{2} + x_3) \rho_0^{\alpha}, \\ C_0^s &= -\frac{1}{4} t_0 (\frac{1}{2} - x_0) - \frac{1}{24} t_3 (\frac{1}{2} - x_3) \rho_0^{\alpha}, \\ C_1^s &= -\frac{1}{8} t_0 - \frac{1}{48} t_3 \rho_0^{\alpha}, \\ C_0^{\tau} &= \frac{3}{16} t_1 + \frac{1}{4} t_2 (\frac{5}{4} + x_2), \\ C_1^{\tau} &= -\frac{1}{8} t_1 (\frac{1}{2} + x_1) + \frac{1}{8} t_2 (\frac{1}{2} + x_2), \\ C_0^{sT} &= \eta_J [-\frac{1}{8} t_1 (\frac{1}{2} - x_1) + \frac{1}{8} t_2 (\frac{1}{2} + x_2)], \\ C_1^{sT} &= \eta_J (-\frac{1}{16} t_1 + \frac{1}{16} t_2), \\ C_0^{\Delta\rho} &= -\frac{9}{64} t_1 + \frac{1}{16} t_2 (\frac{5}{4} + x_2), \\ C_1^{\Delta\rho} &= \frac{3}{32} t_1 (\frac{1}{2} + x_1) + \frac{1}{32} t_2 (\frac{1}{2} + x_2), \\ C_0^{\Delta s} &= \frac{3}{32} t_1 (\frac{1}{2} - x_1) + \frac{1}{32} t_2 (\frac{1}{2} + x_2), \\ C_1^{\Delta s} &= \frac{3}{64} t_1 + \frac{1}{64} t_2, \\ C_0^{\nabla J} &= -\frac{3}{4} W_0, \\ C_1^{\nabla J} &= -\frac{1}{4} W_0, \\ C_0^{\nabla s} &= 0, \\ C_1^{\nabla s} &= 0, \end{aligned}$$

nine of which are independent. Although in this approach $\eta_J=1$, many parametrizations of the Skyrme interaction set $\eta_J=0$. For generalized Skyrme forces with more involved density dependencies, see the references on density dependence cited in Sec. II.A.2. For interactions with generalized spin-orbit interaction one obtains

$$C_0^{\nabla J} = -b_4 - \frac{1}{2} b_4', \quad C_1^{\nabla J} = -\frac{1}{2} b_4', \quad (\text{A2})$$

using the notation introduced by Reinhard and Flocard (1995). In the energy-density functional approach, one has additionally C_T^s , $C_T^{sT} = -C_T^J$, $C^{\Delta s}$, and $C^{\nabla s}$ as independent coupling constants.

APPENDIX B: THE NUCLEON FORM FACTOR

The computation of the charge density following Eq. (105) requires a folding with the intrinsic nucleon form factors. These are taken from electron scattering on protons and deuterons. They are given as the so-called Sachs form factors for isospin 0 and 1 in the form of a dipole fit (Simon *et al.*, 1980),

TABLE VI. The coefficients of the isospin-coupled Sachs form factors of the nucleons, Eq. (B1). The $b_{s,v}$ are given in units of fm^{-2} . The magnetic form factors are taken from Simon *et al.* (1980), the electric form factors from Walther (1986).

S	$a_{s,1}$	$a_{s,2}$	$a_{s,3}$	$a_{s,4}$	$b_{s,1}$	$b_{s,2}$	$b_{s,3}$	$b_{s,4}$
$E, I=0$	2.2907	-0.6777	-0.7923	0.1793	15.75	26.68	41.04	134.2
$E, I=1$	0.3681	1.2263	-0.6316	0.0372	5.00	15.02	44.08	154.2
M	0.6940	0.7190	-0.4180	0.0050	8.50	15.02	44.08	355.4

$$G_s = \sum_{\nu=1}^4 \frac{a_{s,\nu}}{1+k^2/b_{s,\nu}}, \quad (\text{B1})$$

for $s \in \{(E, I=0), (E, I=1), M\}$. The actual coefficients are displayed in Table VI. The isospin-coupled form factors are recoupled for our purposes to proton and neutron form factors, and the relativistic Darwin correction (see, for example, Bjorken and Drell, 1964; Friar and Negele, 1975) has to be added, finally yielding

$$G_{E,q} = \frac{1}{2} (G_{E,I=0} \pm G_{E,I=1}) \left(1 + \frac{\hbar^2 k^2}{2m_q} \right)^{-1/2}. \quad (\text{B2})$$

Note that the nucleon structure is taken into account only approximately because we are folding with the free form factors of the nucleons, thus neglecting medium effects and the off-shell effects of the nucleon.

The charge density $\rho_{\text{ch}}(r)$ is finally obtained from the charge form factor by the Fourier back transformation. But all other information is usually drawn directly from the form factor.

A similar procedure applies for the relativistic mean-field method. The relativistic Darwin corrections is, of course, not needed. And the spin-orbit densities are computed from the tensor densities $\nabla \cdot \sum_n v_n^2 \bar{\psi}_n \hat{\sigma} \psi_n$. For details see Reinhard (1989).

REFERENCES

- Abe, Y., S. Ayik, P.-G. Reinhard, and E. Suraud, 1996, Phys. Rep. **275**, 49.
- Åberg, S., H. Flocard, and W. Nazarewicz, 1990, Annu. Rev. Nucl. Part. Sci. **40**, 439.
- Åberg, S., P. B. Semmes, and W. Nazarewicz, 1997, Phys. Rev. C **56**, 1762; **58**, 3011(E).
- Aboussir, Y., J. M. Pearson, A. K. Dutta, and F. Tondeur, 1992, Nucl. Phys. A **549**, 155.
- Aboussir, Y., J. M. Pearson, A. K. Dutta, and F. Tondeur, 1995, At. Data Nucl. Data Tables **61**, 127.
- Afanasjev, A. V., and P. Ring, 2000, Phys. Rev. C **62**, 031302.
- Afanasjev, A. V., P. Ring, and J. König, 2000, Nucl. Phys. A **676**, 196.
- Anguiano, M., J. L. Egido, and L. M. Robledo, 2001a, Nucl. Phys. A **683**, 227.
- Anguiano, M., J. L. Egido, and L. M. Robledo, 2001b, Nucl. Phys. A **696**, 467.
- Armbruster, P., 2000, Annu. Rev. Nucl. Part. Sci. **50**, 411.
- Audi, G., and A. H. Wapstra, 1995, Nucl. Phys. A **595**, 409.
- Auerbach, N., and A. Klein, 1984, Phys. Rev. C **30**, 1032.
- Auerbach, N., C. Volpe, G. Colo, T. Suzuki, and Nguyen Van Giai, 2001, Nucl. Phys. A **687**, 289c.
- Bäckman, S.-O., A. D. Jackson, and J. Speth, 1975, Phys. Lett. **56B**, 209.
- Baktash, C., B. Haas, and W. Nazarewicz, 1995, Annu. Rev. Nucl. Part. Sci. **45**, 485.
- Balian, R., H. Flocard, and M. Vénéroni, 1999, Phys. Rep. **317**, 251.
- Balian, R., and M. Vénéroni, 1986, Ann. Phys. (N.Y.) **164**, 334.
- Balian, R., and M. Vénéroni, 1988, Ann. Phys. (N.Y.) **187**, 29.
- Balian, R., and M. Vénéroni, 1991, Ann. Phys. (N.Y.) **216**, 351.
- Baran, A., and W. Hohenberger, 1995, Phys. Rev. C **52**, 2242.
- Baran, A., and W. Hohenberger, 1996, Phys. Rev. C **53**, 1571.
- Baranger, M., and M. Vénéroni, 1978, Ann. Phys. (N.Y.) **114**, 123.
- Barranco, F., P. F. Bortignon, R. A. Broglia, G. Colo, and E. Vigezzi, 2001, Eur. Phys. J. A **11**, 385.
- Barranco, F., and R. A. Broglia, 1985, Phys. Lett. **151B**, 90.
- Bartel, J., and K. Bencheikh, 2002, Eur. Phys. J. A **14**, 179.
- Bartel, J., P. Quentin, M. Brack, C. Guet, and H.-B. Håkansson, 1982, Nucl. Phys. A **386**, 79.
- Bassichis, W. H., A. K. Kerman, and J. P. Svenne, 1967, Phys. Rev. **160**, 746.
- Batty, C. J., E. Friedman, H. J. Gils, and H. Rebel, 1989, Adv. Nucl. Phys. **19**, 1.
- Baye, D., and P.-H. Heenen, 1986, J. Phys. A **19**, 2041.
- Beiner, M., H. Flocard, Nguyen Van Giai, and P. Quentin, 1975, Nucl. Phys. A **238**, 29.
- Bell, J. S., and T. H. R. Skyrme, 1956, Philos. Mag. **1**, 1055.
- Bender, M., 1998, Ph.D. thesis (Johann Wolfgang Goethe-Universität, Frankfurt am Main).
- Bender, M., 2000, Phys. Rev. C **61**, 031302(R).
- Bender, M., 2001, in *Proceedings of the International Conference on Fusion Dynamics at the Extremes*, Dubna, Russia, edited by Y. T. Oganessian and V. I. Zagrabaev (World Scientific, Singapore), p. 51.
- Bender, M., T. Cornelius, G. A. Lalazissis, J. A. Maruhn, W. Nazarewicz, and P.-G. Reinhard, 2002, Eur. Phys. J. A **14**, 23.
- Bender, M., J. Dobaczewski, J. Engel, and W. Nazarewicz, 2002, Phys. Rev. C **65**, 054322.
- Bender, M., W. Nazarewicz, and P.-G. Reinhard, 2001, Phys. Lett. B **515**, 42.
- Bender, M., K. Rutz, P.-G. Reinhard, and J. A. Maruhn, 2000a, Eur. Phys. J. A **7**, 467.
- Bender, M., K. Rutz, P.-G. Reinhard, and J. A. Maruhn, 2000b, Eur. Phys. J. A **8**, 59.
- Bender, M., K. Rutz, P.-G. Reinhard, J. A. Maruhn, and W. Greiner, 1998, Phys. Rev. C **58**, 2126.
- Bender, M., K. Rutz, P.-G. Reinhard, J. A. Maruhn, and W. Greiner, 1999, Phys. Rev. C **60**, 034304.
- Bengtsson, R., T. Bengtsson, J. Dudek, G. Leander, W. Nazarewicz, and J. Zhang, 1987, Phys. Lett. B **183**, 1.
- Bennaceur, K., J. Dobaczewski, and M. Płoszajczak, 2000, Phys. Lett. B **496**, 154.
- Berger, J.-F., L. Bitaud, J. Decharge, M. Girod, and K. Dietrich, 2001, Nucl. Phys. A **685**, 1c.
- Berger, J.-F., M. Girod, and D. Gogny, 1984, Nucl. Phys. A **428**, 23c.
- Berger, J.-F., M. Girod, and D. Gogny, 1991, Comput. Phys. Commun. **63**, 365.
- Berger, J.-F., and K. Pomorski, 2000, Phys. Rev. Lett. **85**, 30.
- Bernard, V., and Nguyen Van Giai, 1980, Nucl. Phys. A **348**, 75.
- Bernardos, P., V. N. Fomenko, Nguyen Van Giai, M. Lopez-Quelle, S. Marcos, R. Niembro, and L. N. Savushkin, 1993, Phys. Rev. C **48**, 2665.
- Bertozzi, W., J. Friar, J. Heisenberg, and J. W. Negele, 1972, Phys. Lett. **41B**, 408.
- Bertsch, G. F., 1981, Nucl. Phys. A **354**, 157c.
- Bertsch, G. F., 1991, in *Computational Nuclear Physics I—Nuclear Structure*, edited by K. Langanke, J. A. Maruhn, and S. E. Koonin (Springer, Berlin), p. 75.
- Bertsch, G. F., P. F. Bortignon, and R. A. Broglia, 1983, Rev. Mod. Phys. **55**, 287.
- Bertsch, G. F., and R. Broglia, 1994, *Oscillations in Finite Quantum Systems* (Cambridge University, Cambridge, England).

- Bertsch, G. F., and H. Esbensen, 1991, *Ann. Phys. (N.Y.)* **209**, 327.
- Bertsch, G. F., and K. Stricker, 1976, *Phys. Rev. C* **13**, 1312.
- Bertsch, G. F., and S. F. Tsai, 1975, *Phys. Rep.* **18**, 125.
- Bjorken, J. D., and S. D. Drell, 1964, *Relativistic Quantum Mechanics* (McGraw-Hill, New York).
- Bjørnholm, S., and J. E. Lynn, 1980, *Rev. Mod. Phys.* **52**, 725.
- Blaizot, J. P., 1980, *Phys. Rep.* **64**, 171.
- Blaizot, J. P., J.-F. Berger, J. Dechargé, and M. Girod, 1995, *Nucl. Phys. A* **591**, 435.
- Blaizot, J. P., and D. Gogny, 1977, *Nucl. Phys. A* **284**, 429.
- Blaizot, J. P., D. Gogny, and B. Grammaticos, 1976, *Nucl. Phys. A* **265**, 315.
- Blaizot, J.-P., and G. Ripka, 1985, *Quantum Theory of Finite Systems* (MIT, Cambridge, MA).
- Bloch, C., and A. Messiah, 1962, *Nucl. Phys.* **39**, 95.
- Blum, V., J. Fink, P.-G. Reinhard, J. A. Maruhn, and W. Greiner, 1989, *Phys. Lett. B* **223**, 123.
- Blum, V., G. Lauritsch, J. A. Maruhn, and P.-G. Reinhard, 1992, *J. Comput. Phys.* **100**, 364.
- Blum, V., J. A. Maruhn, P.-G. Reinhard, and W. Greiner, 1994, *Phys. Lett. B* **323**, 262.
- Blunden, P. G., and M. J. Iqbal, 1987, *Phys. Lett. B* **196**, 295.
- Boguta, J., and A. R. Bodmer, 1977, *Nucl. Phys. A* **292**, 413.
- Bohigas, O., A. M. Lane, and J. Martorell, 1979, *Phys. Rep.* **51**, 267.
- Bohigas, O., and P. Leboeuf, 2002, *Phys. Rev. Lett.* **88**, 092502.
- Bohle, D., A. Richter, W. Steffen, A. E. L. Dieperink, N. L. Iudice, F. Palumbo, and O. Scholten, 1984, *Phys. Lett. B* **137**, 27.
- Bohm, D., and D. Pines, 1953, *Phys. Rev.* **92**, 609.
- Bohr, N., and J. A. Wheeler, 1939, *Phys. Rev.* **56**, 426.
- Bonche, P., E. Chabanat, B. Q. Chen, J. Dobaczewski, H. Flocard, B. Gall, P.-H. Heenen, J. Meyer, N. Tajima, and M. S. Weiss, 1994, *Nucl. Phys. A* **574**, 185c.
- Bonche, P., J. Dobaczewski, H. Flocard, P.-H. Heenen, and J. Meyer, 1990a, *Nucl. Phys. A* **510**, 466.
- Bonche, P., J. Dobaczewski, H. Flocard, S. J. Krieger, J. Meyer, and M. S. Weiss, 1990b, *Nucl. Phys. A* **519**, 509.
- Bonche, P., H. Flocard, and P.-H. Heenen, 1987, *Nucl. Phys. A* **467**, 115.
- Bonche, P., H. Flocard, and P.-H. Heenen, 1996, *Nucl. Phys. A* **598**, 169.
- Bonche, P., H. Flocard, P.-H. Heenen, S. J. Krieger, and M. S. Weiss, 1985, *Nucl. Phys. A* **443**, 39.
- Bonche, P., P.-H. Heenen, H. Flocard, and D. Vautherin, 1986, *Phys. Lett. B* **175**, 387.
- Bonche, P., S. E. Koonin, and J. W. Negele, 1976, *Phys. Rev. C* **13**, 1226.
- Bonche, P., S. J. Krieger, P. Quentin, M. S. Weiss, J. Meyer, M. Meyer, N. Redon, H. Flocard, and P.-H. Heenen, 1989, *Nucl. Phys. A* **500**, 308.
- Bonche, P., S. J. Krieger, M. S. Weiss, J. Dobaczewski, H. Flocard, and P.-H. Heenen, 1991, *Phys. Rev. Lett.* **66**, 876.
- Bortignon, P. F., A. Bracco, and R. A. Broglia, 1998, *Giant Resonances: Nuclear Structure at Finite Temperature*, Contemporary Concepts in Physics Series No. 10 (Taylor & Francis, New York).
- Borzov, I. N., S. A. Fayans, E. Krömer, and D. Zawischa, 1996, *Z. Phys. A* **355**, 117.
- Bouyssy, A., J.-F. Mathiot, Nguyen Van Giai, and S. Marcos, 1987, *Phys. Rev. C* **36**, 380.
- Brack, M., 1992, in *International Workshop on Nuclear Structure Models*, Oak Ridge, Tennessee, edited by R. Bengtsson, J. Draayer, and W. Nazarewicz (World Scientific, Singapore), p. 165.
- Brack, M., J. Damgård, A. S. Jensen, H. C. Pauli, V. M. Strutinsky, and C. Y. Wong, 1972, *Rev. Mod. Phys.* **44**, 320.
- Brack, M., C. Guet, and H.-B. Håkansson, 1985, *Phys. Rep.* **123**, 275.
- Brack, M., and P. Quentin, 1975, *Phys. Lett.* **56B**, 421.
- Brink, D. M., and E. Boeker, 1967, *Nucl. Phys. A* **91**, 1.
- Brink, D. M., and A. Weiguny, 1968, *Nucl. Phys. A* **120**, 59.
- Brockmann, R., 1978, *Phys. Rev. C* **18**, 1510.
- Brockmann, R., and R. Machleidt, 1990, *Phys. Rev. C* **42**, 1965.
- Brockmann, R., and H. Toki, 1992, *Phys. Rev. Lett.* **68**, 3408.
- Brown, B. A., 1998, *Phys. Rev. C* **58**, 220.
- Brown, B. A., 2000, *Phys. Rev. Lett.* **85**, 5296.
- Brown, B. A., W. A. Richter, and R. Lindsay, 2000, *Phys. Lett. B* **483**, 49.
- Brown, B. A., and B. H. Wildenthal, 1988, *Annu. Rev. Nucl. Part. Sci.* **38**, 29.
- Buchinger, F., J. M. Pearson, and S. Goriely, 2001, *Phys. Rev. C* **64**, 067303.
- Buchinger, F., *et al.*, 1990, *Phys. Rev. C* **41**, 2883; **42**, 2754(E).
- Bulgac, A., 1980, Hartree-Fock-Bogoliubov approximation for finite systems, preprint FT-194-1980, CIP-IPNE, Bucharest, Romania, nucl-th/9907088.
- Bulgac, A., 2002, *Phys. Rev. C* **65**, 051305(R).
- Bulgac, A., and V. R. Shaginyan, 1999a, *Eur. Phys. J. A* **5**, 247.
- Bulgac, A., and V. R. Shaginyan, 1999b, *Phys. Lett. B* **469**, 1.
- Bulgac, A., and Y. Yu, 2002, *Phys. Rev. Lett.* **88**, 042504.
- Bürvenich, T., D. Madland, J. A. Maruhn, and P.-G. Reinhard, 2002, *Phys. Rev. C* **65**, 044308.
- Bürvenich, T., K. Rutz, M. Bender, P.-G. Reinhard, J. A. Maruhn, and W. Greiner, 1998, *Eur. Phys. J. A* **3**, 139.
- Butler, M. N., D. W. L. Sprung, and J. Martorell, 1984, *Nucl. Phys. A* **422**, 157.
- Butler, P. A., and W. Nazarewicz, 1991, *Nucl. Phys. A* **533**, 249.
- Butler, P. A., and W. Nazarewicz, 1996, *Rev. Mod. Phys.* **68**, 349.
- Calvayrac, F., P.-G. Reinhard, E. Suraud, and C. A. Ullrich, 2000, *Phys. Rep.* **337**, 493.
- Campi, X., and A. Bouyssy, 1978, *Phys. Lett.* **73B**, 263.
- Casten, R. F., 1990, *Nuclear Structure from a Simple Perspective* (Oxford University, New York).
- Caurier, E., J. L. Egido, G. Martínez-Pinedo, A. Poves, J. Retamosa, L. M. Robledo, and A. P. Zuker, 1995, *Phys. Rev. Lett.* **75**, 2466.
- Caurier, E., K. Langanke, G. Martínez-Pinedo, F. Nowacki, and P. Vogel, 2001, *Phys. Lett. B* **522**, 240.
- Caurier, E., and F. Nowacki, 1999, *Acta Phys. Pol. B* **30**, 704.
- Cavinato, M., M. Marangoni, P. Ottaviani, and A. Saruis, 1982, *Nucl. Phys. A* **373**, 445.
- Centelles, M., M. D. Estal, and X. Viñas, 1998, *Nucl. Phys. A* **635**, 193.
- Cescato, M. L., and P. Ring, 1998, *Phys. Rev. C* **57**, 134.
- Chabanat, E., P. Bonche, P. Haensel, J. Meyer, and R. Schaeffer, 1997, *Nucl. Phys. A* **627**, 710.
- Chabanat, E., P. Bonche, P. Haensel, J. Meyer, and R. Schaeffer, 1998, *Nucl. Phys. A* **635**, 231; **643**, 441(E).
- Chang, B. D., 1975, *Phys. Lett.* **56B**, 205.
- Chasman, R. R., J. L. Egido, and L. M. Robledo, 2001, *Phys. Lett. B* **513**, 325.

- Chen, B., J. Dobaczewski, K.-L. Kratz, K. Langanke, P. Pfeiffer, F.-K. Thielemann, and P. Vogel, 1995, *Phys. Lett. B* **355**, 37.
- Chinn, C. R., J.-F. Berger, D. Gogny, and M. S. Weiss, 1992, *Phys. Rev. C* **45**, 1700.
- Colo, G., Nguyen Van Giai, P. F. Bortignon, and R. A. Broglia, 1994, *Phys. Rev. C* **50**, 1496.
- Colo, G., Nguyen Van Giai, and H. Sagawa, 1995, *Phys. Lett. B* **363**, 5.
- Cote, J., and J. M. Pearson, 1978, *Nucl. Phys. A* **304**, 104.
- Cusson, R. Y., P.-G. Reinhard, J. J. Molitoris, H. Stöcker, M. R. Strayer, and W. Greiner, 1985, *Phys. Rev. Lett.* **55**, 2786.
- Cusson, R. Y., P.-G. Reinhard, M. R. Strayer, J. A. Maruhn, and W. Greiner, 1985, *Z. Phys. A* **320**, 475.
- Ćwiok, S., J. Dobaczewski, P.-H. Heenen, P. Magierski, and W. Nazarewicz, 1996, *Nucl. Phys. A* **611**, 211.
- Ćwiok, S., W. Nazarewicz, and P.-H. Heenen, 1999, *Phys. Rev. Lett.* **83**, 1108.
- Dabrowski, J., and P. Haensel, 1976, *Ann. Phys. (N.Y.)* **97**, 452.
- Davies, K. T. R., K. R. S. Devi, S. E. Koonin, and M. R. Strayer, 1985, in *Treatise on Heavy-Ion Physics, Vol. 3 Compound System Phenomena*, edited by D. A. Bromley (Plenum, New York), p. 3.
- Davies, K. T. R., S. J. Krieger, and M. Baranger, 1966, *Nucl. Phys.* **84**, 545.
- Dechargé, J., J.-F. Berger, K. Dietrich, and M. S. Weiss, 1999, *Phys. Lett. B* **451**, 275.
- Dechargé, J., and D. Gogny, 1980, *Phys. Rev. C* **21**, 1568.
- Delaroche, J. P., M. Girod, J. Libert, and I. Deloncle, 1989, *Phys. Lett. B* **232**, 145.
- Delaroche, J. P., *et al.*, 1994, *Phys. Rev. C* **50**, 2332.
- Deloncle, I., J. Libert, L. Bennour, and P. Quentin, 1989, *Phys. Lett. B* **233**, 16.
- de Voigt, M. J. A., J. Dudek, and Z. Szymański, 1983, *Rev. Mod. Phys.* **55**, 949.
- Dickhoff, W. H., and H. Müther, 1992, *Rep. Prog. Phys.* **55**, 1947.
- Dietrich, K., 1996, *Nucl. Phys. A* **606**, 63.
- Dietrich, S. S., and B. L. Bermann, 1988, *At. Data Nucl. Data Tables* **38**, 199.
- Dobaczewski, J., and J. Dudek, 1995, *Phys. Rev. C* **52**, 1827; **55**, 3177(E).
- Dobaczewski, J., and J. Dudek, 1996, *Acta Phys. Pol. B* **27**, 45.
- Dobaczewski, J., and J. Dudek, 2000, *Comput. Phys. Commun.* **131**, 164.
- Dobaczewski, J., J. Dudek, S. G. Rohozinski, and T. R. Werner, 2000a, *Phys. Rev. C* **62**, 014310.
- Dobaczewski, J., J. Dudek, S. G. Rohozinski, and T. R. Werner, 2000b, *Phys. Rev. C* **62**, 014311.
- Dobaczewski, J., H. Flocard, and J. Treiner, 1984, *Nucl. Phys. A* **422**, 103.
- Dobaczewski, J., I. Hamamoto, W. Nazarewicz, and J. A. Sheikh, 1994, *Phys. Rev. Lett.* **72**, 981.
- Dobaczewski, J., P. Magierski, W. Nazarewicz, W. Satuła, and Z. Szymanski, 2001, *Phys. Rev. C* **63**, 024308.
- Dobaczewski, J., and W. Nazarewicz, 1992, *Phys. Rev. C* **47**, 2418.
- Dobaczewski, J., W. Nazarewicz, and P.-G. Reinhard, 2001, *Nucl. Phys. A* **693**, 361.
- Dobaczewski, J., W. Nazarewicz, and M. V. Stoitsov, 2002, in *Proc. of the 3rd International Conference on Exotic Nuclei and Atomic Masses*, Hameenlinna, Finland (Eur. Phys. J. A **15**, 21).
- Dobaczewski, J., W. Nazarewicz, and T. R. Werner, 1996, *Z. Phys. A* **354**, 27.
- Dobaczewski, J., W. Nazarewicz, T. R. Werner, J. F. Berger, C. R. Chinn, and J. Dechargé, 1996, *Phys. Rev. C* **53**, 2809.
- Dreizler, R. M., and E. K. U. Gross, 1990, *Density Functional Theory* (Springer, Berlin).
- Duerr, H.-P., 1956, *Phys. Rev.* **103**, 469.
- Duguet, T., P. Bonche, and P.-H. Heenen, 2001, *Nucl. Phys. A* **679**, 427.
- Duguet, T., P. Bonche, P.-H. Heenen, and J. Meyer, 2002a, *Phys. Rev. C* **65**, 014310.
- Duguet, T., P. Bonche, P.-H. Heenen, and J. Meyer, 2002b, *Phys. Rev. C* **65**, 014311.
- Egido, J. L., J. Lessing, V. Martin, and L. M. Robledo, 1995, *Nucl. Phys. A* **594**, 70.
- Egido, J. L., H. J. Mang, and P. Ring, 1980a, *Nucl. Phys. A* **339**, 390.
- Egido, J. L., H. J. Mang, and P. Ring, 1980b, *Nucl. Phys. A* **334**, 1.
- Egido, J. L., V. Martin, L. M. Robledo, and Y. Sun, 1996, *Phys. Rev. C* **53**, 2855.
- Egido, J. L., and P. Ring, 1982a, *Nucl. Phys. A* **383**, 189.
- Egido, J. L., and P. Ring, 1982b, *Nucl. Phys. A* **388**, 19.
- Egido, J. L., and L. M. Robledo, 1989, *Nucl. Phys. A* **494**, 85.
- Egido, J. L., and L. M. Robledo, 1990, *Nucl. Phys. A* **518**, 475.
- Egido, J. L., and L. M. Robledo, 1991, *Nucl. Phys. A* **524**, 65.
- Egido, J. L., and L. M. Robledo, 1992, *Nucl. Phys. A* **545**, 589.
- Egido, J. L., and L. M. Robledo, 2000, *Phys. Rev. Lett.* **85**, 1198.
- Egido, J. L., L. M. Robledo, and Y. Sun, 1993, *Nucl. Phys. A* **560**, 253.
- Elsenhans, H., H. Müther, and R. Machleidt, 1990, *Nucl. Phys. A* **515**, 715.
- Enami, K., K. Tanabe, and N. Yoshinaga, 2000, *Phys. Rev. C* **61**, 027301.
- Enami, K., K. Tanabe, and N. Yoshinaga, 2001, *Phys. Rev. C* **64**, 044305.
- Engel, J., M. Bender, J. Dobaczewski, W. Nazarewicz, and R. Surman, 1999, *Phys. Rev. C* **60**, 014302.
- Engel, Y. M., D. M. Brink, K. Goeke, S. J. Krieger, and D. Vautherin, 1975, *Nucl. Phys. A* **249**, 215.
- Erkelenz, K., 1974, *Phys. Rep.* **13**, 191.
- Farine, M., J. M. Pearson, and F. Tondeur, 1997, *Nucl. Phys. A* **615**, 135.
- Farine, M., J. M. Pearson, and F. Tondeur, 2001, *Nucl. Phys. A* **696**, 396.
- Fayans, S. A., 1999, *Pis'ma Zh. Eksp. Teor. Fiz.* **70**, 240 [JETP Lett. **70**, 235 (1999)].
- Fayens, S. A., S. V. Tolokonnikov, E. L. Trybov, and D. Zawischa, 1994, *Phys. Lett. B* **338**, 1.
- Fayans, S. A., S. V. Tolokonnikov, E. L. Trykov, and D. Zawischa, 2000, *Nucl. Phys. A* **676**, 49.
- Fayens, S. A., and D. Zawischa, 1996, *Phys. Lett. B* **383**, 19.
- Fink, B., D. Kolb, W. Scheid, and W. Greiner, 1972, *Ann. Phys. (N.Y.)* **69**, 375.
- Fleckner, J., U. Mosel, P. Ring, and H.-J. Mang, 1979, *Nucl. Phys. A* **331**, 288.
- Flocard, H., 1989, *Ann. Phys. (N.Y.)* **191**, 382.
- Flocard, H., and N. Onishi, 1997, *Ann. Phys. (N.Y.)* **254**, 275.
- Flocard, H., P. Quentin, A. K. Kerman, and D. Vautherin, 1973, *Nucl. Phys. A* **203**, 433.
- Flocard, H., P. Quentin, D. Vautherin, M. Vénéroni, and A. K. Kerman, 1974, *Nucl. Phys. A* **231**, 176.

- Friar, J. L., and J. W. Negele, 1975, *Adv. Nucl. Phys.* **8**, 219.
- Friedmann, B., and V. R. Pandharipande, 1981, *Nucl. Phys. A* **361**, 502.
- Friedrich, J., and P.-G. Reinhard, 1986, *Phys. Rev. C* **33**, 335.
- Friedrich, J., and N. Vöglér, 1982, *Nucl. Phys. A* **373**, 192.
- Gaarde, C., J. Rapaport, T. N. Taddeucci, C. D. Goodman, C. C. Foster, D. E. Bainum, C. A. Goulding, M. B. Greenfield, D. J. Horen, and E. Sugarbaker, 1981, *Nucl. Phys. A* **369**, 258.
- Gall, B., P. Bonche, J. Dobaczewski, H. Flocard, and P.-H. Heenen, 1994, *Z. Phys. A* **348**, 183.
- Garett, J. D., G. B. Hagemann, and B. Herskind, 1986, *Annu. Rev. Nucl. Part. Sci.* **36**, 419.
- Garrote, E., J. L. Egido, and L. M. Robledo, 1997, *Phys. Lett. B* **410**, 86.
- Garrote, E., J. L. Egido, and L. M. Robledo, 1998, *Phys. Rev. Lett.* **80**, 4398.
- Giannoni, M. J., and P. Quentin, 1980a, *Phys. Rev. C* **21**, 2060.
- Giannoni, M. J., and P. Quentin, 1980b, *Phys. Rev. C* **21**, 2076.
- Girod, M., J. P. Delaroche, J. F. Berger, and J. Libert, 1994, *Phys. Lett. B* **325**, 1.
- Girod, M., J. P. Delaroche, D. Gogny, and J. F. Berger, 1989, *Phys. Rev. Lett.* **62**, 2452.
- Girod, M., J. P. Delaroche, J. Libert, and I. Deloncle, 1992, *Phys. Rev. C* **45**, R1420.
- Girod, M., and D. Gogny, 1976, *Phys. Lett.* **64B**, 5.
- Girod, M., and B. Grammaticos, 1979, *Nucl. Phys. A* **330**, 40.
- Girod, M., and B. Grammaticos, 1983, *Phys. Rev. C* **27**, 2317.
- Girod, M., and P.-G. Reinhard, 1982a, *Nucl. Phys. A* **384**, 179.
- Girod, M., and P.-G. Reinhard, 1982b, *Phys. Lett.* **117B**, 1.
- Gleissl, P., M. Brack, J. Meyer, and P. Quentin, 1990, *Ann. Phys. (N.Y.)* **197**, 205.
- Gmuca, S., 1992, *Nucl. Phys. A* **547**, 447.
- Goeke, K., F. Grümmer, and P.-G. Reinhard, 1983, *Ann. Phys. (N.Y.)* **150**, 504.
- Goeke, K., and P.-G. Reinhard, 1978, *Ann. Phys. (N.Y.)* **112**, 328.
- Goeke, K., and P.-G. Reinhard, 1980, *Ann. Phys. (N.Y.)* **124**, 249.
- Goeke, K., and P.-G. Reinhard, 1982, Eds., *Proceedings of the International Symposium on Time-dependent Hartree-Fock and beyond*, Bad Honnef, Germany, Lecture Notes in Physics No. 171 (Springer, Berlin).
- Goeke, K., and J. Speth, 1982, *Annu. Rev. Nucl. Part. Sci.* **32**, 65.
- Gogny, D., 1973, in *Proceedings of the International Conference on Nuclear Physics*, Munich, edited by J. de Boer and H. J. Mang (North-Holland, Amsterdam), p. 48.
- Gogny, D., 1975, in *Proceedings of the International Conference on Nuclear Self-Consistent Fields*, International Centre for Theoretical Physics, Trieste, edited by G. Ripka and M. Porneuf (North-Holland, Amsterdam), p. 333.
- Gonzalez-Llarena, T., J. L. Egido, G. A. Lalazissis, and P. Ring, 1996, *Phys. Lett. B* **379**, 13.
- Goodman, A. L., 1974, *Nucl. Phys. A* **230**, 466.
- Goodman, A. L., 1979, *Adv. Nucl. Phys.* **11**, 263.
- Goodman, A. L., 1999, *Phys. Rev. C* **60**, 014311.
- Göppert-Mayer, M., 1948, *Phys. Rev.* **74**, 235.
- Goriely, S., F. Tondeur, and J. M. Pearson, 2001, *At. Data Nucl. Data Tables* **77**, 311.
- Goźdz, A., K. Pomorski, M. Brack, and W. Werner, 1985, *Nucl. Phys. A* **442**, 26.
- Grabmayr, P., A. Mondry, G. J. Wagner, P. Woldt, G. P. A. Berg, J. Lisantti, D. W. Hiller, H. Nann, and E. J. Stephenson, 1994, *Phys. Rev. C* **49**, 2971.
- Grasso, M., Nguyen Van Giai, and N. Sandulescu, 2002, *Phys. Lett. B* **535**, 1.
- Grasso, M., N. Sandulescu, Nguyen Van Giai, and R. J. Liotta, 2001, *Phys. Rev. C* **64**, 064321.
- Griffin, J. J., and J. A. Wheeler, 1957, *Phys. Rev.* **108**, 311.
- Gross, E. K. U., C. A. Ullrich, and U. J. Gossmann, 1994, in *Density Functional Theory*, Vol. 337 of *NATO Advanced Study Institute, Series: B: Physics*, edited by E. K. U. Gross and R. M. Dreizler (Plenum, New York), p. 149.
- Haddad, S., and M. K. Weigel, 1993, *Phys. Rev. C* **48**, 2740.
- Haensel, P., and J. Dąbrowski, 1975, *Nucl. Phys. A* **254**, 211.
- Haensel, P., J. L. Zdunik, and J. Dobaczewski, 1989, *Astron. Astrophys.* **222**, 353.
- Hagino, K., and H. Sagawa, 2001, *Nucl. Phys. A* **695**, 82.
- Hamamoto, I., 1974, *Phys. Rep.* **10**, 63.
- Hamamoto, I., 1999, *Phys. Rev. C* **60**, 031303.
- Hamamoto, I., and H. Sagawa, 1993, *Phys. Rev. C* **48**, R960.
- Hamamoto, I., and H. Sagawa, 2000, *Phys. Rev. C* **62**, 024319.
- Hamamoto, I., H. Sagawa, and X. Z. Zhang, 1997a, *Phys. Rev. C* **56**, 3121.
- Hamamoto, I., H. Sagawa, and X. Z. Zhang, 1997b, *Nucl. Phys. A* **626**, 669.
- Hamamoto, I., H. Sagawa, and X. Z. Zhang, 1997c, *Phys. Rev. C* **55**, 2361.
- Hamamoto, I., H. Sagawa, and X. Z. Zhang, 1998, *Phys. Rev. C* **57**, R1064.
- Hamamoto, I., and X. Z. Zhang, 1995, *Phys. Rev. C* **52**, R2326.
- Han, X., and C. Wu, 1999, *At. Data Nucl. Data Tables* **73**, 43.
- Hansen, P. G., A. S. Jensen, and B. Jonson, 1995, *Annu. Rev. Nucl. Part. Sci.* **45**, 591.
- Hara, K., A. Hayashi, and P. Ring, 1982, *Nucl. Phys. A* **385**, 14.
- Hasse, R. W., and W. D. Myers, 1988, *Geometrical Relationships of Macroscopic Nuclear Physics* (Springer, Berlin).
- Heenen, P.-H., P. Bonche, J. Dobaczewski, and H. Flocard, 1993, *Nucl. Phys. A* **561**, 367.
- Heenen, P.-H., J. Dobaczewski, W. Nazarewicz, P. Bonche, and T. L. Khoo, 1998, *Phys. Rev. C* **57**, 1719.
- Heenen, P.-H., and R. V. F. Janssens, 1998, *Phys. Rev. C* **57**, 159.
- Heenen, P.-H., and J. Skalski, 1996, *Phys. Lett. B* **381**, 12.
- Heenen, P.-H., J. Skalski, P. Bonche, and H. Flocard, 1994, *Phys. Rev. C* **50**, 802.
- Heenen, P.-H., A. Valor, M. Bender, P. Bonche, and H. Flocard, 2001, *Eur. Phys. J. A* **11**, 393.
- Heenen, P.-H., A. Valor, and P. Bonche, 2001, *Acta Phys. Pol. B* **32**, 2375.
- Heiselberg, H., and V. Pandharipande, 2000, *Annu. Rev. Nucl. Part. Sci.* **50**, 481.
- Helm, R. H., 1956, *Phys. Rev.* **104**, 1466.
- Henning, P. A., and P. Manakos, 1987, *Nucl. Phys. A* **466**, 487.
- Heyde, K., P. Van Isacker, M. Waroquier, J. L. Wood, and R. A. Meyer, 1983, *Phys. Rep.* **102**, 291.
- Hill, D. L., and J. A. Wheeler, 1953, *Phys. Rev.* **89**, 1102.
- Hjorth-Jensen, M., E. Osnes, and H. Muether, 1992, *Phys. Scr.* **213**, 102.
- Hoch, T., and P. Manakos, 1990, *Z. Phys. A* **337**, 383.
- Hofmann, S., 1998, *Rep. Prog. Phys.* **61**, 639.
- Hofmann, S., F. P. Heßberger, D. Ackermann, S. Antalic, P. Cagarda, S. Cwiok, B. Kindler, J. Kojouharova, B. Lommel, R. Mann, G. Münzenberg, A. G. Popeko, *et al.*, 2000, *Eur. Phys. J. A* **10**, 5.

- Hofmann, S., and G. Münzenberg, 2000, *Rev. Mod. Phys.* **72**, 733.
- Hohenberg, P., and W. Kohn, 1964, *Phys. Rev.* **136**, B864.
- Holinde, K., 1981, *Phys. Rep.* **68**, 122.
- Holzwarth, G., and G. Eckart, 1978, *Z. Phys. A* **284**, 291.
- Horowitz, C. J., S. J. Pollock, P. A. Souder, and R. Michaels, 2001, *Phys. Rev. C* **63**, 025501.
- Horowitz, C. J., and B. D. Serot, 1982, *Phys. Lett.* **108B**, 377.
- Ineichen, F., M. K. Weigel, and D. Von-Eiff, 1996, *Phys. Rev. C* **53**, 2158.
- Iudice, N. L., 1997, *Prog. Part. Nucl. Phys.* **28**, 556.
- Jaminon, M., and C. Mahaux, 1990, *Phys. Rev. C* **41**, 697.
- Jancovici, B., and D. H. Schiff, 1964, *Nucl. Phys. A* **58**, 678.
- Janssens, R. V. F., and T. L. Khoo, 1991, *Annu. Rev. Nucl. Part. Sci.* **41**, 321.
- Jensen, A. S., and A. Miranda, 1986, *Nucl. Phys. A* **449**, 331.
- Jones, R. O., and O. Gunnarsson, 1989, *Rev. Mod. Phys.* **61**, 689.
- Kaiser, N., S. Fritsch, and W. Weise, 2002, *Nucl. Phys. A* **700**, 343.
- Kamlah, A., 1968, *Z. Phys.* **216**, 52.
- Kautzsch, T., W. B. Walters, M. Hannawald, K.-L. Kratz, V. I. Mishin, V. N. Fedoseyev, W. Böhmer, Y. Jading, P. V. Duppen, B. Pfeiffer, A. Wöhr, P. Möller, *et al.*, 2000, *Eur. Phys. J. A* **9**, 201.
- Kegley, D. R., V. E. Oberacker, M. R. Strayer, A. S. Umar, and J. C. Wells, 1996, *J. Comput. Phys.* **128**, 197.
- Kerman, A. K., 1977, in *Elementary Modes of Excitation in Nuclei—Proceedings of the International School of Physics “Enrico Fermi,” Course LXIX*, Varenna, Italy, edited by A. Bohr and R. A. Broglia (North-Holland, Amsterdam), p. 135.
- Kerman, A. K., J. P. Svenne, and F. M. H. Villars, 1966, *Phys. Rev.* **147**, 710.
- Kinsey, R. R., *et al.*, 1997, The NUDAT/PCNUDAT program for nuclear data, *9th International Symposium of Capture Gamma-Ray Spectroscopy and Related Topics*, Budapest, Hungary. Data extracted from the NUDAT database, version March 20, 1997, National Nuclear Data Center World Wide Web site: <http://www.nndc.bnl.gov/nndc/nudat/>
- Kleban, M., B. Nerlo-Pomorska, J.-F. Berger, J. Dechargé, M. Girod, and S. Hilaire, 2002, *Phys. Rev. C* **65**, 024309.
- Köhler, H. S., 1976, *Nucl. Phys. A* **258**, 301.
- Kohn, W., 1999, *Rev. Mod. Phys.* **71**, 1253.
- Kohn, W., and L. J. Sham, 1965, *Phys. Rev.* **140**, A1133.
- Koonin, S. E., D. J. Dean, and K. Langanke, 1997a, *Annu. Rev. Nucl. Part. Sci.* **47**, 463.
- Koonin, S. E., D. J. Dean, and K. Langanke, 1997b, *Phys. Rep.* **278**, 1.
- Krewald, S., V. Klemt, J. Speth, and A. Faessler, 1977, *Nucl. Phys. A* **281**, 166.
- Krieger, S. J., P. Bonche, H. Flocard, P.-H. Heenen, R. Mehrem, and M. S. Weiss, 1996, *Phys. Rev. C* **54**, 2399.
- Krieger, S. J., P. Bonche, H. Flocard, P.-H. Heenen, and M. S. Weiss, 1994, *Nucl. Phys. A* **572**, 384.
- Krieger, S. J., P. Bonche, H. Flocard, P. Quentin, and M. S. Weiss, 1990, *Nucl. Phys. A* **517**, 275.
- Krivine, H., J. Treiner, and O. Bohigas, 1980, *Nucl. Phys. A* **336**, 155.
- Kruppa, A. T., M. Bender, W. Nazarewicz, P.-G. Reinhard, T. Vertse, and S. Ćwiok, 2000, *Phys. Rev. C* **61**, 034313.
- Kruppa, A. T., P.-H. Heenen, H. Flocard, and R. J. Liotta, 1997, *Phys. Rev. Lett.* **79**, 2217.
- Kruppa, A. T., P.-H. Heenen, and R. J. Liotta, 2001, *Phys. Rev. C* **63**, 044324.
- Kucharek, H., and P. Ring, 1991, *Z. Phys. A* **339**, 23.
- Kutschera, M., and W. Wójcik, 1994, *Phys. Lett. B* **325**, 172.
- Lalazissis, G. A., J. König, and P. Ring, 1997, *Phys. Rev. C* **55**, 540.
- Lalazissis, G. A., S. Raman, and P. Ring, 1999, *At. Data Nucl. Data Tables* **70**, 1.
- Lalazissis, G. A., M. M. Sharma, J. König, and P. Ring, 1994, in *International Conference on Nuclear Shapes and Nuclear Structure at Low Excitation Energies*, Antibes (France), edited by M. Vergnes, D. Goutte, P.-H. Heenen, and J. Sauvage (Editions Frontieres, Gif-sur-Yvette Cedex, France), p. 161.
- Lalazissis, G. A., D. Vretenar, W. Pöschl, and P. Ring, 1998a, *Phys. Lett. B* **418**, 7.
- Lalazissis, G. A., D. Vretenar, W. Pöschl, and P. Ring, 1998b, *Nucl. Phys. A* **632**, 363.
- Lalazissis, G. A., D. Vretenar, and P. Ring, 1999a, *Nucl. Phys. A* **650**, 133.
- Lalazissis, G. A., D. Vretenar, and P. Ring, 1999b, *Phys. Rev. C* **60**, 051302.
- Lalazissis, G. A., D. Vretenar, P. Ring, M. Stoitsov, and L. Robledo, 1999, *Phys. Rev. C* **60**, 014310.
- Lauritsch, G., and P.-G. Reinhard, 1994, *Int. J. Mod. Phys. C* **5**, 65.
- Leander, G. A., R. K. Sheline, P. Möller, P. Olanders, I. Ragnarsson, and A. J. Sierk, 1982, *Nucl. Phys. A* **388**, 452.
- Libert, J., M. Girod, and J.-P. Delaroche, 1999, *Phys. Rev. C* **60**, 054301.
- Lipkin, H. J., 1960, *Ann. Phys. (N.Y.)* **9**, 272.
- Lipkin, H. J., 1961, *Ann. Phys. (N.Y.)* **12**, 452.
- Liu, K.-F., H. Luo, Z. Ma, Q. Shen, and S. A. Moszkowski, 1991, *Nucl. Phys. A* **534**, 1.
- Lutz, M., B. Friman, and C. Appel, 2000, *Phys. Lett. B* **474**, 7.
- Ma, Z.-Y., Nguyen Van Giai, A. Wandelt, D. Vretenar, and P. Ring, 2001, *Nucl. Phys. A* **686**, 173.
- Machleidt, R., K. Holinde, and C. Elster, 1987, *Phys. Rep.* **149**, 1.
- Machleidt, R., and I. Slaus, 2001, *J. Phys. G* **27**, R69.
- Madland, D. G., and J. R. Nix, 1988, *Nucl. Phys. A* **476**, 1.
- Magierski, P., S. Ćwiok, J. Dobaczewski, and W. Nazarewicz, 1993, *Phys. Rev. C* **48**, 1686.
- Mahaux, C., P. F. Bortignon, R. A. Broglia, and C. H. Dasso, 1985, *Phys. Rep.* **120**, 1.
- Mang, H. J., 1975, *Phys. Rep.* **18**, 325.
- Marcos, S., H. Flocard, and P.-H. Heenen, 1983, *Nucl. Phys. A* **410**, 125.
- Marcos, S., H. Flocard, and P.-H. Heenen, 1984, *Phys. Lett.* **134B**, 287.
- Marcos, S., R. Niembro, M. López-Quelle, Nguyen Van Giai, and R. Malfliet, 1989, *Phys. Rev. C* **39**, 1134.
- Martínez-Pinedo, G., and K. Langanke, 1999, *Phys. Rev. Lett.* **83**, 4502.
- Maruhn, J. A., T. A. Welton, and C. Y. Wong, 1976, *J. Comput. Phys.* **20**, 326.
- Matsuo, M., 2001, *Nucl. Phys. A* **696**, 371.
- Meng, J., and P. Ring, 1998, *Phys. Rev. Lett.* **80**, 460.
- Meyer, J., P. Bonche, M. S. Weiss, J. Dobaczewski, H. Flocard, and P.-H. Heenen, 1995, *Nucl. Phys. A* **588**, 597.
- Mizutori, S., J. Dobaczewski, G. A. Lalazissis, W. Nazarewicz, and P.-G. Reinhard, 2000, *Phys. Rev. C* **61**, 044326.
- Möller, P., and J. R. Nix, 1992, *Nucl. Phys. A* **536**, 20.

- Möller, P., J. R. Nix, and K.-L. Kratz, 1997, *At. Data Nucl. Data Tables* **66**, 131.
- Möller, P., J. R. Nix, W. D. Myers, and W. J. Swiatecki, 1995, *At. Data Nucl. Data Tables* **59**, 185.
- Mühlhans, K., K. Neergard, and U. Mosel, 1984, *Nucl. Phys. A* **420**, 204.
- Müther, H., R. Machleidt, and R. Brockmann, 1990, *Phys. Rev. C* **42**, 1981.
- Muthukrishnan, R., and M. Baranger, 1965, *Phys. Lett.* **18**, 160.
- Myers, W. D., 1977, *Droplet Model of Atomic Nuclei* (IFI/Plenum, New York).
- Myers, W. D., and W. J. Swiatecki, 1974, *Ann. Phys. (N.Y.)* **84**, 186.
- Myers, W. D., and W. J. Swiatecki, 1982, *Annu. Rev. Nucl. Part. Sci.* **32**, 309.
- Nadjakov, E. G., K. P. Marinova, and Y. P. Gangrsky, 1994, *At. Data Nucl. Data Tables* **56**, 133.
- Nágy, A., 1998, *Phys. Rep.* **298**, 1.
- Navratil, P., J. P. Vary, and B. R. Barrett, 2000, *Phys. Rev. C* **62**, 054311.
- Nayak, R. C., and J. M. Pearson, 1998, *Phys. Rev. C* **58**, 878.
- Nazarewicz, W., 1993, *Int. J. Mod. Phys. E* **2**, 51.
- Nazarewicz, W., P. Olanders, I. Ragnarsson, J. Dudek, and G. A. Leander, 1984, *Phys. Rev. Lett.* **52**, 1272.
- Nazarewicz, W., and I. Ragnarsson, 1996, in *Handbook of Nuclear Properties*, edited by D. N. Poenaru and W. Greiner (Clarendon Press, Oxford), p. 81.
- Negele, J. W., 1970, *Phys. Rev. C* **1**, 1260.
- Negele, J. W., 1982, *Rev. Mod. Phys.* **54**, 913.
- Negele, J. W., and D. Vautherin, 1972, *Phys. Rev. C* **5**, 1472.
- Negele, J. W., and D. Vautherin, 1975, *Phys. Rev. C* **11**, 1031.
- Nerlo-Pomorska, B., K. Pomorski, J.-F. Berger, and J. Dechargé, 2000, *Eur. Phys. J. A* **8**, 19.
- Nikolaus, B. A., T. Hoch, and D. G. Madland, 1992, *Phys. Rev. C* **46**, 1757.
- Nilsson, S. G., and I. Ragnarsson, 1995, *Shapes and Shells in Nuclear Structure* (Cambridge University, Cambridge, England).
- Nogami, Y., 1964, *Phys. Rev. B* **134**, B313.
- Nolan, P. J., and P. J. Twin, 1988, *Annu. Rev. Nucl. Part. Sci.* **38**, 533.
- Oganessian, Y. T., *et al.*, 2001, *Phys. Rev. C* **63**, 011301(R).
- Onida, G., L. Reining, and A. Rubio, 2002, *Rev. Mod. Phys.* **74**, 601.
- Onsi, M., R. C. Nayak, J. M. Pearson, H. Freyer, and W. Stocker, 1997, *Phys. Rev. C* **55**, 3166.
- Osterfeld, F., 1991, in *Electric and Magnetic Giant Resonances in Nuclei*, edited by J. Speth, International Review of Nuclear Physics No. 7 (World Scientific, River Edge, NJ), p. 536.
- Osterfeld, F., 1992, *Rev. Mod. Phys.* **64**, 491.
- Otsuka, T., 2001, *Nucl. Phys. A* **693**, 383.
- Otsuka, T., M. Honma, T. Mizusaki, N. Shimizu, and Y. Utsuno, 2001, *Prog. Part. Nucl. Phys.* **47**, 319.
- Otten, E. W., 1989, in *Treatise on Heavy-Ion Science*, edited by D. A. Bromley, No. VIII (Plenum, New York), p. 517.
- Oyamatsu, K., I. Tanihata, Y. Sugahara, K. Sumiyoshi, and H. Toki, 1998, *Nucl. Phys. A* **634**, 3.
- Pandharipande, V. R., I. Sick, and P. K. A. deWitt Huberts, 1997, *Rev. Mod. Phys.* **69**, 981.
- Parr, R. G., and W. Yang, 1989, *Density-Functional Theory of Atoms and Molecules* (Oxford University, Oxford).
- Passler, K. H., and U. Mosel, 1976, *Nucl. Phys. A* **257**, 242.
- Pauli, H. C., 1973, *Phys. Rep.* **7**, 35.
- Pearson, J. M., 2001, *Phys. Lett. B* **513**, 319.
- Pearson, J. M., and M. Farine, 1994, *Phys. Rev. C* **50**, 185.
- Pearson, J. M., and S. Goriely, 2001, *Phys. Rev. C* **64**, 027301.
- Perdew, J. P., and A. Zunger, 1981, *Phys. Rev. B* **23**, 5048.
- Peru, S., M. Girod, and J. F. Berger, 2000, *Eur. Phys. J. A* **9**, 35.
- Pethick, C. J., and D. G. Ravenhall, 1995, *Annu. Rev. Nucl. Part. Sci.* **45**, 429.
- Petkov, I. Z., and M. V. Stoitsov, 1991, *Nuclear Density Functional Theory* (Clarendon, Oxford).
- Pfeiffer, B., K.-L. Kratz, J. Dobaczewski, and P. Möller, 1996, *Acta Phys. Pol. B* **27**, 45.
- Pomorski, K., P. Ring, G. A. Lalazissis, A. Baran, Z. Lojewski, B. Nerlo-Pomorska, and M. Warda, 1997, *Nucl. Phys. A* **624**, 349.
- Pöschl, W., D. Vretenar, G. A. Lalazissis, and P. Ring, 1997, *Phys. Rev. Lett.* **79**, 3841.
- Pöschl, W., D. Vretenar, and P. Ring, 1997, *Comput. Phys. Commun.* **103**, 217.
- Pradhan, H. C., Y. Nogami, and J. Law, 1973, *Nucl. Phys. A* **201**, 357.
- Pudliner, B. S., A. Smerzi, J. Carlson, V. R. Pandharipande, S. C. Pieper, and D. G. Ravenhall, 1996, *Phys. Rev. Lett.* **76**, 2416.
- Quentin, P., and H. Flocard, 1978, *Annu. Rev. Nucl. Part. Sci.* **28**, 523.
- Ragnarsson, I., S. G. Nilsson, and R. K. Sheline, 1978, *Phys. Rep.* **45**, 1.
- Raman, S., C. W. Nestor, Jr., and P. Tikkanen, 2001, *At. Data Nucl. Data Tables* **78**, 1.
- Reinhard, P.-G., 1978, *Z. Phys. A* **285**, 93.
- Reinhard, P.-G., 1988, *Z. Phys. A* **329**, 257.
- Reinhard, P.-G., 1989, *Rep. Prog. Phys.* **52**, 439.
- Reinhard, P.-G., 1991, in *Computational Nuclear Physics I—Nuclear Structure*, edited by K. Langanke, J. A. Maruhn, and S. E. Koonin (Springer, Berlin), p. 28.
- Reinhard, P.-G., 1992a, *Phys. Lett. A* **169**, 281.
- Reinhard, P.-G., 1992b, *Ann. Phys. (Leipzig)* **1**, 632.
- Reinhard, P.-G., 1999, *Nucl. Phys. A* **649**, 305c.
- Reinhard, P.-G., M. Bender, T. Bürvenich, C. Reiss, J. A. Maruhn, and W. Greiner, 2000, in *Proceedings of the International Symposium on Models and Theories of the Nuclear Mass*, RIKEN, Japan, edited by N. Tajima and S. Yamaji (RIKEN Rev. **26**, 23).
- Reinhard, P.-G., M. Bender, K. Rutz, and J. A. Maruhn, 1997, *Z. Phys. A* **358**, 277.
- Reinhard, P.-G., and R. Y. Cusson, 1982, *Nucl. Phys. A* **378**, 418.
- Reinhard, P.-G., D. J. Dean, W. Nazarewicz, J. Dobaczewski, J. A. Maruhn, and M. R. Strayer, 1999, *Phys. Rev. C* **60**, 014316.
- Reinhard, P.-G., and D. Drechsel, 1979, *Z. Phys. A* **290**, 85.
- Reinhard, P.-G., and H. Flocard, 1995, *Nucl. Phys. A* **584**, 467.
- Reinhard, P.-G., and J. Friedrich, 1985, *Z. Phys. A* **321**, 619.
- Reinhard, P.-G., J. Friedrich, and N. Voegler, 1984, *Z. Phys. A* **316**, 207.
- Reinhard, P.-G., and Y. K. Gambhir, 1992, *Ann. Phys. (Leipzig)* **1**, 598.
- Reinhard, P.-G., and K. Goeke, 1979, in *Microscopic Optical Potentials*, Proceedings of the Hamburg Topical Workshop on Nuclear Physics, Hamburg, Germany, edited by J. Ehlers, K. Hepp, R. Kippenhahn, H. A. Weidenmüller, and J. Zittartz (Springer Verlag, Heidelberg), p. 440.
- Reinhard, P.-G., and K. Goeke, 1987, *Rep. Prog. Phys.* **50**, 1.

- Reinhard, P.-G., and J. A. Maruhn, 1999, in *Heavy Elements and Related New Phenomena*, edited by W. Greiner and R. K. Gupta (World Scientific, Singapore), Vol. 1, p. 332.
- Reinhard, P.-G., W. Nazarewicz, M. Bender, and J. A. Maruhn, 1996, *Phys. Rev. C* **53**, 2776.
- Reinhard, P.-G., and E. W. Otten, 1984, *Nucl. Phys. A* **420**, 173.
- Reinhard, P.-G., C. Reiss, M. Bender, T. Bürvenich, T. Corneliuss, and J. A. Maruhn, 2000, *Hyperfine Interact.* **127**, 13.
- Reinhard, P.-G., M. Rufa, J. A. Maruhn, W. Greiner, and J. Friedrich, 1986, *Z. Phys. A* **323**, 13.
- Reinhard, P.-G., and C. Toepffer, 1994, *Int. J. Mod. Phys. E* **3**, 435.
- Reinhard, P.-G., H. L. Yadav, and C. Toepffer, 1986, *Nucl. Phys. A* **458**, 301.
- Reiter, P., *et al.*, 2000, *Phys. Rev. Lett.* **84**, 3542.
- Ring, P., 1996, *Prog. Part. Nucl. Phys.* **37**, 193.
- Ring, P., Zhong-Yu Ma, Nguyen Van Giai, D. Vretenar, A. Wandelt, and Li-Gang Cao, 2001, *Nucl. Phys. A* **694**, 249.
- Ring, P., and P. Schuck, 1980, *The Nuclear Many-Body Problem* (Springer, New York).
- Ripka, G., and M. Porneuf, 1975, Eds., *Proceedings of the International Conference on Nuclear Self-Consistent Fields*, International Centre for Theoretical Physics, Trieste (North-Holland, Amsterdam).
- Robledo, L. M., 1994, *Phys. Rev. C* **50**, 2874.
- Robledo, L. M., J. L. Egido, J.-F. Berger, and M. Girod, 1987, *Phys. Lett. B* **187**, 223.
- Robledo, L. M., J. L. Egido, B. Nerlo-Pomorska, and K. Pomorski, 1988, *Phys. Lett. B* **201**, 409.
- Rodriguez-Guzmán, R. R., J. L. Egido, and L. M. Robledo, 2000a, *Phys. Lett. B* **474**, 15.
- Rodriguez-Guzmán, R. R., J. L. Egido, and L. M. Robledo, 2000b, *Phys. Rev. C* **62**, 054319.
- Rodriguez-Guzmán, R. R., J. L. Egido, and L. M. Robledo, 2000c, *Phys. Rev. C* **62**, 054308.
- Rodriguez-Guzmán, R. R., J. L. Egido, and L. M. Robledo, 2002, *Phys. Rev. C* **65**, 024304.
- Rowe, D. J., 1970, *Nuclear Collective Motion* (Methuen, London).
- Rufa, M., P.-G. Reinhard, J. A. Maruhn, W. Greiner, and M. R. Strayer, 1988, *Phys. Rev. C* **38**, 390.
- Runge, E., and E. K. U. Gross, 1984, *Phys. Rev. Lett.* **52**, 997.
- Rusnak, J. J., and R. J. Furnstahl, 1997, *Nucl. Phys. A* **627**, 495.
- Rutz, K., M. Bender, T. Bürvenich, T. Schilling, P.-G. Reinhard, J. A. Maruhn, and W. Greiner, 1997, *Phys. Rev. C* **56**, 238.
- Rutz, K., M. Bender, P.-G. Reinhard, and J. A. Maruhn, 1999, *Phys. Lett. B* **468**, 1.
- Rutz, K., M. Bender, P.-G. Reinhard, J. A. Maruhn, and W. Greiner, 1998, *Nucl. Phys. A* **634**, 67.
- Rutz, K., J. A. Maruhn, P.-G. Reinhard, and W. Greiner, 1995, *Nucl. Phys. A* **590**, 680.
- Sagawa, H., 1992, *Phys. Lett. B* **286**, 7.
- Sagawa, H., 2002, *Phys. Rev. C* **65**, 064314.
- Sagawa, H., and H. Esbensen, 2001, *Nucl. Phys. A* **693**, 448.
- Sagawa, H., T. Suzuki, and Nguyen Van Giai, 1995, *Phys. Rev. Lett.* **75**, 3629.
- Sagawa, H., and Nguyen Van Giai, 1982, *Phys. Lett.* **113B**, 119.
- Samyn, M., S. Goriely, P.-H. Heenen, J. M. Pearson, and F. Tondeur, 2002, *Nucl. Phys. A* **700**, 142.
- Sarriguren, P., E. M. de Guerra, and A. Escuderos, 2001, *Phys. Rev. C* **64**, 064306.
- Sarriguren, P., E. M. de Guerra, and R. Nojarov, 1997, *Z. Phys. A* **357**, 143.
- Satpathy, L., V. S. U. Maheswari, and R. C. Nayak, 1999, *Phys. Rep.* **319**, 85.
- Satula, W., D. J. Dean, J. Gary, S. Mizutori, and W. Nazarewicz, 1997, *Phys. Lett. B* **407**, 103.
- Satula, W., J. Dobaczewski, and W. Nazarewicz, 1998, *Phys. Rev. Lett.* **81**, 3599.
- Satula, W., and R. Wyss, 1994, *Phys. Rev. C* **50**, 2888.
- Satula, W., and R. Wyss, 1997, *Phys. Lett. B* **393**, 1.
- Satula, W., and R. Wyss, 2001a, *Phys. Rev. Lett.* **87**, 052504.
- Satula, W., and R. Wyss, 2001b, *Phys. Rev. Lett.* **86**, 4488.
- Saunier, G., and J. M. Pearson, 1967, *Phys. Rev.* **160**, 740.
- Sauvage-Letessier, J., P. Quentin, and H. Flocard, 1981, *Nucl. Phys. A* **370**, 231.
- Scheid, W., and W. Greiner, 1968, *Ann. Phys. (N.Y.)* **48**, 493.
- Schmid, K. W., and P.-G. Reinhard, 1991, *Nucl. Phys. A* **530**, 283.
- Schmid, R. N., E. Engel, and R. M. Dreizler, 1995a, *Phys. Rev. C* **52**, 164.
- Schmid, R. N., E. Engel, and R. M. Dreizler, 1995b, *Phys. Rev. C* **52**, 2804.
- Serot, B. D., 1992, *Rep. Prog. Phys.* **55**, 1855.
- Serot, B. D., and J. D. Walecka, 1986, *Adv. Nucl. Phys.* **16**, 1.
- Serra, M., and P. Ring, 2002, *Phys. Rev. C* **65**, 064324.
- Serra, M., A. Rummel, and P. Ring, 2002, *Phys. Rev. C* **65**, 014304.
- Sharma, M. M., G. A. Lalazissis, J. König, and P. Ring, 1995, *Phys. Rev. Lett.* **74**, 3744.
- Sheikh, J. A., and P. Ring, 2000, *Nucl. Phys. A* **665**, 71.
- Shen, H., Y. Sugahara, and H. Toki, 1997, *Phys. Rev. C* **55**, 1211.
- Shlomo, S., and G. F. Bertsch, 1975, *Nucl. Phys. A* **243**, 507.
- Simon, G. G., C. Schmitt, F. Borkowski, and V. H. Walther, 1980, *Nucl. Phys. A* **333**, 381.
- Singh, R., and B. M. Deb, 1999, *Phys. Rep.* **311**, 47.
- Skalski, J., 2001, *Phys. Rev. C* **63**, 024312.
- Skalski, J., P.-H. Heenen, and P. Bonche, 1993, *Nucl. Phys. A* **559**, 221.
- Skalski, J., P.-H. Heenen, P. Bonche, H. Flocard, and J. Meyer, 1993, *Nucl. Phys. A* **551**, 109.
- Skyrme, T. H. R., 1956, *Philos. Mag.* **1**, 1043.
- Skyrme, T. H. R., 1959a, *Nucl. Phys.* **9**, 615.
- Skyrme, T. H. R., 1959b, *Nucl. Phys.* **9**, 635.
- Specht, H. J., 1974, *Rev. Mod. Phys.* **46**, 773.
- Speicher, C., R. M. Dreizler, and E. Engel, 1991, *Ann. Phys. (N.Y.)* **213**, 312.
- Speicher, C., E. Engel, and R. M. Dreizler, 1993, *Nucl. Phys. A* **562**, 569.
- Speth, J., and A. van der Woude, 1981, *Rep. Prog. Phys.* **44**, 719.
- Speth, J., and J. Wambach, 1991, in *Electric and Magnetic Giant Resonances in Nuclei*, edited by J. Speth, International Review of Nuclear Physics No. 7 (World Scientific, River Edge, NJ), p. 1.
- Stancu, F., D. M. Brink, and H. Flocard, 1977, *Phys. Lett.* **68B**, 108.
- Stocker, W., and T. V. Chossy, 1998, *Phys. Rev. C* **58**, 2777.
- Stoitsov, M., P. Ring, D. Vretenar, and G. A. Lalazissis, 1998, *Phys. Rev. C* **58**, 2086.
- Stoitsov, M. V., J. Dobaczewski, P. Ring, and S. Pittel, 2000, *Phys. Rev. C* **61**, 034311.
- Stringari, S., 1983, *Ann. Phys. (N.Y.)* **151**, 35.
- Stringari, S., R. Leonardi, and D. M. Brink, 1976, *Nucl. Phys. A* **269**, 87.

- Strutinsky, V. M., 1967, Nucl. Phys. A **95**, 420.
- Sugahara, Y., and H. Toki, 1994, Nucl. Phys. A **579**, 557.
- Sun, Y., L. M. Robledo, and J. L. Egido, 1994, Nucl. Phys. A **570**, 305c.
- Suzuki, T., and H. Sagawa, 2000, Eur. Phys. J. A **9**, 49.
- Szymanski, Z., 1983, *Fast Nuclear Rotation* (Clarendon, Oxford).
- Tajima, N., 2000, in *Proceedings of the International Symposium on Models and Theories of the Nuclear Mass*, RIKEN, Japan, edited by N. Tajima and S. Yamaji (RIKEN Rev. **26**, 87).
- Tajima, N., P. Bonche, H. Flocard, P.-H. Heenen, and M. S. Weiss, 1993, Nucl. Phys. A **551**, 434.
- Tajima, N., H. Flocard, P. Bonche, J. Dobaczewski, and P.-H. Heenen, 1993, Nucl. Phys. A **551**, 409.
- Takahara, S., N. Onishi, and N. Tajima, 1994, Phys. Lett. B **331**, 261.
- Takahara, S., N. Tajima, and N. Onishi, 1998, Nucl. Phys. A **642**, 461.
- Tanihata, I., 1996, J. Phys. G **22**, 157.
- Terasaki, J., H. Flocard, P.-H. Heenen, and P. Bonche, 1997a, Nucl. Phys. A **621**, 706.
- Terasaki, J., H. Flocard, P.-H. Heenen, and P. Bonche, 1997b, Phys. Rev. C **55**, 1231.
- Terasaki, J., P.-H. Heenen, P. Bonche, J. Dobaczewski, and H. Flocard, 1995, Nucl. Phys. A **593**, 1.
- Terasaki, J., P.-H. Heenen, H. Flocard, and P. Bonche, 1996, Nucl. Phys. A **600**, 371.
- Terasaki, J., R. Wyss, and P.-H. Heenen, 1998, Phys. Lett. B **437**, 1.
- Thies, M., 1986, Nucl. Phys. A **460**, 636.
- Titin-Schnaider, C., and P. Quentin, 1974, Phys. Lett. **49B**, 397.
- Tondeur, F., 1979, Nucl. Phys. A **315**, 353.
- Tondeur, F., 1983, Phys. Lett. **123B**, 139.
- Tondeur, F., 1985, Nucl. Phys. A **442**, 460.
- Tondeur, F., D. Berdichevsky, and M. Farine, 1986, Z. Phys. A **325**, 405.
- Tondeur, F., M. Brack, M. Farine, and J. M. Pearson, 1984, Nucl. Phys. A **420**, 297.
- Tondeur, F., S. Goriely, J. M. Pearson, and M. Onsi, 2000, Phys. Rev. C **62**, 024308.
- Towner, I. S., 1987, Phys. Rep. **155**, 263.
- Typel, S., and B. A. Brown, 2001, Phys. Rev. C **64**, 027302.
- Typel, S., and H. H. Wolter, 1999, Nucl. Phys. A **656**, 331.
- Umar, A. S., M. R. Strayer, P.-G. Reinhard, K. T. R. Davies, and J.-S. Lee, 1989, Phys. Rev. C **40**, 706.
- Valor, A., J. L. Egido, and L. M. Robledo, 2000a, Nucl. Phys. A **665**, 46.
- Valor, A., J. L. Egido, and L. M. Robledo, 2000b, Nucl. Phys. A **671**, 189.
- Valor, A., P.-H. Heenen, and P. Bonche, 2000, Nucl. Phys. A **671**, 145.
- van der Woude, A., 1991, in *Electric and Magnetic Giant Resonances in Nuclei*, edited by J. Speth, International Review of Nuclear Physics No. 7 (World Scientific, River Edge, NJ), p. 99.
- Van Giai, Nguyen, and H. Sagawa, 1981, Phys. Lett. **106B**, 379.
- Vautherin, D., and D. M. Brink, 1972, Phys. Rev. C **5**, 626.
- Vautherin, D., and M. Vénéroni, 1969, Phys. Lett. **29B**, 203.
- Ventura, J., A. Polls, X. Viñas, and E. S. Hernandez, 1994, Nucl. Phys. A **578**, 147.
- Villars, F., 1957, Annu. Rev. Nucl. Sci. **7**, 185.
- Von-Eiff, D., H. Freyer, W. Stocker, and M. K. Weigel, 1995, Phys. Lett. B **344**, 11.
- Von-Eiff, D., S. Haddad, and M. K. Weigel, 1994, Phys. Rev. C **50**, 1244.
- Von-Eiff, D., J. M. Pearson, W. Stocker, and M. K. Weigel, 1994, Phys. Lett. B **324**, 279.
- Von-Eiff, D., W. Stocker, and M. K. Weigel, 1994, Phys. Rev. C **50**, 1436.
- Vretenar, D., H. Berghammer, and P. Ring, 1993, Phys. Lett. B **319**, 29.
- Vretenar, D., G. A. Lalazissis, and P. Ring, 2000, Phys. Rev. C **62**, 045502.
- Vretenar, D., N. Paar, P. Ring, and G. A. Lalazissis, 2001a, Nucl. Phys. A **692**, 496.
- Vretenar, D., N. Paar, P. Ring, and G. A. Lalazissis, 2001b, Phys. Rev. C **63**, 047301.
- Vretenar, D., N. Paar, P. Ring, and T. Nikišić, 2002, Phys. Rev. C **65**, 021301(R).
- Vretenar, D., A. Wandelt, and P. Ring, 2000, Phys. Lett. B **487**, 334.
- Walecka, J. D., 1974, Ann. Phys. (N.Y.) **83**, 491.
- Walther, V. H., 1986, private communication.
- Waroquier, M., K. Heyde, and G. Wenes, 1983, Nucl. Phys. A **404**, 269.
- Werner, T. R., J. A. Sheikh, W. Nazarewicz, M. R. Strayer, A. S. Umar, and M. Misu, 1994, Phys. Lett. B **333**, 303.
- Wilson, A. N., *et al.*, 1996, Phys. Rev. C **54**, 559.
- Wong, C. W., 1970, Nucl. Phys. A **147**, 563.
- Wong, C. Y., 1975, Phys. Rep. **15**, 283.
- Wood, J. L., K. Heyde, W. Nazarewicz, M. Huyse, and P. Van Duppen, 1992, Phys. Rep. **215**, 101.
- Woods, P. J., and C. N. Davids, 1997, Annu. Rev. Nucl. Part. Sci. **47**, 541.
- Xu, F. R., R. Wyss, and P. M. Walker, 1999, Phys. Rev. C **60**, 051301.
- Yamagami, M., and K. Matsuyanagi, 2000, Nucl. Phys. A **673**, 123.
- Yamagami, M., K. Matsuyanagi, and M. Matsuo, 2001, Nucl. Phys. A **693**, 579.
- Yoshida, S., H. Sagawa, and N. Takigawa, 1998, Phys. Rev. C **58**, 2796.
- Zheng, D. C., D. W. L. Sprung, and H. Flocard, 1992, Phys. Rev. C **46**, 1355.
- Zimanyi, J., and S. A. Moszkowski, 1990, Phys. Rev. C **42**, 1416.